Comparative Study of Microstructure and Properties of Thermal Sprayed MCrAlY Bond Coatings

A Thesis Presented

By

Michael William Inglima

To

The Graduate School

in Partial Fulfillment of the Requirements

for the Degree of

Master of Science

In

Materials Science and Engineering

Stony Brook University

August 2014

Stony Brook University
The Graduate School

Michael William Inglima

We, the thesis committee for the above candidate for the
Master of Science degree, hereby recommend
acceptance of this thesis.

Sanjay Sampath – Thesis Advisor
Distinguished Professor
Department of Materials Science and Engineering

Jason Trelewicz – Second Reader
Assistant Professor
Department of Materials Science and Engineering

Gary Halada – Third Reader
Assistant Professor
Department of Materials Science and Engineering

This thesis is accepted by the Graduate School

Charles Taber
Dean of the Graduate School

Abstract of the Thesis

Comparative Study of Microstructure and Properties of Thermal Sprayed MCrAlY Bond Coatings

By

Michael William Inglima

Master of Science

In

Materials Science and Engineering

Stony Brook University

2014

A series of experiments were performed in order to observe certain process-property trends in thermally sprayed MCrAlY bond coatings for thermal barrier coating (TBC) applications in gas-turbine engines. Firstly, the basis of gas-turbine operation and design is discussed with a focus on the Brayton cycle and basic thermodynamic properties with respect to both the thermal and fuel efficiency of the turbine. The high-temperature environment inside the gas-turbine engine creates an extremely corrosive medium in which the engineering components must operate with sufficient operating life times. These engineering constraints, both thermal/fuel efficiency and operating life, pose a serious problem during long operation as well as thermal cycling of a civil aerospace engine. The concept of a thermal barrier coating is introduced along with how these coatings protect the internal engineering components, mostly in the hot-section of the turbine, and increase both the efficiency as well as the operating life of the components. The method used to create TBC's is then introduced being thermal spray processing along with standard operating procedures (SOP) used during coating deposition. The main focus of the experiments was to quantify the process-property trends seen during thermal spray processing of TBC's with respect to the adhesion and thermally grown oxide (TGO) layer, as well as how sensitive these properties are to changing variables during coating deposition. The design of experiment (DOE) method was used in order to have sufficient statistical process control over the output as well as a standard method for quantifying the results. A total of three DOE's were performed using two main types of thermal spray processes being high-velocity oxygen fuel (HVOF) and atmospheric plasma spray (APS), with a total of five different types of torches which are categorized by liquid-fuel, gas-fuel, and single cathode plasma. The variables used in the proceeding experiments were mainly spray distance, air/fuel ratio, raster speed, powder feed rate, combustion pressure, current, primary and secondary gas flow, as well as three different powder chemistries. The results of the experiments showed very clear process-property trends with respect to mean bond strength of the coatings as well as TGO growth on the as-sprayed coating surface. The effect of either increasing/decreasing the melting index of the powder as well as increasing/decreasing the kinetic energy of the particles is shown with corresponding cross-sectional microstructures of the coating interfaces. The temperature and velocity of the particles were measured with spray diagnostic sensors as well as using an in-situ curvature property sensor (ICP) to monitor the stress-states of the coatings both during deposition as well as residual stresses, and how these might affect the bond strength. An SOP referred to as furnace cycling was used to quantify the TGO growth of the bond coatings by measuring the thickness via a scanning electron microscope (SEM) as well as performing energy dispersive x-ray spectroscopy (EDX) on the coatings to measure chemical changes.

Table of Contents

List of Figures

List of Tables

1. INTRODUCTION

1.1. THE GAS-TURBINE ENGINE

As with most engineering systems, the gas-turbine engine is a highly complex power producing system that has endless applications in our ever energy intensive society. The two main applications of said system is for civil aerospace and aviation, and the other is for power production on a large scale. These two main applications can then be further refined to define the types of gas-turbine engines, either aviation turbine type (turbofan) or the larger version, which is a commercial/industrial land-based turbine, or a combination of both which is termed an "aeroderivative" turbine. Each type of gas-turbine has the same four basic sub-systems, or sections, in the engine and a broad overview of each is discussed. [1]

Firstly, the compressor section which is comprised of a low-pressure and high-pressure stage, in which ambient air is forced into the turbine, and a series of vanes and rotors compress the air to a very high pressure, typically defined as an overall pressure ratio which is the difference in the stagnation pressure at the front and rear of the compressor (ΔP_{comp}) and in the case of the GE90 is ≈ 42:1 ratio. The next two sections are commonly referred to as the "hot section" of the turbine which consists of a combustion section where either a gas or liquid fuel (typically a highly refined hydrocarbon such as kerosene or methane) is introduced into a chamber with the highly compressed air and ignited to produce a high energy combustion reaction. The next section consists of the actual power producing turbine, being a disc with turbine blades fixed radially along the circumference. The hot combustion gases are forced out of the chamber and are incident onto the turbine blades and transfer their energy into the turbine to spin the rotor. The last section can be thought of as a “de-compressor” in which the hot compressed gases are then rapidly exhausted, and therefor decompressed, out of the engine creating a jet propulsion effect, and where the name “jet engine” comes from. The power output of a gas-turbine engine is measured in megawatts (MW) and are rated as such, and can vary from 20-500 MW, depending on the size and application of the engine. Most common civil aviation gas-turbines are in the 20-50 MW range and are a sub-type known as turbofan engines, having a large fan that is a pre-stage before the compressor, whereas the larger commercial turbines are in the 200-500 MW range, depending on how efficient the engine is and if it is a combined cycle setup. [1]

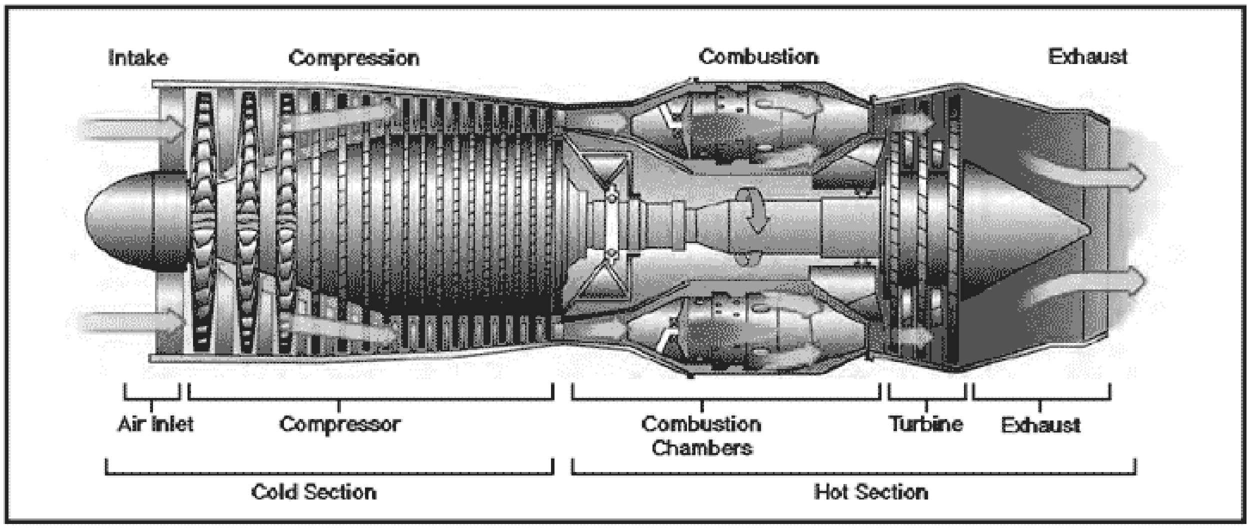

Images.google.com

FIGURE 1: *Cross-sectional view of a gas-turbine engine.*

1.1.2. GAS-TURBINE THERMODYNAMICS (BRAYTON CYCLE)

The basis upon which the gas-turbine engine works is called the Brayton cycle which is considered a steady-flow thermodynamic cycle. The engine transitions between 4 states, which are analogous to the 4 sections or stages in the turbine, which consist of an isentropic compression, an isobaric combustion, a second isentropic expansion (decompression), and a second isobaric heat exchange with the surroundings. The work required/done to either compress the air (**w_{12}**) or decompress (**w_{34}**) the hot gases, and the heat gained (**q_{23}**) and released (**q_{41}**) is shown in the following P-V and T-S graphs which outline the Brayton cycle: [2]

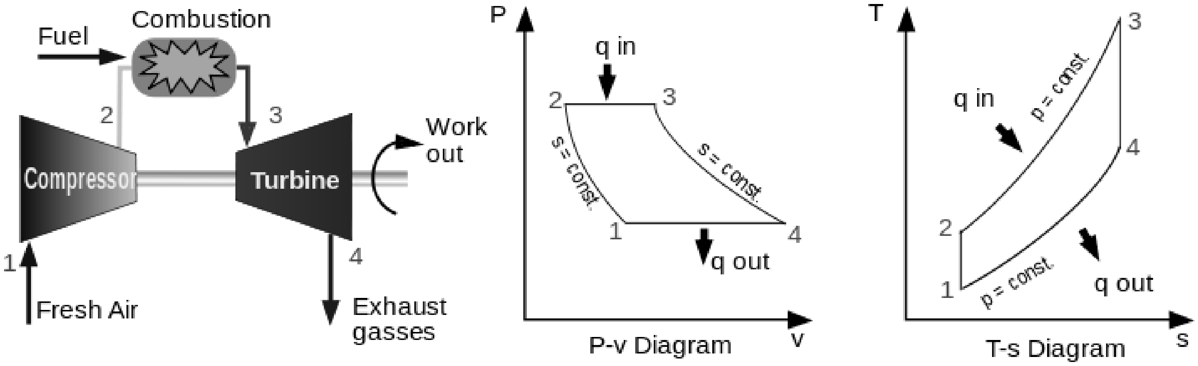

Web.mit.edu

FIGURE 2: *Graphical thermodynamic representation of Brayton cycle.*

The most important factors in this cycle, in terms of an industrial gas-turbine is the work output (**w_{34}**) and the heat released (**q_{23}**) after the cycle is completed which produce the power output, where civil aviation turbines are concerned the thermal efficiency of the engine is of great concern and is calculated as such;

$$\boldsymbol{w_{12} = h_1 - h_2 = c_P(T_1 - T_2)}$$

$$\boldsymbol{w_{34} = h_3 - h_4 = c_P(T_3 - T_4)}$$

$$\boldsymbol{w_{net} = w_{12} + w_{34}}$$

$$\boldsymbol{q_{23} = h_3 - h_2 = c_P(T_3 - T_2)}$$

$$\boldsymbol{q_{41} = h_1 - h_4 = c_P(T_1 - T_4)}$$

$$\boldsymbol{q_{net} = q_{23} + q_{41}}$$

$$\boldsymbol{\eta_{th} = \frac{w_{net}}{q_{23}}}$$

Given the inlet temperature from the combustor, where $\mathbf{T_{in} = q_{23}}$, it can be shown that increasing $\mathbf{T_{in}}$ will therefor increase the thermal efficiency, and in turn increase the fuel efficiency, of the gas-turbine engine. This increasing inlet temperature creates many problems where materials are concerned inside the turbine, and will be discussed further in the next section. The fuel cycle used in modern turbine engines is a basic complete combustion reaction between air and a refined hydrocarbon fuel, such as kerosene, which is a very carbon heavy molecule, therefor producing a large amount of enthalpy when reacted with oxygen, this reaction can be seen below; [2-3]

Paraffin Series:

C_nH_{2n+2}; $2C_nH_{2n+2} + (3n+1)O_2 \rightarrow 2nCO_2 + (2n+2)H_2O$

Complete Combustion of Kerosene:

$C_{12}H_{26(l)} + {}^{37}/_{2}O_{2(g)} \rightarrow 12CO_{2(g)} + 13H_2O_{(g)}$; $\Delta H^\circ = -7513$ kJ

Air-Fuel Ratio: $\frac{A}{F} = \frac{m_{air}}{m_{fuel}}$

Percent Theoretical Air: $\frac{\frac{A}{F}_{actual}}{\frac{A}{F}_{stoichiometric}} * 100\%$

Percent Excess Air: $\frac{\frac{A}{F}_{actual} - \frac{A}{F}_{stoichiometric}}{\frac{A}{F}_{stoichiometric}} * 100\%$

1.1.3. MOTIVATION FOR INNOVATION

The main motivation for innovating new designs of gas-turbine engines is simply to increase the fuel efficiency, which in turn will sell more engines and netting the company more profit in the long run. This can be done a number of ways yet the focus has been, especially in modern turbofan engines, on increasing the inlet temperature (**T_{in}**) from the combustor, which will increase the thermal efficiency (**η_{th}**) of the engine, as well as the net power output, and in turn increase the fuel efficiency of the turbine. This increasing inlet temperature (currently, $T_{in} \leq 1700\ ^{o}C$) creates a very high-temperature environment in the hot section of the turbine, in most cases exceeding the melting point of the materials used inside of the engine, necessitating advanced heat flux mitigation techniques such as applying thermal sprayed thermal barrier coatings (**TBC**), which consist of a dense metallic bond coating layer and a thick porous ceramic top coating, onto both the combustor linings and turbine blades. These TBC's provide an excellent solution to the high-temperature environment inside the hot section of the engine. [4]

1.2. HIGH-TEMPERATURE ENVIRONMENT

Due to the nature of the high energy combustion reaction taking place inside the hot section of the turbine, it creates a high-temperature environment ($T_{in} \leq 1700\ ^{o}C$) which the materials inside of the engine must endure. The materials inside the hot section start to degrade the closer to their respective melting points the temperatures become, possibly exceeding the tolerances that the engine was originally designed for. The gas-turbine engine parts must have specific minimum operating lifetimes before being repaired or replaced, in the case of an irreparable part failing, the turbine must be overhauled and/or decommissioned being deemed unfit for operation. This requires the use of special types of alloys with high melting points, as well as high resistance to thermal creep and oxidation, to retain room temperature bulk properties of the materials, such alloys of nickel and cobalt are very commonly used. The relative operating temperatures versus the minimum operating lifetime of various systems is seen below as well as the temperature capabilities and melting points of materials used in gas-turbine engines; [5]

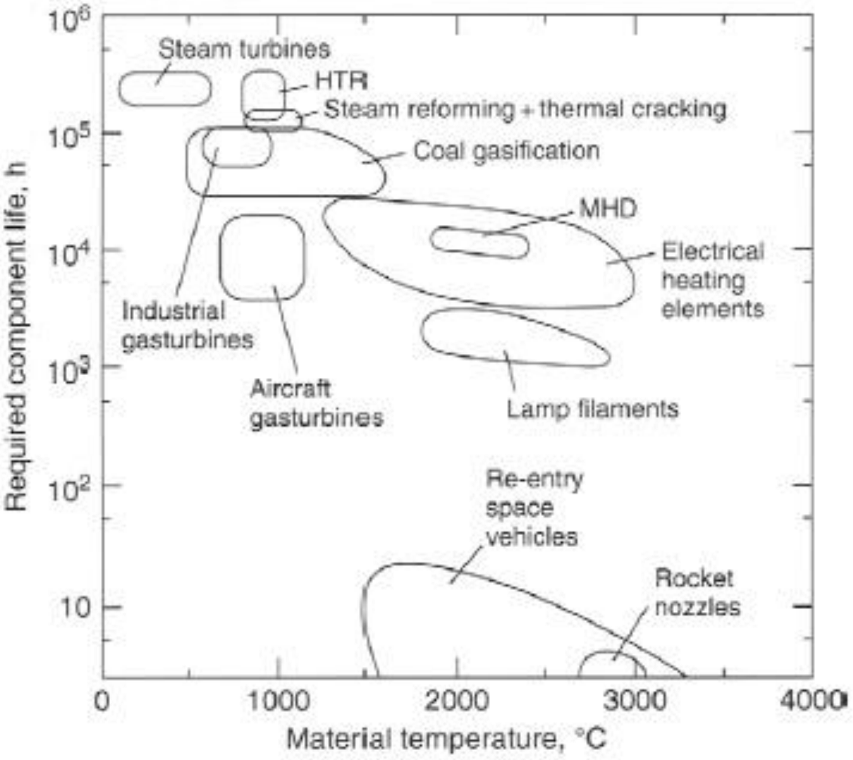

Bose et al.

FIGURE 3: *Various high-temperature systems compared to gas-turbines with required thermal cycle life.*

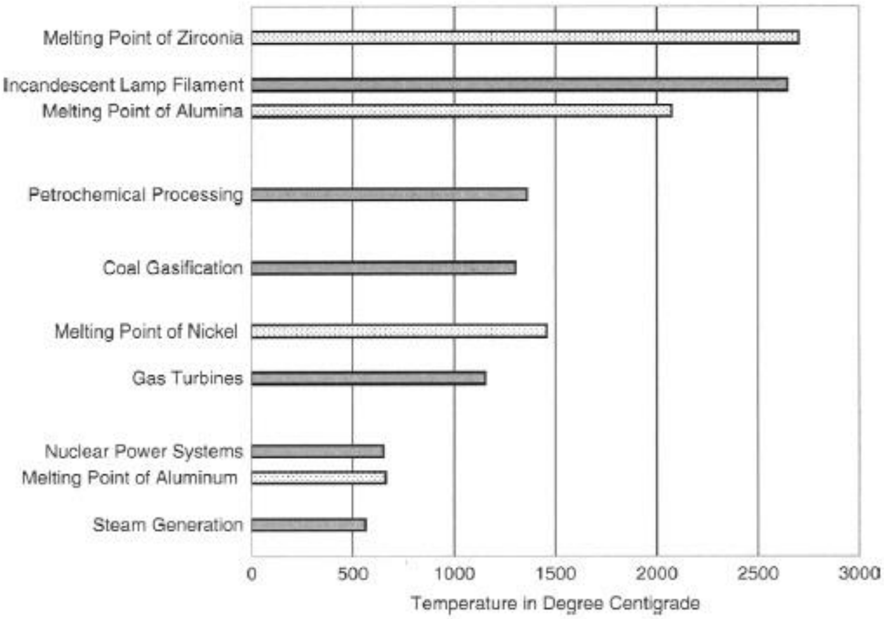

Bose et al.

FIGURE 4: *Nominal temperatures for industrial systems compared with melting points of critical coating materials.*

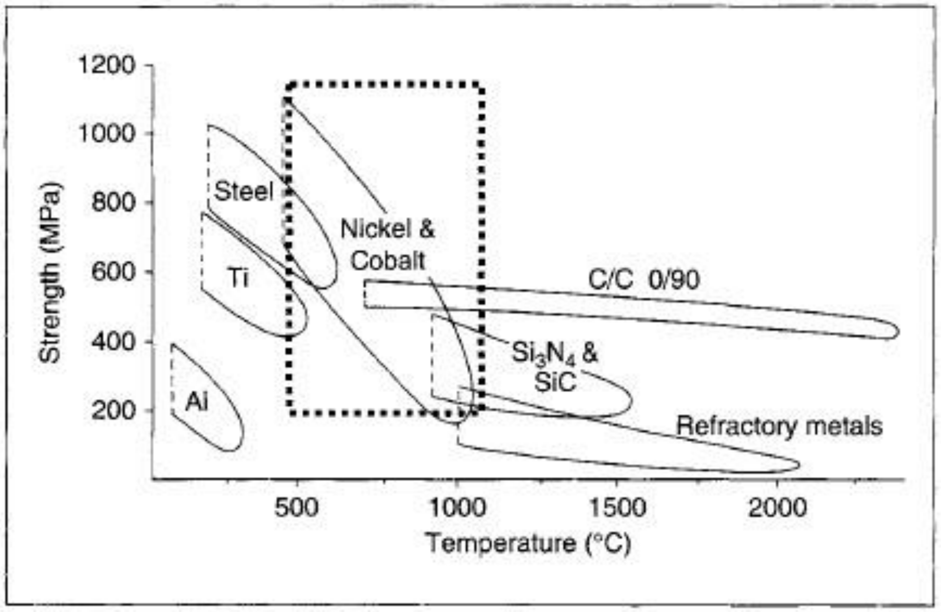

Bose et al.

FIGURE 5: *High-temperature strength retention of nickel-cobalt based superalloys compared with other metals and alloys.*

1.2.1. HOT CORROSION

The environment in which a turbine blade is subjected to is extremely harsh in terms of very high temperatures, and also a corrosive atmosphere in which thermally accelerated oxidation and sulfidation processes exist. This environment is extremely caustic even for a nickel superalloy (**NSA**) that exhibits very good high-temperature oxidation properties. The operation of a gas turbine engine produces many contaminants, namely CO_2, water vapor and in cases of incomplete combustion, hydrocarbons and/or sulfides. The combustion reaction taking place in the turbine is an oxy-fuel chemical reaction between the fuel, typically a refined kerosene, and highly compressed air entering the chamber after the second stage high pressure compressor section. [5]

The combustion reaction produces CO_2 and H_2O vapor which are the main high-temperature oxidizing agents inside the turbine. If the combustion reaction is incomplete, having not enough oxygen to completely combust all the hydrocarbon fuel, typically 10 – 50% excess oxygen is needed for complete combustion, other contaminants are produced such as sulfates/sulfides, left over hydrocarbon fuel, and some carbon. The presence of these sulfates leads to another type of corrosion taking place called sulfate-induced hot corrosion, or high-temperature sulfidation. This process penetrates the TBC with sulfide ions and weakens the coating, and can also lead to sulfide stress cracking in the substrate which is a form of hydrogen embrittlement. The highly engineered TBC chemistry is crucial in the prevention of high-temperature corrosion where the addition of cobalt and tantalum help to mitigate this process, as well as chromium and aluminum which form a protective oxide layer on the bond coating surface. [5]

1.2.1.1. HIGH-TEMPERATURE OXIDATION

The presence of excess CO_2 and H_2O vapor inside the combustion chamber, under temperatures ≤ 1700 ^{o}C can act as a super oxidizing agent. These oxidants traditionally at room temperature consist of elements with high oxidation states such as; H_2O_2, MnO_4^-, CrO_3, $Cr_2O_7^{2-}$, OsO_4, or highly electronegative compounds such as; O_2, F_2, Cl_2, Br_2, which strip away electrons from the substrate and oxidize it. This process is highly accelerated by the high-temperature environment in which water vapor acts as the main oxidizing agent. This process is particularly harmful for the TBC because the ceramic traditionally used consists of a partially-stabilized zirconia; 7YSZ, 7 mol% Y_2O_3 – ZrO_2; or 4YSZ, 4 mol% Y_2O_3 – ZrO_2, which chemically are oxygen transparent materials. This oxygen transparency allows the high-temperature oxidizing agent to leeche AlO and CrO out of the bond coating, making it unstable and prone to premature failure. The bond coating traditionally will form a thermally grown oxide (**TGO**) layer onto the coating surface to protect both the substrate material and the TBC. [5-6]

The rate of oxidation depends on activation energies of the transient oxides that are formed and the difference in gibbs free energy which will predict how spontaneous the reaction is, and in which direction it will proceed. The activation energy can be thought of as a hill that must be surpassed in order to start the oxidation reaction, which in the high-temperature environment is supplied by the thermal energy from the combustion reaction. The oxygen atoms in the H_2O vapor are atomized and are adsorbed onto the surface of the coating, which then seek the state of lowest potential energy and diffuse Al out of the metallic bond coating, forming Al_2O_3 as an oxide scale. The rate of oxidation is determined by the activation energy, free energy, and activity coefficients and can be seen below, as well as a figure depicting the oxidation kinetics process: [5-6]

$$k_{ox} = k_1 \exp\left(-\frac{\Delta G_{active}}{RT}\right) = k_1 \exp\left(\frac{\Delta S_{active}}{R}\right) exp\left(-\frac{\Delta H_{active}}{RT}\right)$$

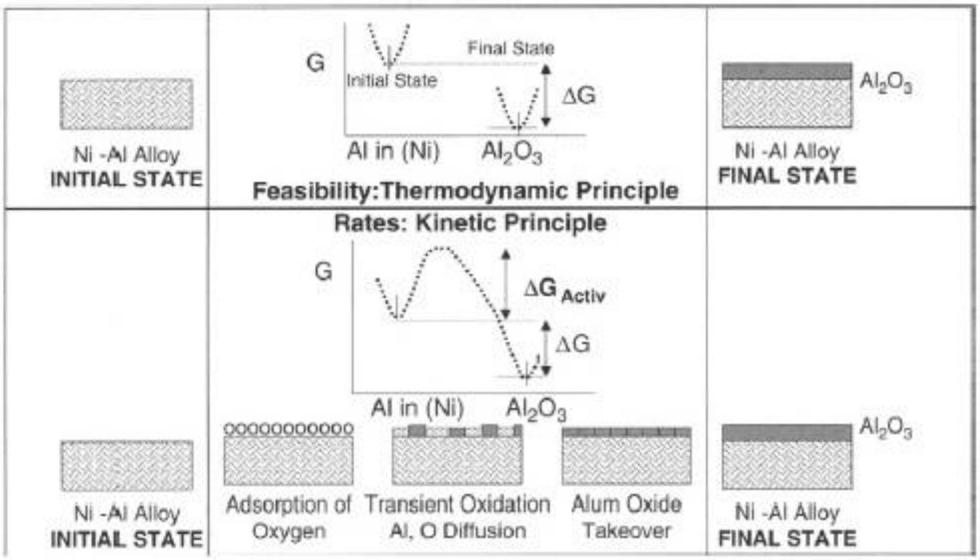

Bose et al.

FIGURE 6: *Illustration of activation energy barrier required for oxidation.*

1.3. NICKEL-COBALT BASED SUPERALLOY TURBINE BLADES

The hot-section of the gas-turbine engine contains the main power producing turbine which consists of a main rotor shaft with circular discs concentric with the shaft, where turbine blades are fixed radially around the circumference of the disc. The turbine blades must not only endure the high-temperature corrosive environment, they must also maintain their bulk properties and dimensional stability under the very large rotational forces imparted onto the blades as the turbine spins at high RPM. Material selection is very important for turbine blades, which are generally metal alloys, as they must have excellent properties such as high melting point, tensile, creep, and fatigue strength, toughness, and low density. Examples of such materials that have been used for this application include various titanium alloys (Ti-6Al-4V, Ti-6Al-2Sn-4Zr-2Mo), high strength bainitic steels, work-hardened nickel-iron alloys, and precipitate-hardened austenitic nickel-cobalt based superalloys (**NSA**), which are the most common. This unique class of complex alloys have very high-strength across a wide temperature range, as well as excellent corrosion resistance, making them an obvious choice for turbine blade applications. The large rotational forces imparted onto the turbine blade, of which creep is most important, require the material do have different properties in different directions which is called anisotropy, and can be achieved by manufacturing the blades with specific crystal structures. The method used is called directional solidification, where the cast alloy is controlled via grain growth directions and can produce blades with columnar grain structure or most commonly a single crystal turbine blade, which requires the addition of a grain selector which allows only one crystal grain to grow into the mold, and can be seen below; [6]

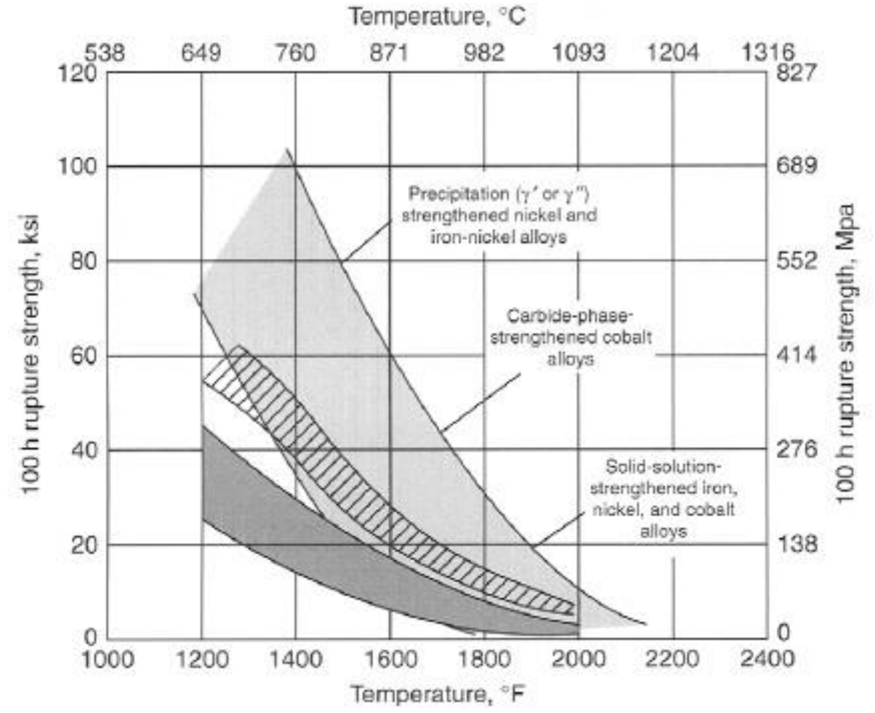

Bose et al.

FIGURE 7: *NSA creep rupture strength as a function of temperature.*

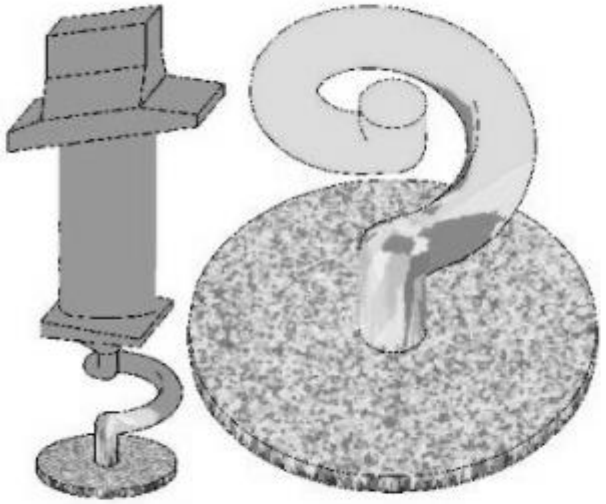

Machine design.com

FIGURE 8: *Example of single crystal turbine blade casting with grain selector.*

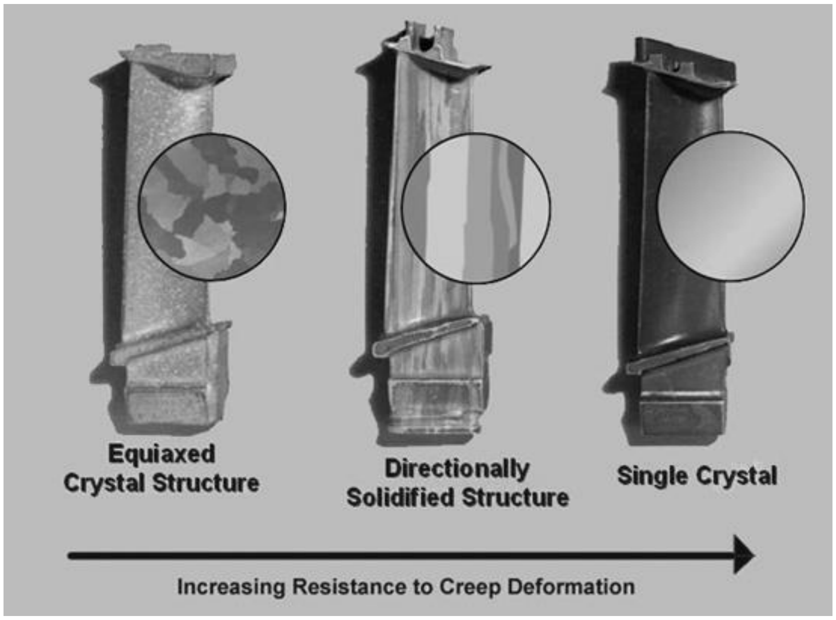

Rolls-royce.com

FIGURE 9: *Increasing creep deformation resistance as function of anisotropic crystal structure in turbine blades.*

A significantly important property of nickel, from a chemical and engineering standpoint, is its ability to resist corrosion, especially at high temperatures. This is due to the formation of a preferentially grown oxide scale on the surface of the metal, which will be seen that can be controlled via the dopants used. At room temperature elemental nickel has a typical oxidation state of Ni^{+1} to Ni^{+2} and a relatively low electronegativity (≈ 1.9), which makes it highly susceptible to oxidation from highly electronegative oxygen (≈ 3.5) in the ambient environment. This forms a scale layer composed of Nickel (II) oxide, NiO, or less commonly Nickel (III) oxide, Ni_2O_3, on the surface of the metal, as seen below; [6-7]

$$\mathbf{Ni^{+1} + O_2 \rightarrow 1/2NiO^{+2}}$$

$$\mathbf{2Ni^{+1} + 1.5O_2 \rightarrow Ni_2O_3^{+2}}$$

The process of protecting the substrate material involves depositing a TBC onto the surface, which in this case consists of what is referred to as an MCrAlY bond coating, and a 7YSZ ceramic top coating. The bond coating is of particular interest being the primary failure mechanism for the TBC, which will be discussed later. This coating has a chemistry of NiCoCrAlY which is a highly engineered mixture and has a very similar composition to the NSA substrate material for which it was designed, and the oxidation properties can be tailored by adding various elements. Before defining the specific chemical combination of dopants used in MCrAlY powder, it is necessary to define and understand the crystal structure of nickel, and how these elements form substitutional/interstitial alloys. Nickel has a unit cell configuration of face centered cubic (FCC) with an atomic radius of 124 pm, and a van der waal's radius of 163 pm. At this time it is convenient to consider the structure and phase transformation of nickel superalloys (NSA) in order to better understand the crystal structure of the powder. These are composed of a nickel base or matrix, doped with cobalt and chromium, and other trace elements which are usually proprietary.

These NSA materials are categorized depending on their chemical composition and/or metallurgy, common types are Hastelloy, Inconel (IN713), Rene alloys (Rene 80), Haynes alloys, and CMSX (CMSX-4) which are single crystal alloys. The highly corrosion resistant properties of NSA comes from the addition of chromium and aluminum into the nickel-cobalt matrix. [8]

The microstructure of these alloys typically consist of two phases, a **γ** – phase and a **γ'** – phase**,** which arise through the processing and cold working of the NSA called precipitation hardening, where there exists a **γ** – matrix and **γ'** – intermetallic precipitates. These phases consist of the nickel-cobalt **γ** – matrix which is a solid solution in an FCC configuration, and the **γ'** – intermetallic precipitate phase, typically Ni_3Al in an LI_2 crystal structure, which is cuboid in shape. The aluminum atoms are randomly placed in the **γ** – matrix, having a larger atomic radius (≈ 143 pm) than the nickel atoms (≈ 124 pm), which cannot occupy the tetrahedral or octahedral interstices in the FCC lattice, which is also true for chromium (≈ 128 pm). The LI_2 structure of Ni_3Al consists of atoms of aluminum occupying the vertices of the cubic cell and form a sublattice A, whereas the nickel atoms occupy the center of the FCC faces and form the sublattice B. The stoichiometry of this phase is not usually balanced, mainly caused by a high vacancy concentration in one of the sublattices. The **γ'** – intermetallic precipitate phase can solute many types of other elements in its sublattices, such as chromium, cobalt, yttrium, tantalum, rhenium, hafnium, and silicon with some others placed in the **γ** – matrix, which can be seen below; [9]

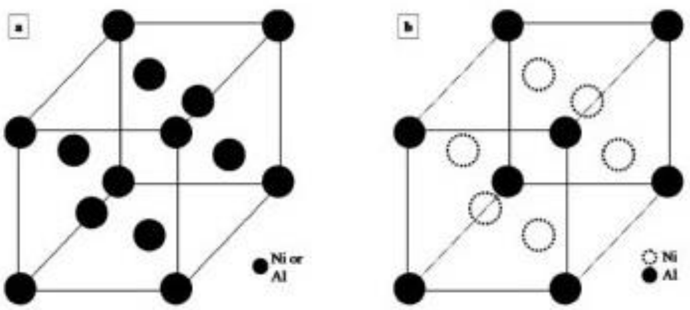

Singh et al.

FIGURE 10: *Crystal Structure of NSA showing γ and γ' Phase Transformation*

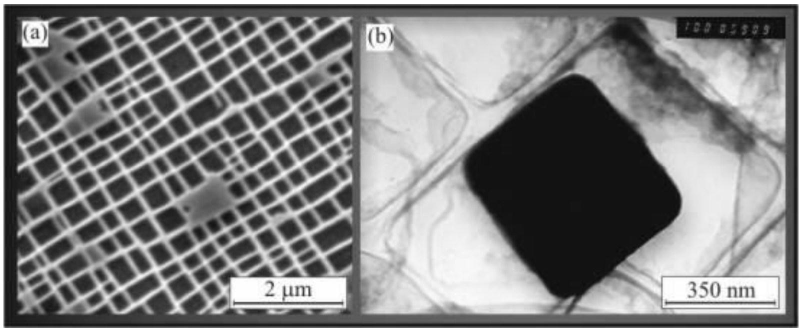

Umms.sav.sk

FIGURE 11: *TEM Micrograph of Single Crystal NSA Microstructure*

1.4. THERMAL BARRIER COATING (TBC)

The anatomy of a thermal barrier coating is rather simple, it consists of a metallic substrate, in the case of turbine blades it is most commonly a nickel superalloy. A metallic bond coating is applied to the substrate surface, in the scope of this application it will be referred to as an MCrAlY coating. The final layer is a ceramic top coating, currently the standard is a partially-stabilized zirconia (7 – 7.5YSZ). The bond coating layer is extremely important as it is specifically designed to have high bond strength to the substrate, as well as bond to the ceramic top coating improving the interfacial fracture toughness of the TBC. The surface roughness of the as-sprayed bond coating is a critical parameter as this is directly linked to the thermal cycle life of the TBC as well. This functionally graded coating effectively arrests the high heat flux seen by the substrate material, preserving the bulk properties of the alloy and maintaining dimensional stability of the turbine blade. The cross-sectional microstructure of a typical TBC can be seen below, with a dual-layer bond coating, TGO, and zirconia top-coat, as well as respective nominal thicknesses; [10]

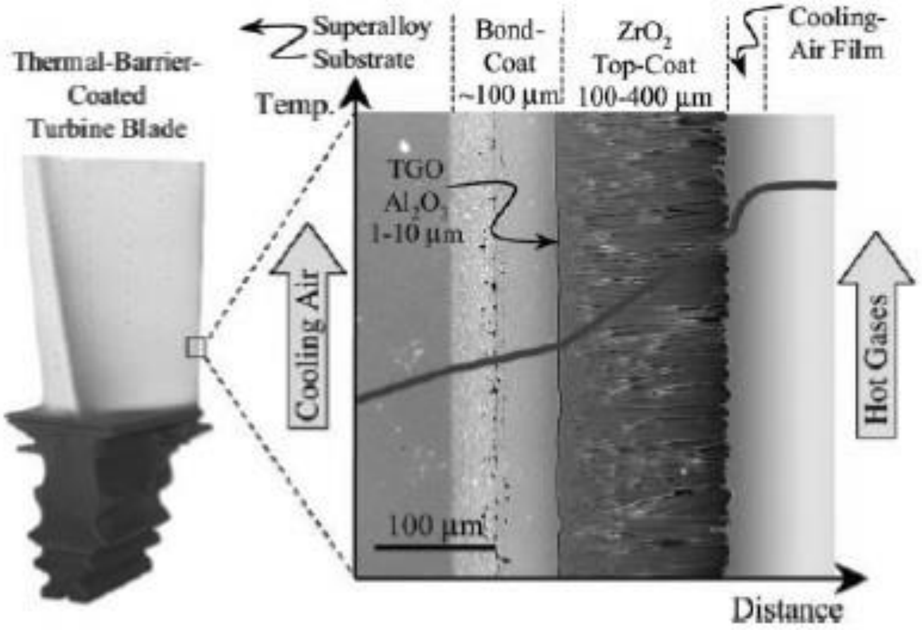

Padture et al.

FIGURE 12: *TBC Microstructure showing NSA Substrate, Bond Coat, TGO, and Top Coat*

1.5. BOND COATING

The primary purpose of this coating is to bond the ceramic top-coating to the substrate, as well as to grow an oxide layer onto the as-sprayed surface. The main type of bond-coating material used are known as MCrAlY alloys, although other materials can/have been used in the past such as NiAl, NiCr, or other nickel based alloy blends. The MCrAlY family is comprised of NiCrAlY, CoCrAlY, NiCoCrAlY, and CoNiCrAlY, as can be seen have either a nickel or cobalt matrix metal and alloyed with chromium, aluminum and yttrium. This bond-coating material has a special property which is to preferentially grow an oxide layer onto the surface after the coating has been thermally cycled a number of times. This would normally be seen as a negative attribute in any other application yet these materials were specifically designed for this purpose. The thermally grown oxide layer grows linearly with temperature and time and reaches a parabolic asymptote after a certain number of thermal cycles, depending on the coating chemistry as well as the type of processing used to deposit the coating. [10-11]

The chemistry of the MCrAlY powder is very similar to the chemistry of the NSA substrate for a specific reason, mainly to minimize further oxidation of the coating via the thermally grown oxide (**TGO**) layer, leeching of elements from the substrate, and improved adhesion of the bond coating to the substrate. This makes the coating highly customizable and tailorable to specific applications, mainly in very high-temperature environments. The alloying elements of aluminum and titanium create the $\boldsymbol{\gamma'}$ – phase which can be precisely controlled by careful precipitation hardening of the alloy. [11]

Some alloys are processed by a two-phase heat treatment which creates the dispersion of the cuboidal $\boldsymbol{\gamma'}$ – phase particles known as primary phase, with a finer dispersion of $\boldsymbol{\gamma'}$ – phase particles between them known as secondary phase. This is done specifically to improve the oxidation resistance of the alloy, where aluminum, chromium, boron, hafnium, rhenium, tantalum, silicon and yttrium $\boldsymbol{\gamma'}$ – intermetallic secondary phase particles are added. The aluminum and chromium form oxide layers that can passivate the surface and prevent any further oxidation of the coating, whereas the boron, yttrium, and hafnium improve the adhesion of the oxide layer to the coating by increasing the chemical activity of aluminum in the coating. The amount of chromium and aluminum in the coating will serve as a leeching reservoir in order to grow the oxide layer, the ratio of chromium/aluminum is very critical in order to avoid coating embrittlement. The presence of cobalt and tantalum in the coating improves the ductility and hot corrosion resistance as well. [11]

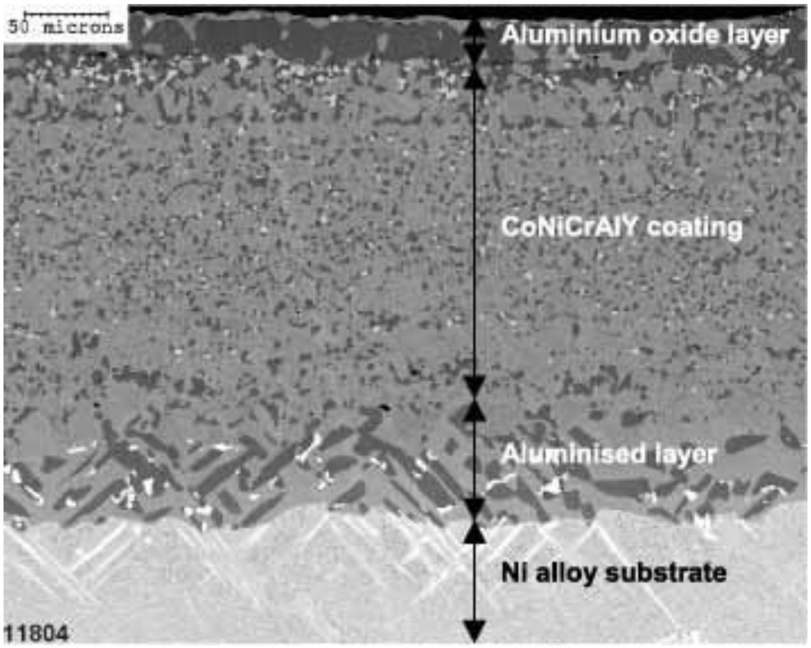

Twi-global.com

FIGURE 13: *Nominal microstructure of a dense MCrAlY bond-coating.*

1.6. THERMALLY GROWN OXIDE (TGO)

The defining characteristic of the MCrAlY bond coating is the ability to passivate the surface with a thermally grown oxide (TGO) layer. As previously discussed this is achieved by the leeching of aluminum and chromium from the bond coating to form an oxide layer on the surface of aluminum oxide in an alpha phase, $\boldsymbol{\alpha - Al_2O_3}$, which is a crystalline form of corundum, with a Trigonal (Hexagonal Scalenohedral) crystal structure, and is most commonly known as sapphire.

The oxide layer is typically grown after the thermal barrier coating (TBC) is applied to the substrate, in the case of a gas turbine onto the blades, and is put into production where it is subjected to many thermal cycles as the engine is run from take-off to landing. The TGO layer is a crucial aspect of the MCrAlY bond coating, which dictates the adhesion of the ceramic top layer to the bond coating, and is the defining factor of the overall thermal cycle life of the TBC. [12]

This oxide layer is very complicated in terms of how fast it is grown and to what thickness, dictated by the oxidation kinetics, and the highly engineered chemistry of the coating. As was stated before specific elements are added to the MCrAlY alloy in order to try to mitigate and control the growth of the TGO layer. As the TBC is thermally cycled to $\approx 1100\ ^{o}C$ the TGO starts to rapidly grow in a hyperbolic function and as the TGO thickness increases, the TGO growth rate starts to slow and reach an asymptotic relationship. This temperature in a gas turbine engine is known as the inlet temperature and is a crucial factor in the efficiency of the turbine, where in new designs the inlet temperatures could reach $\geq 1600\ ^{o}C$. [12-13]

The specific phases of the bond coating (BC) can affect the growth of the TGO and make the coating more unstable, such as in the case of Pt – aluminide, which forms an unstable β – phase field and can be seen in the Ni – Al – Pt ternary phase diagram. These unstable phases will affect how the TGO layer reacts under thermal cycling, where it tends to bunch up or form a wavy surface with a specific amplitude and, is analogous to a sine function. This wavy nature of the TGO is caused by the thermal mismatch between the TGO and the bond coating, caused by the difference in the coefficient of thermal expansion (CTE), or ΔCTE_{BC-TGO}, which causes a large interfacial strain energy in an elastic/plastic deformation system. The large interfacial strain caused by the TGO growth volume expansion can be quantified by the relationships for the stress a radius **r** away from the center of curvature and the stress at the surface of curvature: [13]

$$\boldsymbol{\sigma_{rr} = -\frac{2E(m-1)h}{3(1-\upsilon)mR}}$$

$$\boldsymbol{\sigma_{\theta\theta} = \sigma^{i}_{\theta\theta} + \frac{E(m-1)}{3(1-\nu)m}\left[\frac{r}{R} - \left(1 - \frac{h}{R}\right)\right]}$$

Where, **E** is young’s modulus, **m** is the ratio of new TGO volume to the consumed bond coat volume, **h** is TGO thickness, **R** is radius of concave surface, $\boldsymbol{\nu}$ is Poisson’s ratio, and $\boldsymbol{\sigma^{i}_{\theta\theta}}$ is the hoop stress at the growth interface. [13]

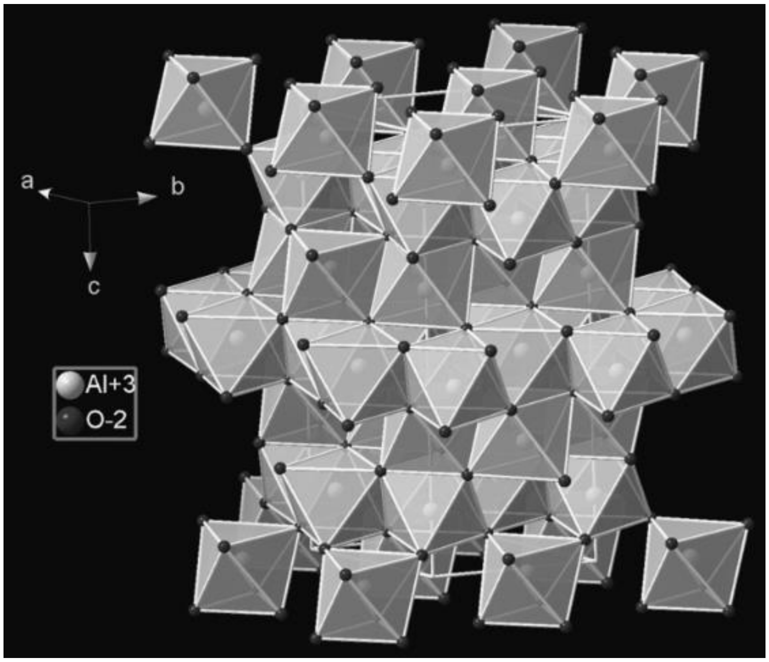

NIMSoffice

FIGURE 14: *Trigonal Crystal Structure of* $\alpha - Al_2O_3$ *(TGO)*

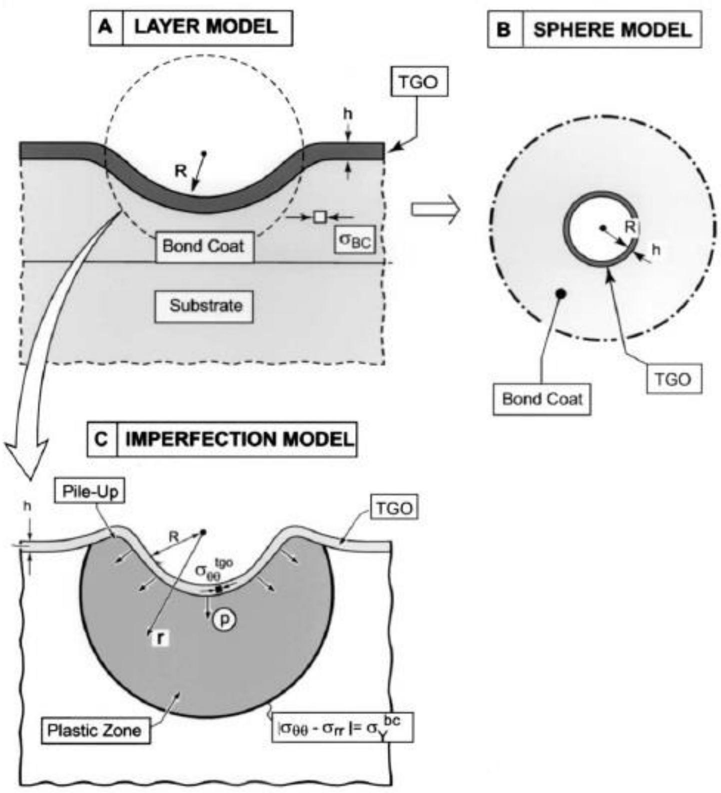

Karlsson et al.

FIGURE 15: *Stress-Strain Models for TGO Growth*

1.7. TOP COATING

The ceramic top-coating of the TBC is the actual thermal barrier material which protects the substrate from overheating and losing dimensional stability, or in extreme cases can also partially melt, with the inlet temperatures exceeding the melting point of NSA. The low thermal conductivity, low coefficient of thermal expansion (CTE), and high melting point of ceramics make them an ideal choice for TBC applications, and these properties can be improved through processing of the coating as well. The ceramic has the capacity to absorb thermal energy by imparting a stress onto the substrate and forming what is known as a bi-layer curvature stress-strain relationship. The material exhibits anelastic behavior where during this curvature it will return back to its original state after cooling down, yet not following the same stress-strain path. This curious property of the ceramic allows the coating to endure intense thermal cycling without suffering from thermal shock cracking and spallation of the coating, which dense bulk ceramics exhibit. The porosity of the top-coating also plays a crucial role as the higher the porosity of the coating, the lower the thermal conductivity of the ceramic, with the only caveat being that ≥ 12 – 15% porosity the coating loses strength and tends to degrade. This can be overcome by forming a dense vertically cracked microstructure in the top-coating which allows for bi-layer curvature and keeps the anelastic property while not losing strength or degrading. This microstructure currently can only successfully be achieved by using a thin film coating technique known as electron beam physical vapor deposition (**EB-PVD**), though new atmospheric plasma spray (**APS**) methods are being developed which can achieve the same microstructure. The most common ceramic used for TBC applications is a partially stabilized zirconia (**PSZ**) where the crystal lattice of zirconium dioxide is stabilized at room temperature by adding a yttria dopant. [14-15]

1.7.1. ZIRCONIUM DIOXIDE (ZIRCONIA)

Zirconium is a transition metal, having a crystal structure of hexagonal close packed (HCP), in the same group as titanium and hafnium, which all have similar properties. This metal has very good corrosion properties and forms many organic and inorganic compounds, most notably zirconium dioxide, ZrO_2, and most commonly called zirconia, having a monoclinic crystal structure at room temperature. The phase transitions pure zirconia can undertake are ≤ 1170 ^oC monoclinic, 1170 ^oC ≤ tetragonal ≤ 2370 ^oC, 2370 ^oC ≤ cubic < 2715 ^oC, having a melting point of 2715 ^oC, with the higher temperatures exhibiting higher symmetry which is normal. [15]

When zirconia is cooled from a molten state it exhibits three phase transformations, from cubic → tetragonal → monoclinic, the last monoclinic phase has a much greater volume than either the cubic or tetragonal phase. This volume expansion upon cooling puts a large strain energy on to the crystal lattice which manifests itself in a large residual stress in the material, and has the tendency to crack, being a brittle ceramic. It is therefore desirable to retain the cubic phase of zirconia while reducing the tetragonal phase, and eliminating the phase transformation to monoclinic. This is done by doping the zirconia with oxides such as magnesium oxide (MgO), calcium oxide (CaO), gadolinium oxide (Gd_2O_3), and most commonly with yttrium oxide (Y_2O_3) or yttria. This oxide dopant tends to stabilize the zirconia crystal structure making it more stable at room temperature, after being quenched from a molten state. The degree to which the zirconia matrix is stabilized depends on the amount of dopant added, and the percentage of either the tetragonal or cubic phase present. [15-16]

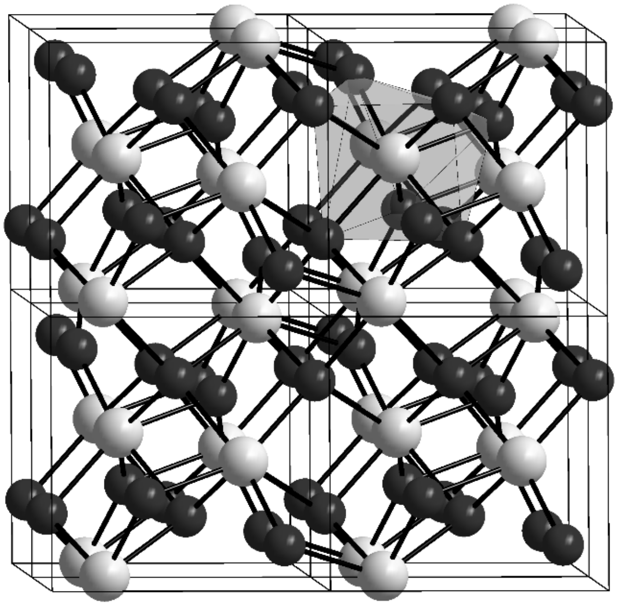

Orci, open source

FIGURE 16: *Monoclinic Crystal Structure of Zirconium Dioxide at 25 ^{o}C*

1.7.2. YTTRIA-STABILIZED ZIRCONIA (YSZ)

The most common phase of YSZ ceramic used for TBC applications is the 7YSZ, 7 mol% $Y_2O_3 – ZrO_2$ which has very good thermal and mechanical properties. This composition is ideal for a TBC application because it is the highest mol% of dopant that can be added without becoming a fully-stabilized zirconia, such as cubic zirconia, which is extremely stiff and cannot be melted well enough. This composition of YSZ also has a very high melting point of ≈ 2750 °C, a low thermal conductivity (2.20 W/m*K) and low CTE mismatch (0.1 – 0.5) with the TGO layer. The properties of this ceramic are also highly process dependent, being mainly EB-PVD and APS. The process used to deposit these powders will either create a columnar grain structure (EB-PVD) or a more porous composite structure (APS). It has also been shown that a problem arises when a YSZ ceramic is deposited with EB-PVD and is thermally cycled in a furnace. During the thermal cycling, usually from room temperature to ≥ 1150 °C, for as many cycles until failure, it has been shown that due to certain microstructural changes, the thermal conductivity of the YSZ tends to increase linearly with temperature, due to the ceramic being sintered. [16]

This 7YSZ ceramic processed by EB-PVD was shown to have an increase in thermal conductivity and thermal diffusivity at a substantial rate after the first 20 -1 hr cycles. The values tended toward an asymptotic relationship after 20 cycles and after performing Raman spectroscopy on the coating, it was determined that this increase in both thermal conductivity and diffusivity, was due to a decrease in the defect concentration in the ceramic. The porosity of the coating is a crucial aspect of the TBC as the thermal conductivity is inversely proportional to the porosity of the ceramic. The increase in thermal conductivity is attributed to the decrease in porosity, mostly this happens when the ceramic sinters together at high temperatures, both reducing its fracture toughness and porosity, and becoming less compliant and more brittle. The microstructure of

7YSZ ceramic coatings tend to form what is a known as a dense vertically cracked structure which is a columnar growth mechanism. [16-17]

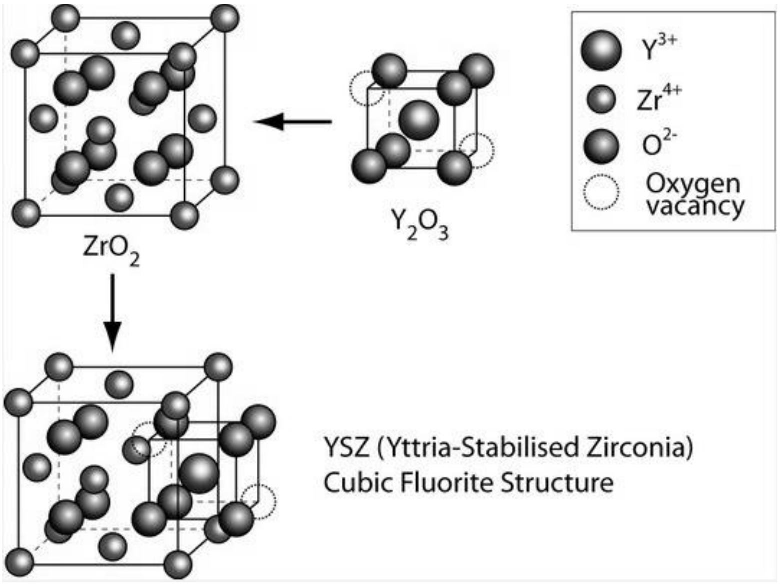

Doitpoms.ac.uk

FIGURE 17: *Cubic Fluorite Crystal Structure of YSZ*

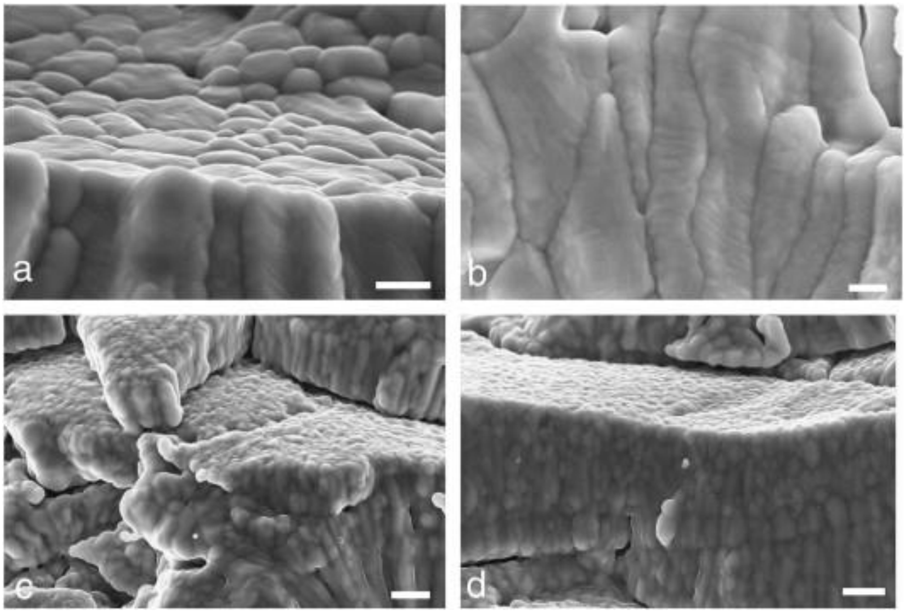

Sampath et al.

FIGURE 18: *SEM Micrograph of APS 7YSZ Microstructure Formation*

1.8. THERMAL SPRAY PROCESSING

Thermal barrier coatings can be applied using various coating deposition processes such as electron beam physical vapor deposition, chemical vapor deposition, thin-film vacuum processes, and thermal spray processing. The latter of these deposition processes has become the standard coating technique used by original equipment manufacturers (OEM) to apply TBC's to their parts and in the case of gas-turbine engines, thermal spray processing is used to deposit coatings on parts in virtually every section. In the cold section (compressor) of the turbine there are abradable coatings, which are designed to create the seals where parts rub against each other and wear the coatings off. The hot-section has mainly TBC's on both the combustor liners and turbine blades, as well as the exhaust section. This form of "thick-film" processing has become very popular because of its low-cost and versatility in coating materials, where if it is able to be melted can be applied using thermal spray. [18]

There are many different kinds of thermal spray processes yet in the case of TBC's the most common are atmospheric plasma spray (APS) and high-velocity oxygen fuel (HVOF), as well as some vacuum plasma techniques such as low-pressure plasma spray (LPPS). The concept is the same in all of these being either metallic or ceramic powder is injected into a high energy heat source and melted, the molten particles are then ejected from the heat source (plume) by the high-velocity gases exiting the gun. The molten particles travel through a short distance in air and are then incident onto the substrate surface, experiencing an extreme quenching rate on the order of 1.0×10^6 $^oC/s$ which rapidly solidifies the particles. After the first layer of particles are deposited onto the surface, known as splats, the next wave of molten particles are then deposited onto the splats and start to form a "brick and mortar" style coating. These coatings have inherent flaws in them such as voids, inclusions, un-melted particles, and also foreign objects such as entrained grit from the surface preparation process. These flaws can be designed into the coating, as is the case in the ceramic top coat which has a porous microstructure, and can also have vertical cracks running through thickness of the coating, which improves the properties of the coating. Examples of both the thermal spray process and a cross-section of a typical coating microstructure can be seen below: [18-19]

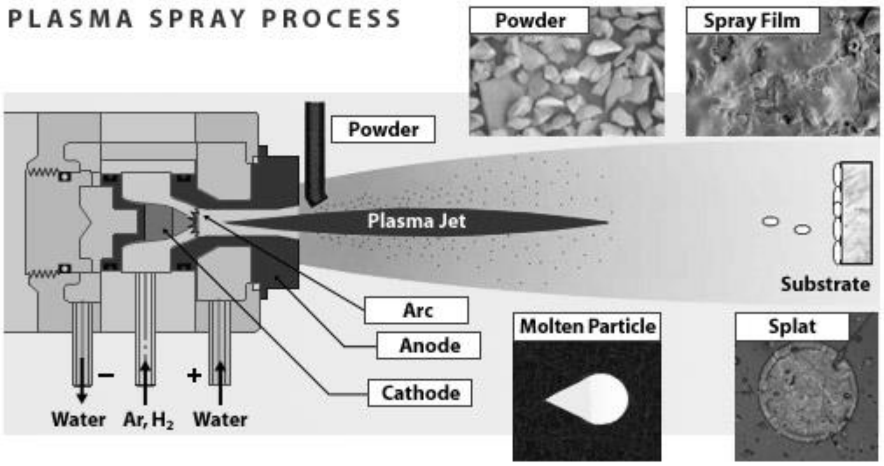

Thermalsprayusa.com

FIGURE 19: *Example of plasma spray process showing various stages of coating.*

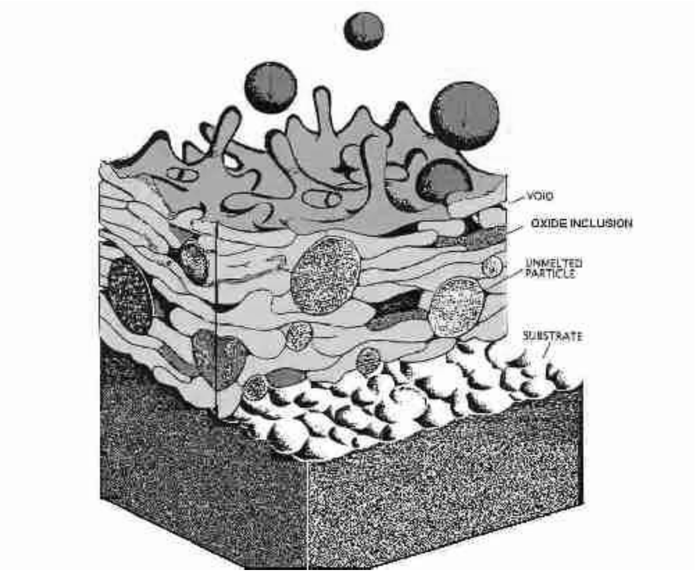

Thermalsprayusa.com

FIGURE 20: *Example of thermal spray deposition process including flaws in coating.*

1.8.1. ATMOSPHERIC PLASMA SPRAY (APS)

The most common thermal spray deposition process is known as atmospheric plasma spray, or air plasma spray (APS), and is mainly used to spray ceramic powders. This process takes advantage of the extreme amount of thermal energy contained in a superheated ionized gas, which is said to be in a plasma state. In physics, this plasma is one of four states of matter, being solid, liquid, gas, and plasma. This plasma is analogous to a superheated gas, in APS the primary gas used to create the plasma is typically argon, in which it is passed through a high-voltage electrical arc and strips away its electrons, ionizing the gas. The plasma has a very high temperature, typically ≥ 10,000 ^{o}C, which is sufficient to melt most materials such as ceramics, refractory metals, and most oxides/carbides. The amount of enthalpy in the plasma can be raised by introducing a secondary gas, most commonly hydrogen or helium, which is then ionized and adds additional thermal energy. [20]

1.8.1.1. PLASMA GENERATION/APS TORCH DESIGN

In the APS process the way the plasma is generated is very important as this can affect the efficiency of melting the particles, and also the amount of heat transfer to the material inside the plume. Most simple plasma torch designs use a straight channel in which the primary gas is flowed through, which also acts as the cathode, and is convergent into a smaller aperture. This aperture contains the anode in the circuit and is called the nozzle, where the high-voltage electrical arc discharges to. The argon flows through the nozzle and is ionized by the electrical arc and creates the superheated plasma, which is “pushed” out of the aperture by a force in the $\hat{z}$ direction, called the Lorentz force. This so called “pinching effect” is what gives the plasma its velocity as it exits the nozzle. The nozzle is made from conductive metal, such as copper, which is electrically insulated from the outside of the torch so that the arc does not discharge in random places, only on the anodic nozzle surface. [20-21]

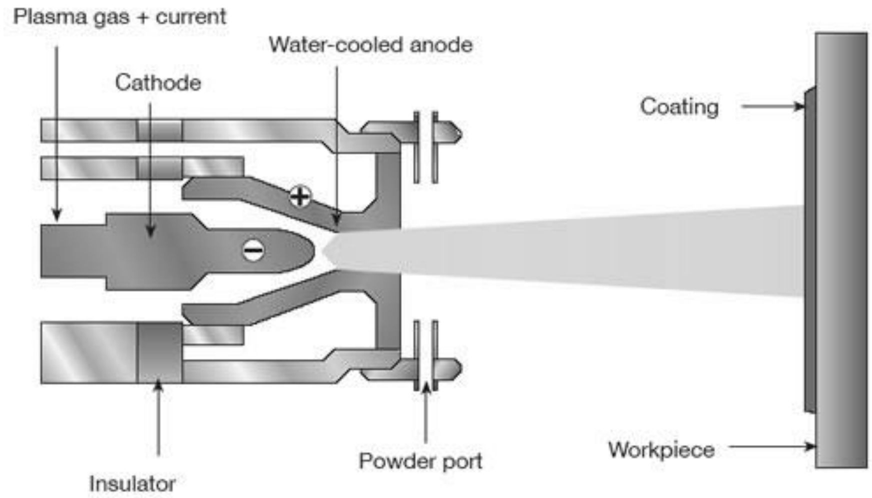

Sulzermetco.com

FIGURE 21: *Cross-sectional view of APS torch.*

These torches used a direct current supply and can either be transferred or non-transferred arc designs. If the anode and cathode are both housed inside the torch the plasma is generated internally and can lose some enthalpy due to the water cooling inside the torch, which is known as DC non-transferred arc design. If the cathode is inside the body and the anode is outside of the torch, being part of the nozzle, then it is a DC transferred arc design. There have been new innovations in DC transferred arc designs dealing with arc stabilization, which lets the arc travel farther inside the nozzle, creating a larger and more uniform plasma, and improves heat transfer and melting efficiency. The parameters use when performing experiments with APS deal with overall DC current, which in a Sulzer-Metco F4 model APS torch, range from $350 \leq I \leq 550$ amps (A), primary gas flow rate $30 \leq Q_P \leq 60$ standard liters per minute (SLPM), and secondary gas flow rate $2 \leq Q_S \leq 8$ SLPM. The APS process has a high particle temperature but a low particle velocity in a ratio of ≈ 21.5, some different torch designs have a higher particle velocity termed high-velocity plasma spray (HVPS) such as a Praxair SG100 torch. [22]

1.8.1.2. EXTERNAL POWDER INJECTION

The powder is delivered from a hopper style feeder which houses a spinning disc, stirrer, and feed line. The carrier gas typically used in APS is also argon and acts as an inert carrier fluid to deliver the powder to the torch. The stirrer and disc both spin at a specified rate, generally in revolutions per minute (RPM), and the feed rate must be dialed in using a weighted method. The disc is set to a standard rate, such as 10% or 10 RPM, the carrier gas is turned on at a low nominal flow rate, and the powder is fed through the line into a pre-weighed bag for 60 seconds. The bag is then weighed again and the feed rate is determined in mass per unit time, usually in grams per minute or g/min. This method is fairly accurate and allows the user to calculate higher feed rates by extrapolating the linear relationship between disc RPM and feed rate, which assumes a scalar quantity. [22-23]

During torch operation the feed rate is set, for example if the feed rate at a disc rotation of 10% is 20 g/min (FR_{10}), at 60 g/min then the disc rate would be set at 30%. The powder is carried to the torch by the argon carrier gas through the feed line to the powder injector. The injector on an APS torch is fixed on a ring to the outer housing of the nozzle, and is normal to the plasma jet unit vector direction ($\hat{z}$), in the - $\hat{y}$ unit vector direction. This is referred to as an external injector, due to the fact that the powder is being injected externally to the torch. When the powder is fed into the plasma jet it feels a force in the $\hat{z}$ direction and forms a parabolic arc travelling both in the - $\hat{y}$ and $\hat{z}$ directions. This parabolic tendency of powder direction in the plume necessitates an optimization process in order to insure the powder assumes a straight vector in the $\hat{z}$ direction and is incident and normal to the substrate surface. [23]

1.8.1.3. INJECTION OPTIMIZATION

The process of injection optimization includes both visual and sensor inspection with in-situ plume measurement sensors such as Tecnar Accuraspray or DPV2000. The parabolic trajectory of the powder in the plume is a function of carrier gas flow rate and also some variables due to the plume velocity. If the powder stream is over-injected, being that the powder is travelling too far down into the plume, or in some cases straight through, this needs to be corrected. The stream can also be under-injected which is when the powder stream is not travelling far enough into the plume. In the F4 model there is only one single external injector so the process is somewhat simplified. Using the DPV sensor, which is a single particle sensor, a very low feed rate is used, typically anywhere from 2-5 g/min is sufficient to get a reading. The sensor measures the particle temperature, velocity, size, and relative energy. This is achieved via the emissivity of the material, and the relative intensity of the particle in a binary imaging system. The torch is set to a nominal center parameter, in the case of MCrAlY bond coating would be $I = 550$ A, $Q_P = 47.5$ SLPM, $Q_S = 6.0$ SLPM, and the carrier gas flow rate (Q_C) is varied from $1.0 \leq Q_C \leq 6.0$ SLPM. Each time the Q_C is changed a visual inspection of the plume is done via a monitor and camera system. It is extremely hazardous to look directly at the plasma because it produces ultraviolet radiation which can damage your eyes. Once the powder stream is visually in the middle of the plume this is cross referenced with the data from the DPV2000 sensor. It records ≈ 2,500 particles and produces histograms of the particle temperature, velocity, size, and relative energy. The particle temperature is especially important when using this sensor to ensure that the particles are being sufficiently melted, and in an area of highest enthalpy, being the middle of the plasma jet. [23]

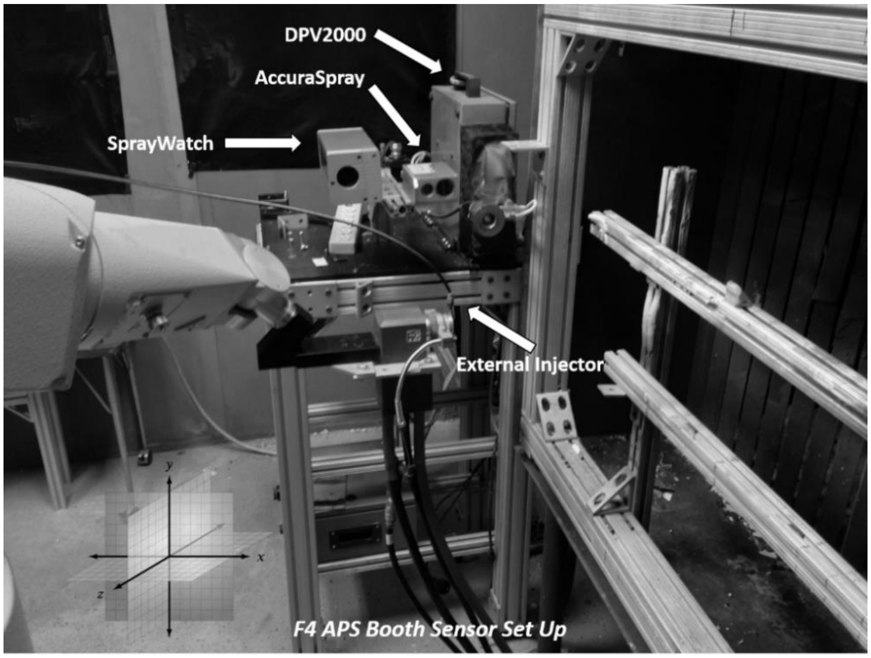

FIGURE 22: *F4 APS Booth Setup with Sensor Array and Direction Coordinates*

1.8.2. HIGH-VELOCITY OXYGEN FUEL (HVOF)

The majority of experiments performed herein were with a process called high-velocity oxy fuel (HVOF) spraying. This type of thermal spray process differs greatly from APS in many ways and is very useful when spraying metallic and intermetallic powders. It is possible to spray ceramics with certain types of HVOF torches as long as the powder particles are very fine and have a low melting point. This process takes advantage of the chemical reaction that takes place between a hydrocarbon fuel in an oxygen rich environment. This combustion reaction produces a large amount of enthalpy, especially in a fuel rich condition, which has adverse effects on the torch. There are two main types of HVOF torches being gas fuel and liquid fuel and also the type of fuel used varies. The two main types used in these experiments were two liquid fuel torches using kerosene as the hydrocarbon fuel (TAFA JP5000, Sulzer-Metco WJ410), and a hydrogen gas fuel type of torch (Sulzer-Metco DJ2600). These HVOF torches produce a very high particle velocity due to the convergent-divergent jet nozzle combustion chamber design, sometimes ≥ 1000 m/s which is very fast in terms of thermal spray. The combination of high enthalpy production and high velocity make this process ideal for spraying metallic and some cermet/carbide powders, which require a very dense coating structure. [24]

1.8.2.1. COMPLETE COMBUSTION REACTION

The combustion reaction taking place inside an HVOF torch is relatively the same as in the gas-turbine engine. The hydrocarbon fuel differs in that it is not as refined as in a gas-turbine engine which requires a cleaner burner derivative of kerosene. The liquid kerosene fuel is combined in the combustion chamber with pure oxygen, and ignited with a spark plug, or a hydrogen pilot flame is sometimes used. The complete combustion of kerosene in “air” requires at least 10 – 50% excess oxygen to combust all of the fuel. This produces an enthalpy of reaction of, ΔH^{o}_{rxn} = -7513 kJ in a stoichiometric ratio of oxygen to fuel. This ratio is exceptionally important when process engineering as this is very application specific, and which will be seen, can have a great effect on the quality of the coating. The incomplete combustion of kerosene fuel can leave large amounts of unreacted carbon, which can infiltrate and be deposited onto the coating, and also can remain in the copper barrel which is referred to as barrel loading. The HVOF torch is designed to be run on mostly oxygen rich conditions, therefor completely combusting all of the fuel with excess oxygen. [25]

1.8.2.2. HVOF TORCH DESIGN

The liquid fuel HVOF torch has a simple, yet effective, design which incorporates 5 different sections. The kerosene is atomized in the rear section of the combustion chamber, which is mixed with oxygen, and contains the spark plug for ignition. The next section is the combustion chamber where the fireball is produced and builds up pressure very fast. The end of the combustion chamber has a convergent-divergent jet nozzle design which is where the high velocity of the plume is achieved. This jet nozzle rapidly compresses the hot gases then immediately decompresses the gas and is expelled at high velocities into the next section. This compression of hot gases produces a large combustion pressure which also adds energy to the particles as they exit the combustion chamber. The liquid fuel HVOF torch (JP5000, WJ410) have an internal injection section which houses two radial injectors on both sides of a cylindrical section where the powder is injected into the jet. [25]

The last section is a copper barrel which stabilizes the plume and keeps the particles molten until they exit the barrel, referred to as the dwell time of the particles. The barrel length also has some effects on the overall particle temperature and velocity, due to the increase or decrease of particle dwell time. The plume in the liquid fuel torch tends to be long and a large cross-sectional area, giving it very good deposition area coverage, whereas a gas fuel torch (DJ2600) has a shorter and thinner plume. The barrel and combustion chamber are water cooled as with the APS process, this prevents the copper barrel and chamber from warping or melting due to the large amount of heat produced. The gas fuel torch design differs in that it has a single axial injector contained in the back of the torch, and the combustion chamber is more complex and contains small mixing vanes and not a single large chamber like the liquid fuel torches. [25-26]

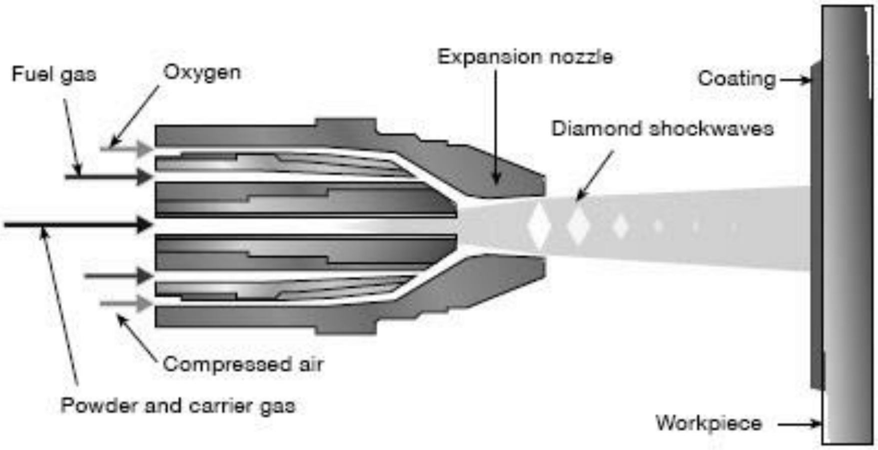

Sulzermetco.com

FIGURE 23: *Cross-sectional view of HVOF torch.*

1.8.2.3. AIR/FUEL RATIO

The most important processing parameter to consider when making an MCrAlY bond coating with HVOF is the air/fuel ratio. This is defined as the mass of air, or oxygen in this case, to the mass of fuel being used, $A/F = m_{air}/m_{fuel}$ and can be converted into flow rates when the stoichiometric flow is known, and assumes a scalar quantity. This scalar quantity turns out to be 1:275 fuel to oxygen, for every standard cubic foot per hour (SCFH) of fuel used, 275 SCFH of oxygen is required to combust all the hydrocarbon fuel. This is a linear relationship and can be scaled up depending on the amount of fuel desired. If a fuel flow rate of 5.0 gallons per hour (GPH) is required then the oxygen flow rate would be 5.0*275 = 1375 SCFH. This is a stoichiometric ratio, being an A/F = 1.0, and serves as the bench mark for calculating other ratios. This relationship can be used to analyze other conditions for the A/F used, such as if a parameter used was F = 4.8 GPH and Air = 2000 SCFH, the stoichiometric ratio would be 4.8*275 = 1320 which can be divided by the new flow rate 1320/2000 and take the inverse to acquire the air/fuel ratio which would be A/F = 1.515. The typical range for a liquid fuel HVOF torch is $0.85 \leq A/F \leq 1.5$

where most parameters are stoichiometric or higher. The liquid fuel torch is not designed to run very fuel rich conditions, having an A/F < 1.0 which presents many problems with overheating and barrel loading. [26]

1.8.2.4. GAS FUEL vs. LIQUID FUEL

The two major types of HVOF torches consist of either gas-fuel (GF) type or liquid-fuel (LF) type and can vary in many respects. Both the TAFA JP5000 and Sulzer-Metco WJ410 are liquid-fuel torches and use liquid hydrocarbon fuels such as kerosene. The Sulzer-Metco DJ2600 is a gas-fuel torch and uses hydrogen gas as the fuel. The main advantages/disadvantages between choosing either a GF or LF torch is entirely application dependent, and also a cost-benefit analysis (CBA) can be done, which is a systematic approach to estimating the strengths and weaknesses of alternatives that satisfy functional requirements, such as the type of hydrocarbon fuel used. The specific energy/energy density of many types of hydrocarbon fuels are compared to the price per unit volume of fuel and then ranked 1-6 depending on which fuel has the best price/unit volume or price/unit energy: [26]

Fuel	***Specific Energy (MJ/kg)***	***Energy Density (MJ/L)***	***Price ($/L)***	***Price/GJ ($/GJ)***	***Rank ($/L) vs. ($/GJ)***
Hydrogen (H_2)	141.80	5.60	1.22	0.91	**4/1**
Methane (CH_4)	55.50	9.25	0.58	1.07	**1/2**
Propene (C_3H_6)	45.80	19.02	0.67/lb	31.90	**2/3**
Propane (C_3H_8)	50.35	26.00	0.79	35.90	**3/5**
Butane (C_4H_{10})	49.50	28.30	4.0/kg	80.80	**6/6**
Kerosene ($C_{12}H_{26}$)	46.20	35.10	1.62	33.15	**5/4**

TABLE 1: *Cost-benefit Analysis of HVOF Hydrocarbon Fuels*

It can be seen that methane (CH_4) has the best \$/L and \$/GJ of energy which would be an optimal choice when considering which type of gas-fuel to use. The methane can be stored as compressed natural gas (CNG) in a large tank as well as liquid oxygen, which is commonly seen in manufacturing settings. The majority of DJ2600 torches are run on hydrogen gas, though it is more expensive it does not contain any elemental carbon which can make a finer coating with no carbon deposits, and also no barrel loading that is seen in liquid-fuel torches using carbon heavy fuels like kerosene. [26]

1.8.2.5. RADIAL/AXIAL POWDER INJECTION

Both the JP5000 and WJ410 style liquid-fuel torches use a different powder injection design, where the powder is injected radially from either side in a cylindrical section directly after the jet nozzle. This poses a problem with the powder streams either being over injected or under injected, which can cause stream over-lap or weak stream injection which can erode the barrel over time. The reason for such a powder injection design is due to the rear fuel injection system which connects directly to the combustion chamber, not allowing an internal axial injection system. The powder stream must be optimized in order to allow for maximum deposition efficiency and heat transfer to the powder within the jet, this also effects coating consistency and adhesive/cohesive bonding. The DJ2600 gas-fuel torch uses an internal axial powder injection system which is a single injector located in the rear housing of the torch. This is a much better design as powder injection optimization is only a function of carrier gas flow rate through one injector. This is possible due to the combustion chamber being housed around the injection section and comprised of smaller combustion cylinders and not a single large combustion chamber that is seen with the liquid-fuel torches. [26]

1.8.2.6. INJECTION OPTIMIZATION

The process of powder injection optimization for HVOF torches is similar to that in APS except for the fact that the powder injection takes place internally instead of externally with respect to the torch. This is typically done by using the Tecnar Accuraspray sensor and turning the torch $^{o}90$ around the $\hat{x}$ axis so that both radial injectors are now normal to the plane of the sensor. Two powder feed lines are connected separately to each injector and connected to a twin feeder system and N_2 carrier gas is fed through both lines, to keep any hot combustion gases from exiting the injector fittings. Typically a low feed rate of approximately 10 g/min is used during this process to minimize waste of powder. The left hand side injector which is now at the bottom is used while the right hand side injector, now being at the top has no powder feed. The carrier gas flow rate (Q_C), which in HVOF torches is nitrogen, is set to a nominal value and varied by steps of either 2-4 SCFH in a range of +/- 10 SCFH to get enough data points for a good trend. [27]

The powder is fed to the bottom injector and data is acquired through the Accuraspray sensor typically for 10 seconds, being that the sensor takes one reading every second. The powder stream is also visually inspected to check for signs of over/under injection which is sometimes subjective but is used in conjunction with the data from the sensor. The mean plume intensity readings are analyzed for every change in Q_C and plotted in an x-y scatter format. A trend-line is then applied to check for the global maxima and corresponding Q_C and is then determined as the optimal Q_C for the specific powder injection. This is done when a new type of powder is used in the torch, which depending on the density and morphology, can vary the Q_C greatly. If it is suspected that there exists secondary peaks in the trend, then the range of Q_C is varied in increments of 1 SCFH to get finer structure to the trend. The global maxima of the trend-line will tell you the greatest mean plume intensity captured by the sensor. This value corresponds to the Q_C which delivers the powder stream into the center of the plume. This is very important as you want maximum heat transfer to the powder when injected to allow for complete melting of the particles. [28]

If the powder is under-injected, visually the stream can be seen riding the barrel wall and only exiting in a straight line from the left hand side or bottom side of the barrel. If the powder stream is over-injected, visually the stream will be crossing the center of the plume into the right hand side of the barrel which would be the top. Typically this is only done with radial injection style torches whereas with the DJ2600 torch, having internal axial injection system a nominal flow rate is used depending on the powder density and morphology. This value is typically 28.5 SCFH and does not vary much depending on the powder, which was optimized by Sulzer-Metco when they designed the torch, making it much easier to switch powder and not have to use a lengthy complicated powder injection optimization process. [29]

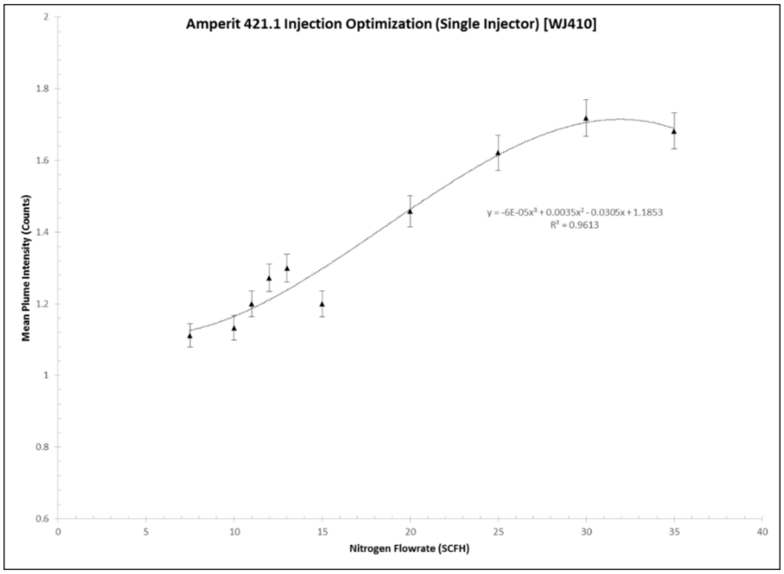

FIGURE 24: *Injection Optimization Trend with Maximum Intensity at 30 SCFH* Q_C

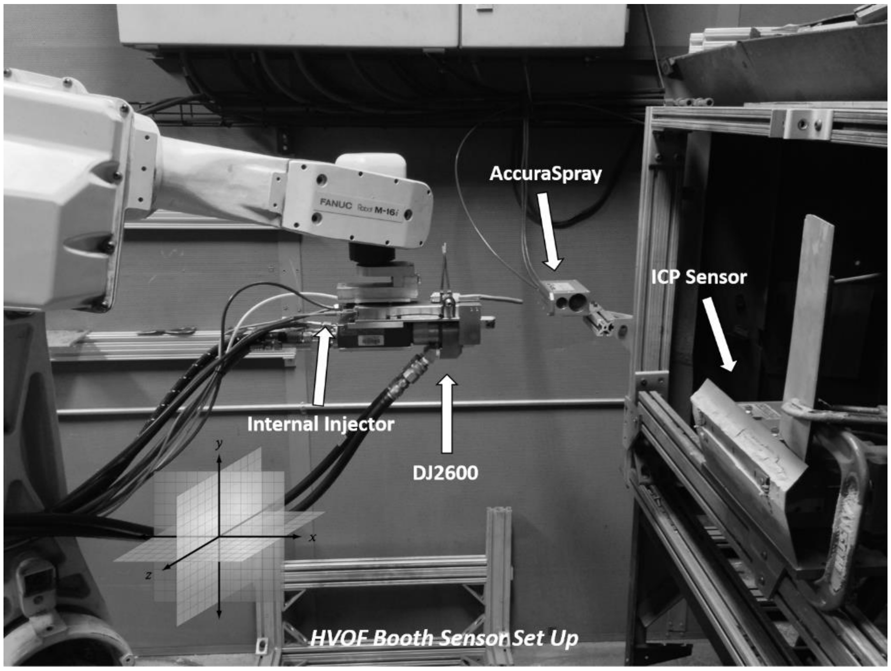

FIGURE 25: *HVOF Booth Setup with Sensor Array and Direction Coordinates*

1.8.3. LOW-PRESSURE PLASMA SPRAY (LPPS)

The last type of processing used in these experiments is called low-pressure plasma spray (LPPS) which is a vacuum deposition process and has many advantages over APS processing, especially when it comes to bond coatings. This process is similar to other vacuum depositon processes in that it takes place inside a vacuum chamber in an evacuated environment. LPPS is a low-velocity and high temperature process, similar to APS but inside a vacuum chamber. This process can produce very dense coatings with high surface roughness which is optimal when spraying MCrAlY bond coatings. The torch is mounted horizontally inside the chamber and the vacuum chamber is then pumped down to a vacuum level (VL) of approximately 13 – 93 Pa, or 0.00189 – 0.0135 PSIG, which is termed as a medium vacuum level. The chamber is then filled with argon gas to act as an inert medium atmosphere, and typically heated to 120 ^oC to avoid any thermal shock reactions. [30]

The plasma is created with a DC electrical field in the range of 50 – 60 V and a power of 1 – 500 W, which would produce a current of 8.5 – 50 Amps. The plasma produced in an LPPS system is much larger than with APS and can be up to ten times larger, which produces a large amount of enthalpy and maximum heat transfer to the powder particles. The volatile plasma byproducts are pumped out by the vacuum pump so they will not affect the coating. This process is ideal for spraying MCrAlY coatings as there is an oxygen devoid environment and produces no unwanted oxides during processing. The coating is very dense and also has a high surface roughness, which may need to be finished or ground post processing to achieve the optimal surface roughness. The high intial cost of the LPPS system is a drawback, where an entire turn-key LPPS system can cost in excess of $100,000. The LPPS coatings used in these experiments were sprayed by Mitsubishi Heavy Industries and then analyzed in the laboratory. [30]

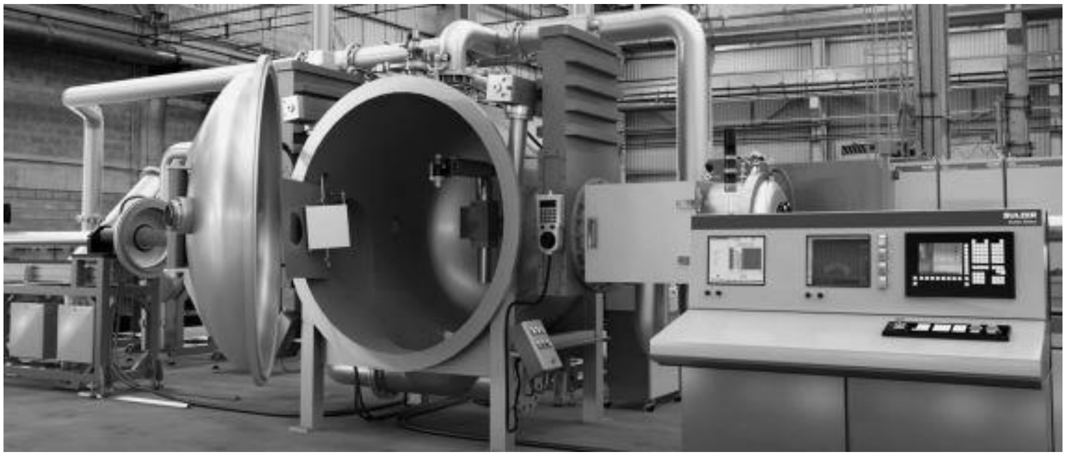

Sulzer.com

FIGURE 26: *Sulzer-Metco LPPS System with Vacuum Chamber*

1.9. PARTICLE SIZE CHARACTERIZATION

One of the most important aspects of thermal spraying powders is determining the mean particle size, or particle size range, which can be done with a particle size analyzer. The mean particle size is important due to the nature of how the powder is fed into the torch, taking accurate sensor measurements, overall surface roughness of the coating, and also how well the particles are melting inside the plume deemed the melting index of the powder. The powders can either fine or coarse, where a fine "HVOF Cut" powder is typically anywhere from $22 \leq D \leq 45$ μm and a coarser "Plasma Cut" powder can be anywhere from $80 \leq D \leq 150$ μm particle diameter. The more fine particles in the powder will lower the melting temperature, requiring less enthalpy of melting, and can achieve complete melting at a lower temperature. A coarser powder has more mass, and requires greater enthalpy of melting, and can cause only partial melting of the particles, which may or may not be favorable depending on the coating application. The most accurate way of determining the D_{50} or mean particle size of the powder is to use a particle size analyzer. [31]

The most common instrument used for particle size analysis is a Beckman-Coulter laser diffraction particle size analyzer (PSA). This instrument is complicated and works off a principle called Mie theory of light scattering using laser diffraction. It can produce particle size in differential volume, number, and surface area in one measurement, and has a sizing range from $1.7\text{E-}9 \leq D_{50} \leq 2.0\text{E-}3$ m, which is a very broad range making it a very accurate and versatile instrument. The laser diffraction technique utilized by this instrument, also known as static light scattering, depends on many parameters such as sample dispersion, using a large detector array to capture the maximum amount of scattered light, and also is the sample is aqueous or non-aqueous. The laser diffraction technique correlates the pattern or scattered light which is measured most commonly as the intensity at different angles, to the particle size distribution of the particles. The particle size is calculated by using differential volumes of the particles to a calibrated known sample and is cross-referenced with the laser diffraction data to make a very accurate measurement. [31]

1.10. IN-SITU SPRAY DIAGNOSTICS

In order to properly process a thermal spray coating the in-situ mean particle temperature and velocity need to be measured, using various plume sensors, as well as single particle sensors. These in-situ plume diagnostic sensors mainly work of the principle of emmisivity of materials in order to measure the temperature, in terms of particle intensity. Metals in general have a low emmisivity, in the case of HVOF sprayed bond coatings, a low-emmision sensor head must be applied in order to acquire a signal from the material. Whereas in the case of APS sprayed ceramics, which have a high emmisivity, employ a high-emmision sensor head. These measurements are most commonly performed using a low powder feed rate, such as 10 g/min for metals, and 4 g/min for ceramics, so as not to waste powder. In the case when a plume diagnostic measurement is to be taken before making a coating, the measurements are taken at the full feed rate. It is important to first measure the single particle temperature, velocity, and diameter, in the molten state, in order to fully understand the melting index and how dense the coating will be, where a higher velocity will produce a denser coating. The entire plume can be measured at the full feed rate in order to understand how well the particles are melting and also how much a higher feed rate will tend to quench the plume by consuming too much enthalpy. Generally plume diagnostics are taken for a range of processing parameters to build first order process maps and get an idea of the T-v space for a material. [32]

1.10.1. PARTICLE DWELL TIME

The molten state of the particles measured by the in-situ plume sensors is largely a function of particle dwell time. This is defined as the time the particle resides inside of the plume, whether before or after exiting the barrel, in the case of HVOF which has a much longer plume than in the case of APS torches. This long plume is produced by the large jet flame that exits the combustion chamber at high velocities. When the particles are injected after the combustion chamber they are melted inside the jet flame and are carried by the plume mixing with other molten particles before exiting the plume where they will travel through air and are incident onto the substrate surface. This dwell time is important as a longer time inside the plume will increase the melting of the material and also give it extra kinetic energy. In the case of HVOF processing the barrel length adds to this effect by containing the plume for a longer time inside a longer barrel whereby it increases the particle melting and a small increase in kinetic energy. Where bond coating powders are concerned this is important because it can cause overheating of the material and raising the exit temperature into the next stage which is the particle flight time. [32]

1.10.2. PARTICLE FLIGHT TIME

The amount of time the molten particles travel through the environment, after exiting the plume is termed as the particle flight time. This can be controlled to some extent by the barrel length in HVOF torches, but mainly by choosing an appropriate spray distance. It has been shown that the longer amount of particle flight time, caused by a large spray distance, increases the temperature of the particles, demonstrated by an increase in particle intensity as seen by the in-situ sensors, in terms of MCrAlY powders. This can be seen as pre-oxidation of the particles as the redox reaction is exothermic, releasing energy after the reaction which is displayed as an increased particle temperature. This necessitates a minimization of particle flight time in order to mitigate and reduce the amount of pre-oxidation of the powder. The particle flight time can also affect the density of the coating where an increase in particle flight time reduces the kinetic energy of the particles and can reduce the melting index of the material. A decrease in particle flight time can effectively increase the melting index and kinetic energy of the particles that are incident onto the substrate surface, increasing the coating density. The melting index of the material is process dependent and is defined as the ratio of the particle melting temperature (T_m), particle flight time, particle velocity (v), spray distance (L), and diameter of the particles (D) where: [32-33]

$$\mathbf{MI(\%)} = \frac{(\boldsymbol{T}-\boldsymbol{T_m})\Delta \boldsymbol{t_{fly}}}{\boldsymbol{D^2}} \; ; \; \Delta \boldsymbol{t_{fly}} = \frac{\mathbf{2}\boldsymbol{L}}{\boldsymbol{v}}$$

1.10.3. SPRAY DISTANCE

An important control factor in processing thermal spray coatings is choosing a proper spray distance that will achieve optimal coating properties. This must meet the following requirements:

Melting Index

Wettability

Density

Porosity

Residual Stress

Evolving Stress

Surface Roughness

Pre-Oxidation of Powder

This is the first line of defense for achieving optimal process-property relations when spraying a new type of coating. Typically when spraying an MCrAlY bond coating a small spray distance is favorable as this decreases particle flight time, increases melting index and kinetic energy, increases density, and also produces a nominal surface roughness. The caveat to a small spray distance is it is inversely proportional to residual stress in the coating, also the increase in kinetic energy (KE) causes the semi-molten particles to harden the substrate surface through the shot peening effect, which can either be beneficial or detrimental depending on the coating thickness and application. The shot peening effect is mainly seen in very dense and hard materials such as tungsten carbide, WC (CoCr) and chrome carbide, CrC (NiCr) which are used for damage tolerant coatings. The MCrAlY powders have a lower peening effect, being not as dense and having a lower melting temperature, which can be neglected for the most part when choosing a spray distance. The nominal spray distance used for processing bond coatings is generally 8” ≤ L ≤ 12” inches, which is also process and torch dependent, where in these experiments were sprayed at a distance of 12” for HVOF and 100 mm for APS. [33]

1.10.4. TORCH RASTER SPEED

The speed at which the torch travels with respect to the substrate surface is the torch raster speed and is controlled by a robot which manipulates the torch during spraying. This aspect of thermal spraying is very important as the raster speed affects many properties of the coating. It has been shown that torch raster speed is proportional to coating deposition efficiency, as well as spray angle. The slower the torch rasters over the surface of the substrate the more powder that is being deposited, increasing the efficiency of deposition. This can also affect the residual stress and localized heating of the substrate which can have negative effects on the coating properties. [33]

In the case of HVOF the particles are moving at very high velocities (≥ 800 m/s) so a high raster speed is needed, generally 1000 mm/s, to ensure consistency and density of the coating, as well as prevent overheating and warping of the substrate, which can also be caused by the large amount of force felt by the high velocity particles. It has also been shown that raster speed has an effect on the evolving stress of the coating, which can be related to the higher deposition efficiency and greater thickness/pass of the coating. A raster speed of 750 mm/s has been seen to reduce evolving stress of the coating while increasing surface roughness and slightly decrease the temperature. [34]

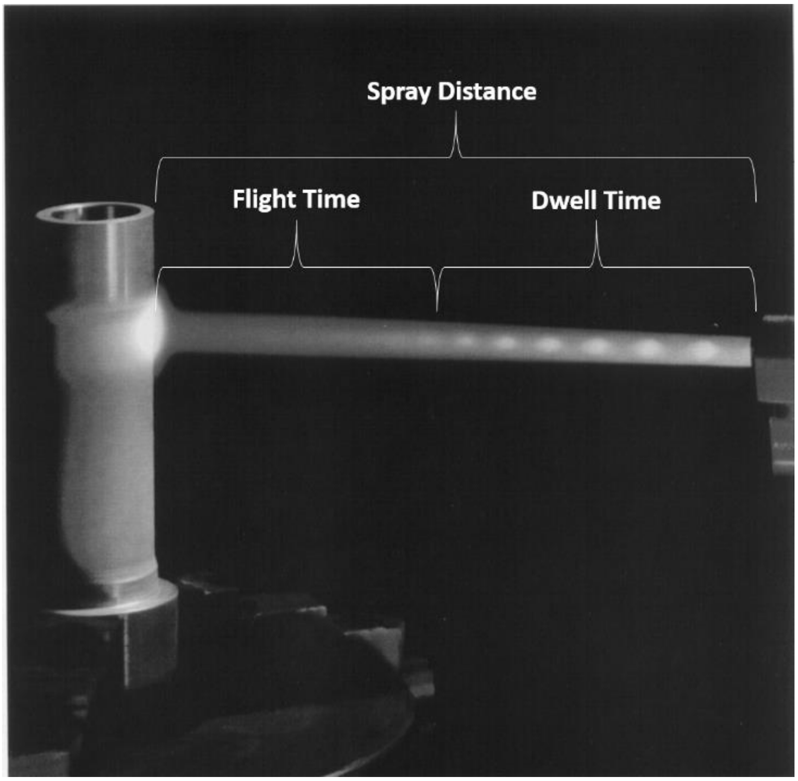

FIGURE 27: *Schematic of Particle Flight and Dwell Time*

1.10.5. 1ST ORDER PROCESS MAPS

The generation of so called first order process maps is done largely using the in-situ plume diagnostic sensors. These can be made using the data output from the Accuraspray sensor by taking the mean values for particle temperature and velocity as well as the standard deviation for both, in order to understand the variance in the data. After the mean values are calculated they can be plotted in an x-y scatter format where mean particle velocity on the x-axis and mean particle temperature on the y-axis. This will produce a first order process map wherein many different parameters and also different processes can be compared depending on their location and grouping in the T-v space of the map. This can be done for any type of material and in the case of bond coatings it is very useful in order to understand whether or not a parameter is too energetic causing the particles to oxidize during particle flight, in an oxygen containing medium. If there is a visible increase in particle temperature when the spray distance is moved farther away, indicating longer particle flight time, can be seen as evidence of pre-oxidation of the particles. [35]

The processing parameters take into account spray distance, raster speed, A/F ratios, Q_C, Q_P, Q_S, Current, Barrel Length, Spray Angle, and Substrate material. All of these variables can be varied, and in the case of designing an experiment, are considered the control variables, and all have an effect on the T,v space. Processes and parameters that exists in the top left corner of the process map are deemed high MI, low KE conditions, in the middle of the space are the central conditions, which are also reference points, and on the bottom right corner are the low MI, high KE conditions. The Accuraspray sensor tends to have large error when calculating the mean particle temperature due to the nature of the sensor and the emissivity of the material, as well as bright spots on the camera. [35]

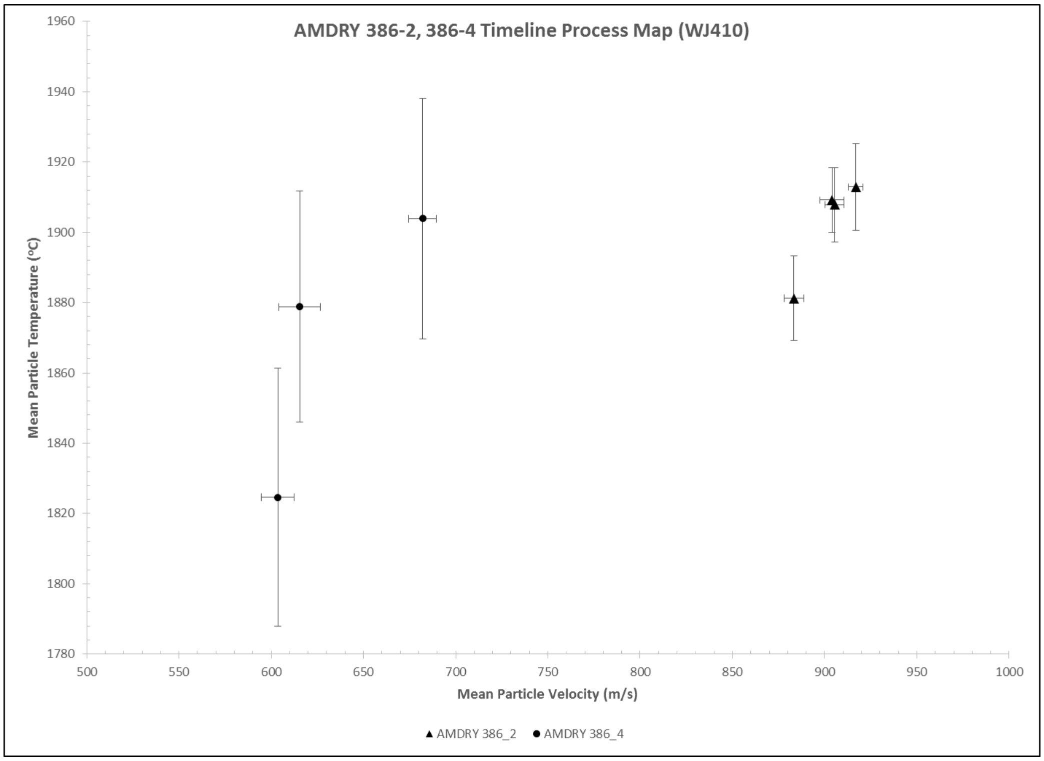

FIGURE 28: *Example of Process Map with Large Temperature Error*

1.11. STRESS-STATE MEASUREMENT

In order to understand the state of the as sprayed coating, stress-state measurements must be made using in-situ sensors. This is typically done with what is known as an In-situ Curvature Property sensor (ICP) which measures the levels of stress between the coating and substrate as the powder is being deposited. This sensor works on the property of bi-layer curvature, when a thin film coating is deposited onto a beam and then slowly cooled, the coating and beam tend to go either into tension or compression and bend the beam to relieve stress. This stress relieving bending of the coating and beam can be measured by the sensor with the use of 3 lasers incident onto the back of the beam. [36]

These 3 lasers measure a displacement in distance between the laser aperture and the beam when it is reflected back to the sensor. If the beam has the tendency to bend inward, reducing the displacement measured, the coating is said to be in tension, as the system cools the coating pulls on the substrate surface bending the beam inward. If the reverse is seen, where the beam has the tendency to bend outward with respect to the sensor, the coating is said to be in compression, analogous to gripping down on the substrate surface and bending it outward. The 3 laser displacements that are measured can be seen as an overall curvature of the beam from a set position and are in the units of m^{-1} as well as measuring the beam temperature during spraying through the use of two contact thermocouples. The overall coating thickness is important because this can have a great effect on the residual stress in the coating, as well as the quenching stress during cooling. [36]

The curvature, thickness, and temperature data from the ICP sensor can then be used to calculate both the evolving stress of deposition, $\frac{dk}{dt}$, being the stress build up after each pass of deposition, and the quenching stress/residual stress in the coating. This is done through the use of the Brenner-Senderoff formula for thin film coatings, as well as the Stoney formula which does not take the elastic modulus of the coating into account:

Brenner-Senderoff Formula

$$\sigma_q = \frac{E'_S t_S (t_S + \beta^{5/4} \Delta t_D)}{6 \Delta R \Delta t_D}; \;\; \beta = \frac{E'_D}{E'_S}$$

Stoney Formula

$$\sigma_q = \frac{E'_S t_S^2}{6 \Delta R \Delta t_D}$$

Where, E'_S = Effective Substrate Modulus, E'_D = Effective Coating Modulus, t_S = Substrate Thickness, Δt_D = Deposited Coating Thickness, ΔR = Change in Radius of Curvature of Beam due to Quenching Stress. The residual stress in the coating after deposition will have a great effect on the interfacial adhesion strength, which is an important property of an MCrAlY bond coating, affecting the thermal cycle life of the TBC. [36]

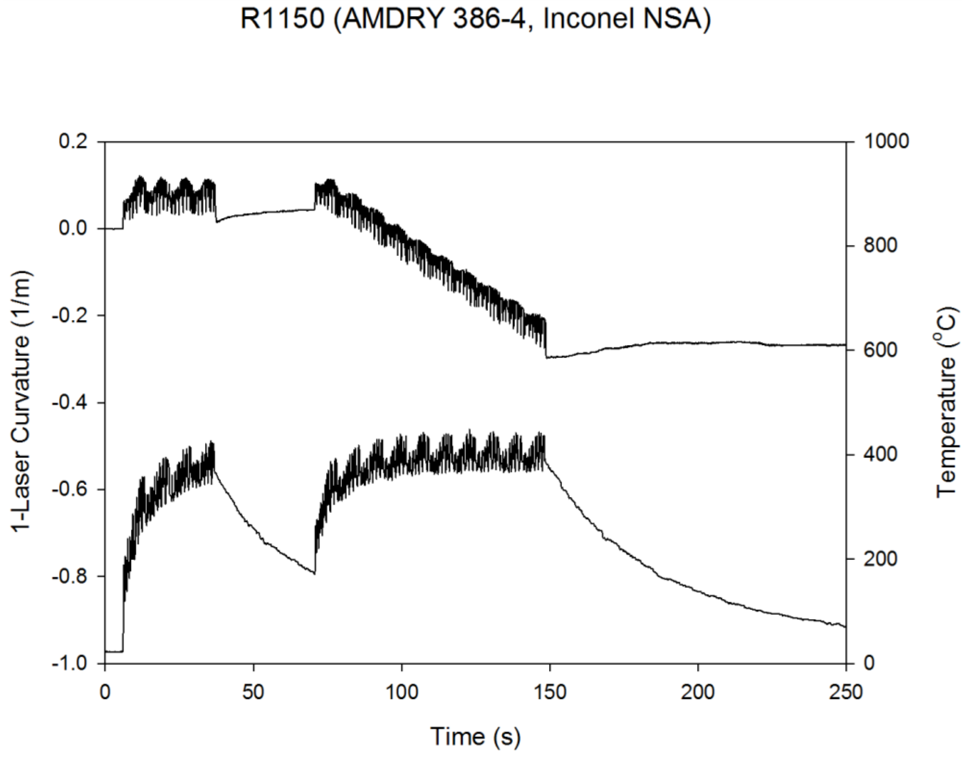

FIGURE 29: *Example of ICP Data Output with Beam Curvature and Temperature*

1.12. MICROSTRUCTURAL ANALYSIS

After the bond coating is sprayed onto the ICP beam is can then be analyzed through metallographic and microscopy methods. The beam is cut using a low-speed diamond saw in order to preserve the interface of the coating and the substrate, which is of importance. After the beam is cut into approximately 10.5 x 3.0 x 25.75 mm coupons it can then be de-burred and set into a mold which is filled with epoxy and hardened over a 24 hour period. The sample can now be polished with an automatic polishing machine and differing grit SiC paper in order to be able to image the coating-substrate interface, typically with an optical microscope. After the interface has been imaged at magnifications of 50X and 100X the sample can then be imaged with a scanning electron microscope (SEM) if a much larger magnification is needed, depending on how small the feature size is in the coating. This interfacial cross-section shows the microstructure of the as-sprayed coating which resembles a brick and mortar structure, being the molten splats, which resemble lamella, that overlap and cool on the substrate surface forming the coating. This method is important in terms of MCrAlY coatings and can aid in visual inspection of many variables such as porosity, density of coating, inclusions, voids, inter-lamellar oxide growth, foreign particles, interface between bond coating and substrate, and to some extent the surface roughness or morphology. [37-38]

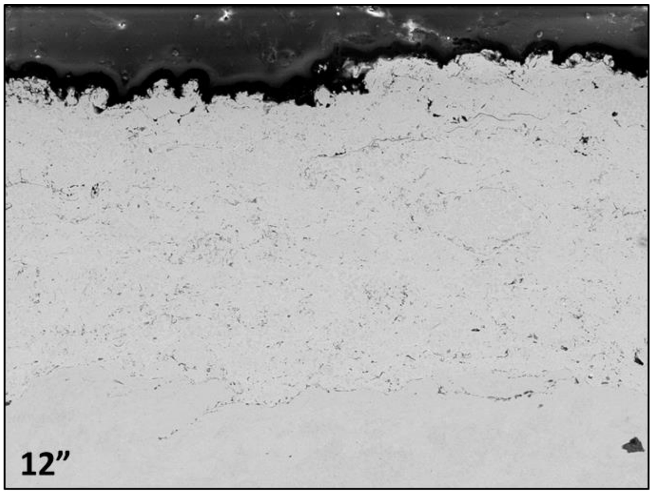

FIGURE 30: *Nominal HVOF Sprayed MCrAlY Microstructure*

1.13. ADHESION TESTING (ASTM C633-13)

The culmination of the process engineering of MCrAlY coatings is with a standard process of bond testing the coatings to analyze the adhesion/cohesion strength. The standard is created by ASTM International and its designation is C633-13 which is titled “Standard Test Method for Adhesion or Cohesion Strength of Thermal Spray Coatings”. This process involves manufacturing a set-up that can be used in conjuction with a tensile testing machine such as an Instron tester. The apparatus consists of coupons or slugs which are to be sprayed, along with threaded couplings which are pinned into the jaws of the tensile testing machine, a schematic of the apparatus can be seen below: [39]

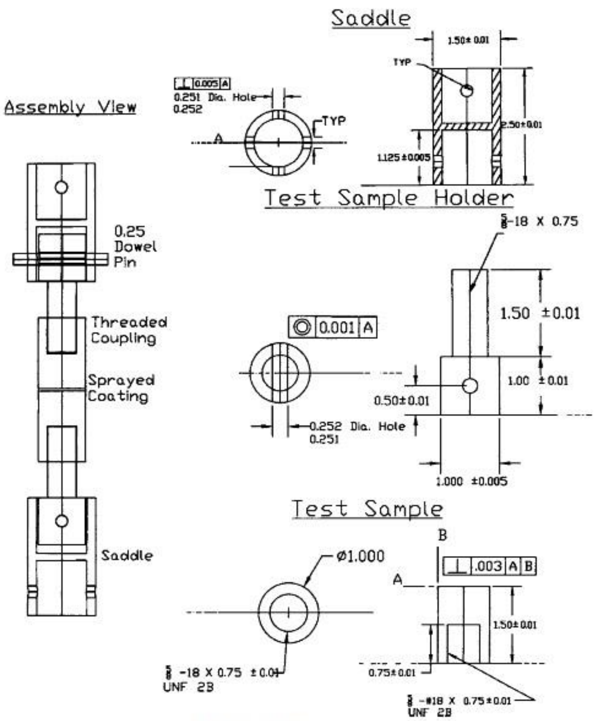

Metric Equivalents

in.	3⁄16	1⁄4	3⁄4	1	1 1⁄8	1 7⁄16	1 1⁄2	2 1⁄2
(*mm*)	(4.8)	(6.4)	(19)	(25.4)	(29)	(37)	(38)	(64)

ASTM International, C633-13

FIGURE 31: *Schematic of ASTM C633-13 Testing Apparatus*

The test samples consist of low-carbon, 1020 steel and are first grit blasted to roughen the surface, the coating is then applied on top of the test sample in the standard procedure. Another blank test sample is also grit blasted and used as the top fixture of the assembly. The two samples are then fixed together using a high-strength thermoset polymer epoxy, such as FM-1000 or MasterBond EP15, which the latter was used during these experiments. The samples are set into a fixture and 150 grams of weight is placed on top of the samples to ensure they stay concentric and the epoxy bonds only to the test samples. The samples are then placed inside a low-temperature furnace at a temperature of 300 – 350 ^{o}F for a period of 60 – 90 minutes. The samples are then taken out of the furnace and are ready to be tested, but must also be inspected to ensure the epoxy set properly while being cured. The testing sample is threaded onto the apparatus which is attached to the tensile testing machine. A constant cross head travel, or strain rate, of 0.013 – 0.021 mm/s is applied to the fixture until the coating fails under the load. This produces a graph of extension of the cylinder vs. applied load in kN and an example can be seen below: [39]

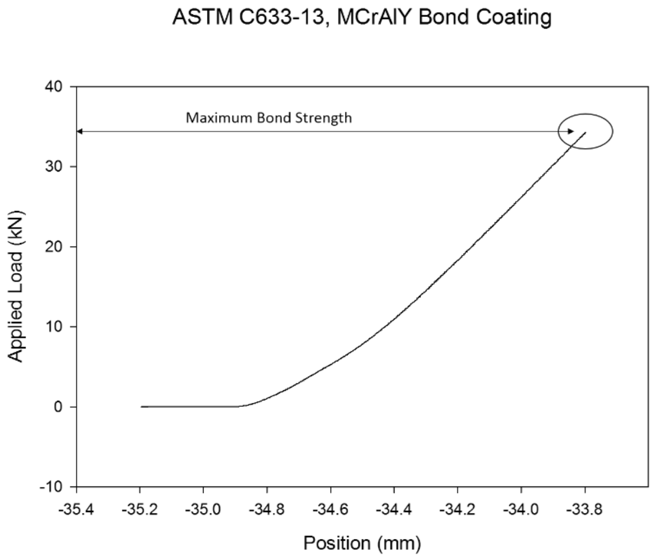

FIGURE 32: *Typical Bond Testing Load vs. Position Data*

The maximum applied load is a force with the units of kN, which can be converted into units of stress or MPa, by dividing the load by the cross-sectional area of the specimen, to obtain the bond strength of the coating. The failure mechanism of the coating can be either adhesive or cohesive, or many combinations of the two depending on where the failure occurred. The most common location for MCrAlY failure is adhesive at the coating/substrate interface, although it will be shown that this mechanism can change when the powder is sprayed with APS, specifically with the Sulzer-Metco Sinplex torch, a diagram of the various failure locations is seen below: [39-40]

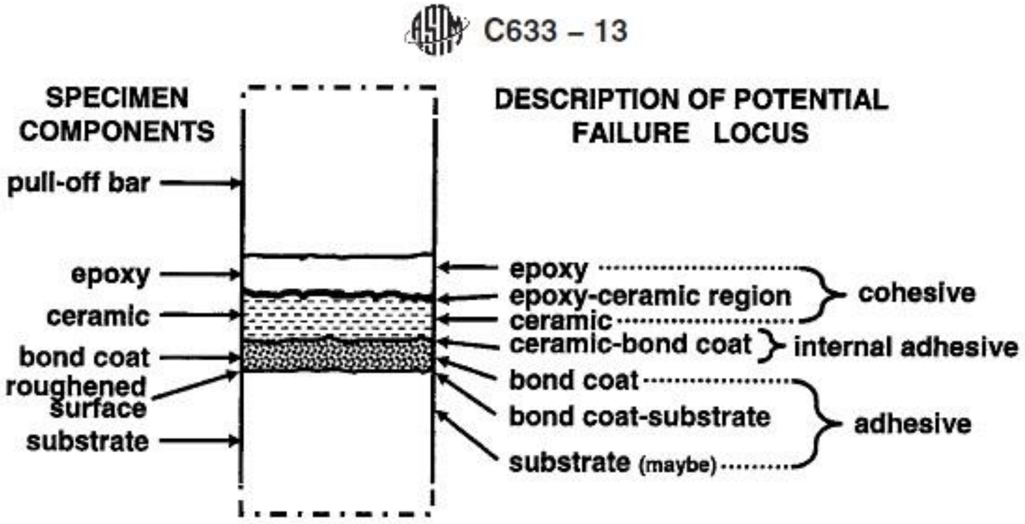

ASTM International, C633-13

FIGURE 33: *Potential Failure Loci in Bond Testing Experiment*

1.14. THERMAL CYCLING AND TGO GROWTH

In order to understand how specific processing parameters are affecting the oxidation kinetics of the bond coating, the as-sprayed coatings have to be furnace cycled in order to see how the TGO layer grows. This is an effective tool in understanding how changing the processing of the coating will either accelerate or hinder the TGO layer growth with the latter being preferable to the former. The unsprayed powder is also furnace cycled in order to understand how the pure MCrAlY chemistry grows the TGO and use this as a reference to our as-sprayed bond coatings. This process is fairly simple as the powder and/or bond coated samples are placed inside a high-temperature furnace which is ≈ 1,100 ^{o}C and kept in this isothermal environment for typically 24 hours and then taken out. As the TGO growth is a thermally activated process this is the most effective way or measuring this property without the use of highly sophisticated and expensive instruments. The bond coatings and powder can be cycled in a range from $1 \leq N \leq 20$, 24-hr cycles which would be in a time range of $24 \leq t_c \leq 480$ hrs inside the furnace. The bond coated samples are then cross-sectioned and analyzed under an SEM to inspect the TGO layer growth on the surface of the coating. This can be measured in an approximate manner using the SEM and a relative growth rate can be calculated depending on how many cycles the coating has gone under. A schematic of how the TGO layer grows on the interface between the bond coating and ceramic top coating after thermal cycling can be seen below: [41-43]

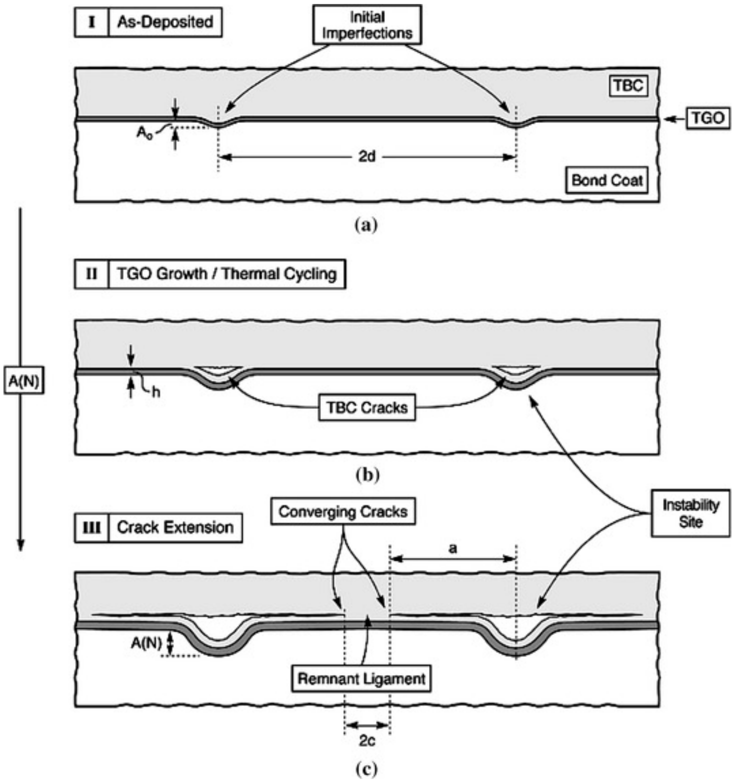

Springerimages.com

FIGURE 34: *Schematic of TGO Growth after Furnace Cycling*

2. PROBLEM STATEMENT

The need for longer engine life as well as higher hot-section inlet temperatures has created a wide field of issues related to how materials react with this high-temperature environment, especially in terms of creating new types of TBC's that can achieve these goals. These issues have led to new research being done in terms of thermal spray processing of TBC's in the areas of creating new microstructures of ceramic top coatings, as well as optimizing the processing of the metallic bond coating. It has been shown that the premature thermal cycle failure of TBC's can be attributed to incorrect processing of the bond coating, as well as insufficient process control. In order to achieve an optimal thermal cycle life for TBC's the bond coating must be optimized in terms of process engineering. This can be achieved by first understanding the process-property relationships in terms of thermal spray coatings. This step is crucial in understanding the materials science behind how the coating functions and how to engineer them to meet and/or exceed expectations. These coatings are extremely important in protecting the substrate materials in the hot-section of gas-turbine engines, without a TBC the turbine blades would lose dimensional stability and eventually melt the material. An understanding of how specific thermal spray processing of these coatings affects both the TGO growth, and in turn how this will affect the adhesion strength of the interfacial layers, is the directed focus of the proceeding experiments. Through the use of certain design of experiment (DOE) methods, the process-property relationships affecting TGO growth and adhesion strength can be ascertained and quantified, given consistent data which produce clear signal-to-noise values. This can be done by selecting crucial variables in each process, such as spray distance, raster speed, air to fuel ratio, barrel length, etc., as well as a significant number of variable levels, which can be realistically quantified and understood. The results of said experiments are listed in detail in section 4 of the document.

3. EXPERIMENTAL METHODS

3.1. DESIGN OF EXPERIMENT (D.O.E.)

The processing of thermal spray coatings has to be rigorous in order to achieve the optimal properties that are desired. This can be done using a design of experiment (DOE) method which is a statistical process designed to minimize the number of experiments having to be performed while also giving the maximum amount of combinations of variables. The taguchi method for designing experiments was used throughout the experiments performed within which was created specifically for industrial processes, like thermal spraying coatings. This method follows three specific guidelines which are: [44]

1.) *Quality must be inherent in the part and not inspected for quality afterwards*
2.) *Quality is achieved by minimization of the deviation from a target value, and should be immune to uncontrollable environmental error.*
3.) *The cost of quality should be a function of the deviation from the target value, and the losses should be measured as a system wide variable.*

This method of DOE is considered an orthogonal array type which uses said arrays to statistically vary the control parameters, variables, and levels of the variables. The specific steps that need to be taken while designing a Taguchi style DOE is firstly you have to define the target value which can be a maximum and minimum in the processing equipment. Secondly, define the design parameters that affect the process, and also the levels of these parameters or variables. The creation of orthogonal arrays is the most important step as it is dependent on the number of variables and also the number of levels. The experiments are then performed and all the data taken, and lastly a data analysis to determine the magnitude of effect that the different variables have on the performance and quality of the part, termed the signal-to-noise ratio (SN). This method has some drawbacks as it does not test every permutation and combination of the variables and control parameters as well as not taking into account the interaction between the variables. A flow diagram of the Taguchi method, an orthogonal array, and signal-to-noise ratio equations can be seen below: [44]

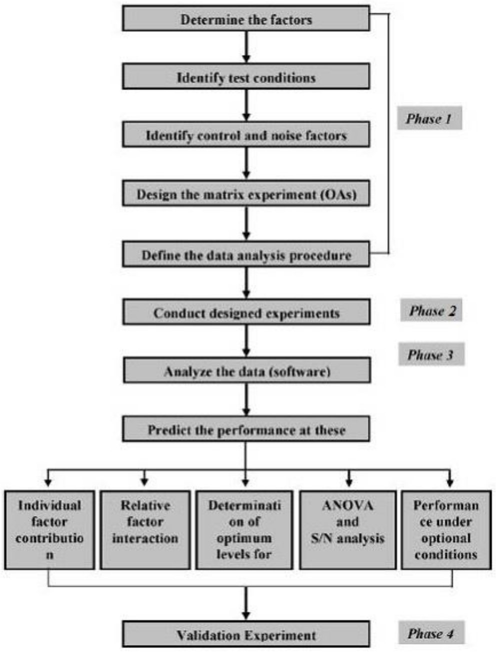

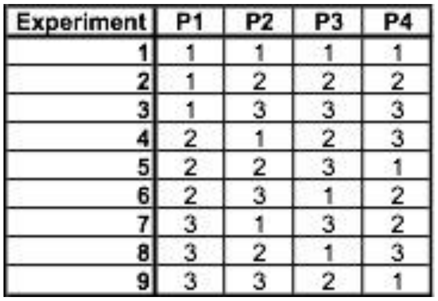

Experiment	P1	P2	P3	P4
1	1	1	1	1
2	1	2	2	2
3	1	3	3	3
4	2	1	2	3
5	2	2	3	1
6	2	3	1	2
7	3	1	3	2
8	3	2	1	3
9	3	3	2	1

$$SN_i = 10 \log \frac{\bar{y_i}^2}{{s_i}^2}$$

$$Where$$

$$\bar{y}_i = \frac{1}{N_i} \sum_{u=1}^{N_i} y_{i,u}$$

$$s_i^2 = \frac{1}{N_i - 1} \sum_{u=1}^{N_i} (y_{i,u} - \bar{y}_i)$$

$$i = Experiment\ number$$

$$u = Trial\ number$$

$$N_i = Number\ of\ trials\ for\ experiment\ i$$

Fraley et al.

FIGURES 35 – 37: *Taguchi Method Flow Chart, Orthogonal Array, SN Ratios*

3.1.1. EXPERIMENTAL PLAN

3.1.1.1. D.O.E. 1

The most important process parameters that are involved with bond coat processing, in terms of HVOF spraying are the A/F ratio, Spray distance, Torch type. and Powder type. The first combination that was tested was the use of a JP5000/WJ410 liquid-fuel torch and AMPERIT 421.1 NiCoCrAlTaHfReY powder. This DOE was performed to understand the effects of varying the barrel length, feed rate, spray distance, combustion pressure, A/F ratio, spray angle, and to a lesser extent the substrate roughness. The following DOEs were performed in succession and the resulting data was compiled using MiniTab statistical software:

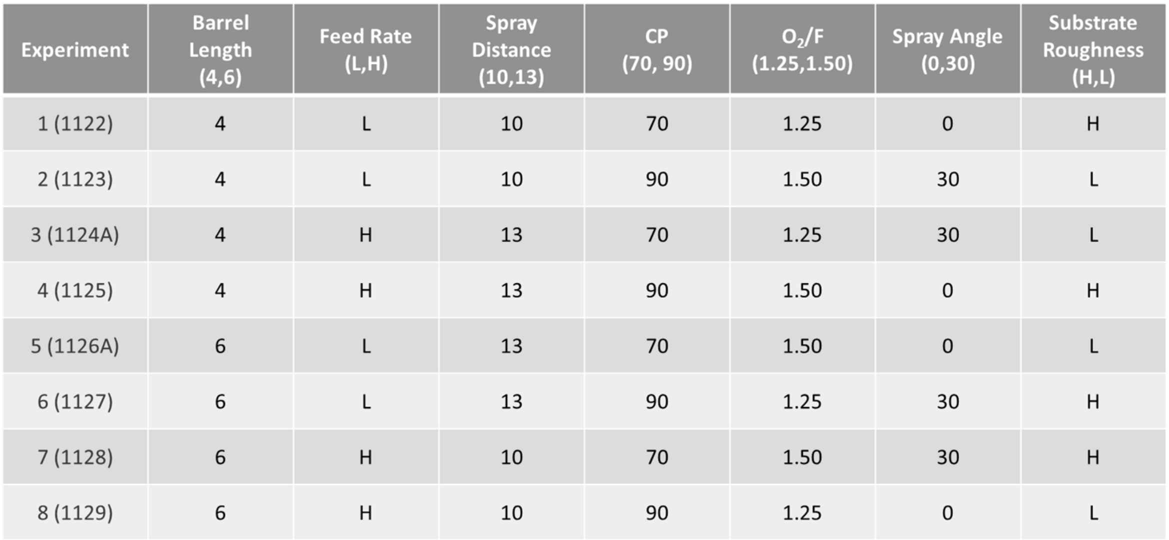

Experiment	Barrel Length (4,6)	Feed Rate (L,H)	Spray Distance (10,13)	CP (70, 90)	O_2/F (1.25,1.50)	Spray Angle (0,30)	Substrate Roughness (H,L)
1 (1122)	4	L	10	70	1.25	0	H
2 (1123)	4	L	10	90	1.50	30	L
3 (1124A)	4	H	13	70	1.25	30	L
4 (1125)	4	H	13	90	1.50	0	H
5 (1126A)	6	L	13	70	1.50	0	L
6 (1127)	6	L	13	90	1.25	30	H
7 (1128)	6	H	10	70	1.50	30	H
8 (1129)	6	H	10	90	1.25	0	L

TABLE 2: *D.O.E. 1 using AMPERIT 421.1 and WJ410, L8 Array with 7 variables and 2 levels*

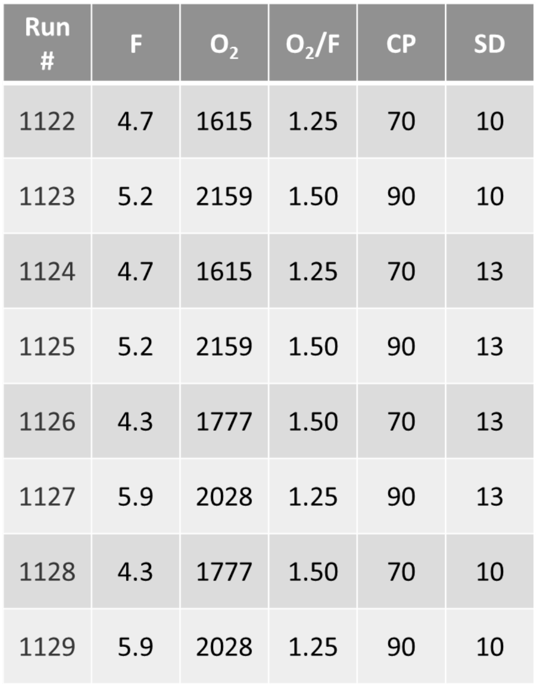

Run #	F	O_2	O_2/F	CP	SD
1122	4.7	1615	1.25	70	10
1123	5.2	2159	1.50	90	10
1124	4.7	1615	1.25	70	13
1125	5.2	2159	1.50	90	13
1126	4.3	1777	1.50	70	13
1127	5.9	2028	1.25	90	13
1128	4.3	1777	1.50	70	10
1129	5.9	2028	1.25	90	10

TABLE 3: *Processing conditions used for D.O.E. 1*

Element	Unit	Value	Lower Limit	Upper Limit
Ni	%	44.88	-	-
Cr	%	18.2	17.0	19.0
Al	%	6.73	6.25	6.75
Co	%	10.2	9.0	11.0
Ta	%	5.85	5.75	6.25
Re	%	2.1	1.8	2.2
Hf	%	0.5	0.4	0.6
Y	%	0.3	0.2	0.4
Si	%	1.0	0.8	1.2

TABLE 4: *H.C. Starck AMPERIT 421.1 Powder Chemistry*

3.1.1.2. D.O.E. 2

The purpose of this next D.O.E. was to understand the effects of barrel length, spray angle, raster speed, and A/F ratio, and a different powder chemistry. The processing combination used was with a JP5000/WJ410 liquid-fuel torch and Sulzer-Metco XPT449 pure NiCoCrAlY powder without any other reactive rare earth elements. The following data was obtained and analyzed via in-situ diagnostics and microstructural analysis:

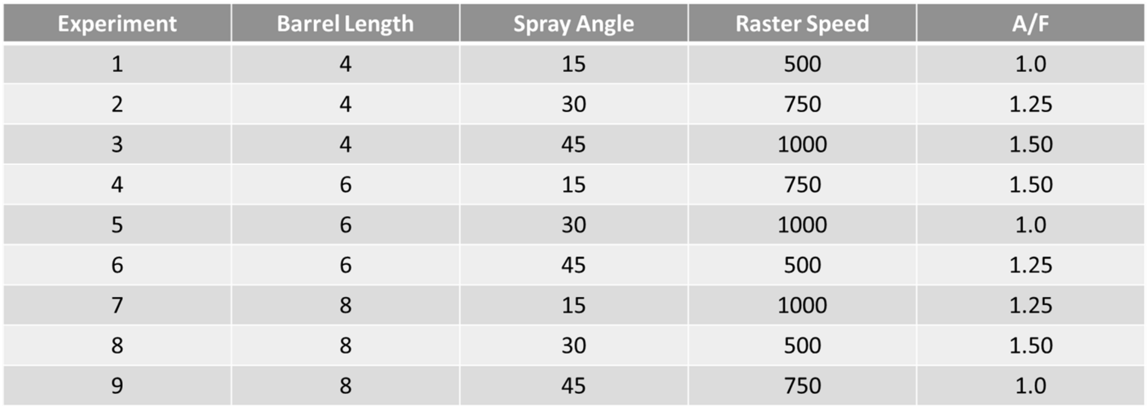

Experiment	Barrel Length	Spray Angle	Raster Speed	A/F
1	4	15	500	1.0
2	4	30	750	1.25
3	4	45	1000	1.50
4	6	15	750	1.50
5	6	30	1000	1.0
6	6	45	500	1.25
7	8	15	1000	1.25
8	8	30	500	1.50
9	8	45	750	1.0

TABLE 5: *D.O.E. 2 using XPT449 and WJ410, L9 Array with 4 variables and 3 levels*

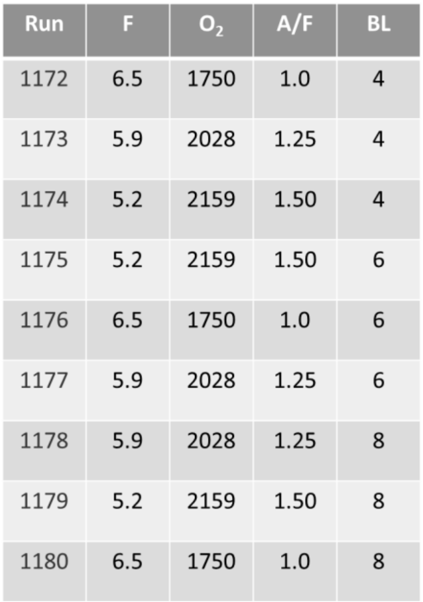

Run	F	O_2	A/F	BL
1172	6.5	1750	1.0	4
1173	5.9	2028	1.25	4
1174	5.2	2159	1.50	4
1175	5.2	2159	1.50	6
1176	6.5	1750	1.0	6
1177	5.9	2028	1.25	6
1178	5.9	2028	1.25	8
1179	5.2	2159	1.50	8
1180	6.5	1750	1.0	8

TABLE 6: *Processing conditions used for D.O.E. 2*

SULZER METCO – XPT449

**PURE NICOCRALY POWDER, EXACT CHEMISTRY UNKNOWN**

3.1.1.3. D.O.E. 3

The final D.O.E. was performed with a sulzer-metco DJ2600 gas-fuel HVOF torch using hydrogen fuel, in order to get a comparison between liquid-fuel and gas-fuel torches. The powder to be used is an advanced NiCoCrAlTaHfSiY bond coating alloy which exhibits excellent hot corrosion protection as well as improved thermal creep and toughness. The experiment matrix can be seen below as well as the powder chemistry:

Experiment	Spray Distance	Raster Speed	Spray Angle	A/F
1	8	500	0	0.75
2	8	750	30	0.9
3	8	1000	45	1.05
4	9	500	30	1.05
5	9	750	45	0.75
6	9	1000	0	0.9
7	10	500	45	0.9
8	10	750	0	1.05
9	10	1000	30	0.75

TABLE 7: *D.O.E. 3 using AMDRY 386-2 and DJ2600*

Element	Unit	Value	Lower Limit	Upper Limit
Ni	%	-	Bal.	Bal.
Co	%	-	18.0	26.0
Cr	%	-	13.0	21.0
Al	%	-	10.0	15.0
Ta	%	-	-	-
Y	%	-	0.1	1.0
Hf	%	-	0.1	1.0
Si	%	-	0.1	0.7
Other	%	-	≥5.0	≤5.0

TABLE 8: *Sulzer-Metco AMDRY 386-2, 386-4 Powder Chemistry*

3.1.1.4. ADHESION TESTING MATRIX

Sample #	*Process*	*Torch*	*A/F*	*Thickness (µm)*
1	EPOXY	N/A	N/A	N/A
2	EPOXY	N/A	N/A	N/A
3	HVOF	WJ410	1.00	450
4	HVOF	WJ410	1.00	800
5	HVOF	WJ410	1.00	1200
6	HVOF	WJ410	0.85	500
7	HVOF	WJ410	1.00	500
8	HVOF	WJ410	1.50	500
9	HVOF	DJ2600	0.85	500
10	HVOF	DJ2600	1.00	500
11	HVOF	DJ2600	1.15	500
12	HVOF	WJ410	1.00	500
13	HVOF	JP5000	1.00	500
14	HVOF	JP5000	1.50	500
15	APS	F4	N/A	650
16	APS	F4	N/A	650
17	APS	SIN	N/A	1000
18	APS	SIN	N/A	1000

All JP500/WJ410 Samples sprayed at 12 inch Spray Distance
All DJ2600 Samples sprayed at 10 inch Spray Distance
All APS Samples sprayed at 100 mm Spray Distance
HVOF Feed Rate = 70 g/min

APS Feed Rate = 60 g/min
F4 Conditions: I = 350 A, PG = 35.5, SG = 2.0, CG = 1.5
Sinplex Conditions: I = 300 A, PG = 35.5, SG = 2.0, CG 1.5
3 Samples/Experiment
54 Samples Total

4. RESULTS AND DISCUSSION

The following results were obtained from the design of experiment method used to analyze the main effects and signal-to-noise ratio (SN #) obtained from the output of the various experiments. The SN #'s display the sensitivity the process has to changing certain variables, as well as which variables have the greatest effect on a certain output parameter. The output parameters that were measured using in-situ diagnostic sensors include mean particle velocity and temperature of the plume. This output is used to create the first order process maps which can be seen in the following figures. The stress-state measurements that were measured using an ICP sensor can be seen plotted with time vs. beam curvature and substrate temperature. Lastly the microstructure can be seen in the cross-sectioned images taken with an optical microscope, where the main analysis is done with visual inspection. These techniques can lead to an analysis of the output parameters and can show deviations from normal values, if the meet expectations in terms of trending, as well as observing large changes in the output parameter values, being the higher SN #'s which have the greatest effect on the process.

4.1. HVOF

4.1.1. D.O.E. 1

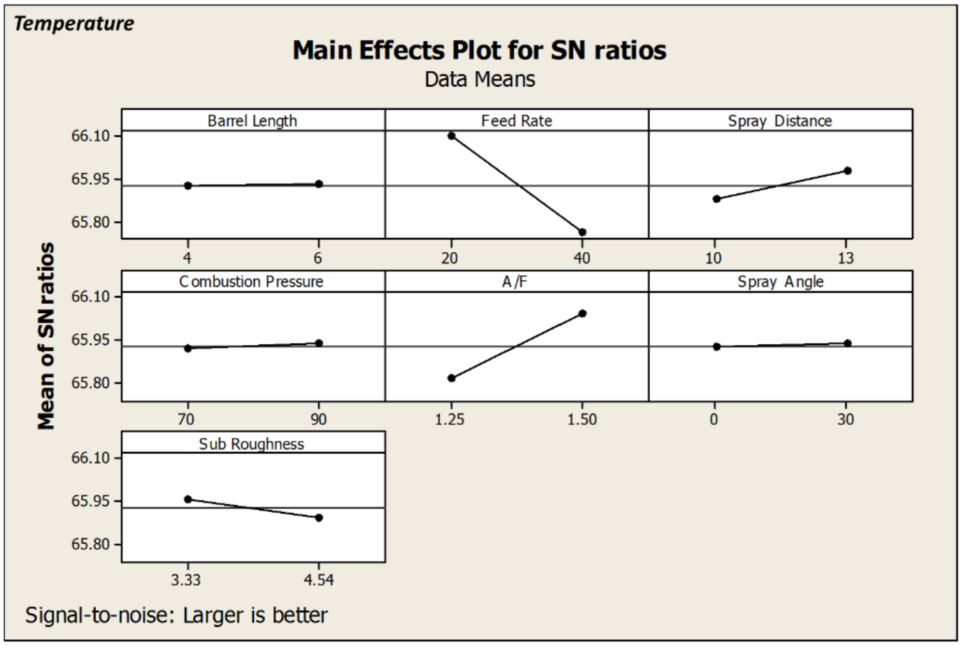

FIGURE 38: *D.O.E. 1 Main Effects plot for Temperature SN Ratios*

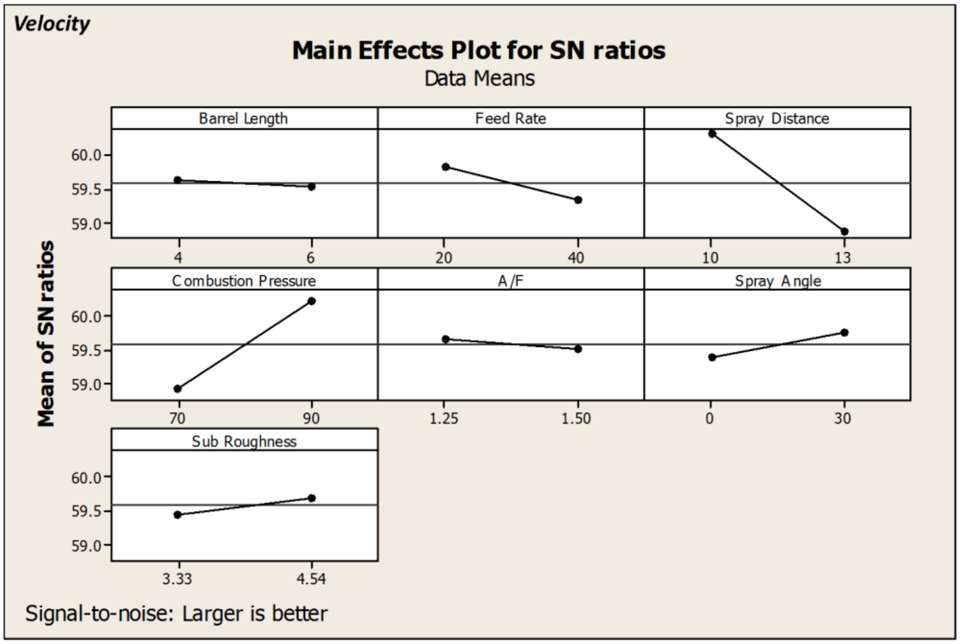

FIGURE 39: *D.O.E. 1 Main Effects plot for Velocity SN Ratios*

The proceeding main effects plots for SN ratios were calculated with MiniTab statistical software using the Taguchi method for design of experiments. The seven input variables can be seen as well as in the top left corner is the output parameter which is mean particle temperature and velocity. The variables with the highest SN #'s that effect temperature are typically the spray distance, feed rate, and A/F ratio which is to be expected as increasing the spray distance also increases particle flight time in air and therefor cooling the particles. Increasing the powder feed rate has a quenching effect on the plume which has a fixed amount of enthalpy which gets consumed with more powder. The A/F ratio can be seen to have an effect on the temperature as a higher ratio creates an oxidizing flame which then superoxidizes the particles in flight therefor increasing their mean temperature in the plume. The variables having the largest SN #'s for velocity can be seen to be spray distance, combustion pressure, as well as feed rate and barrel length to a lesser degree and is to be expected.

4.1.1.1. PROCESS MAPS

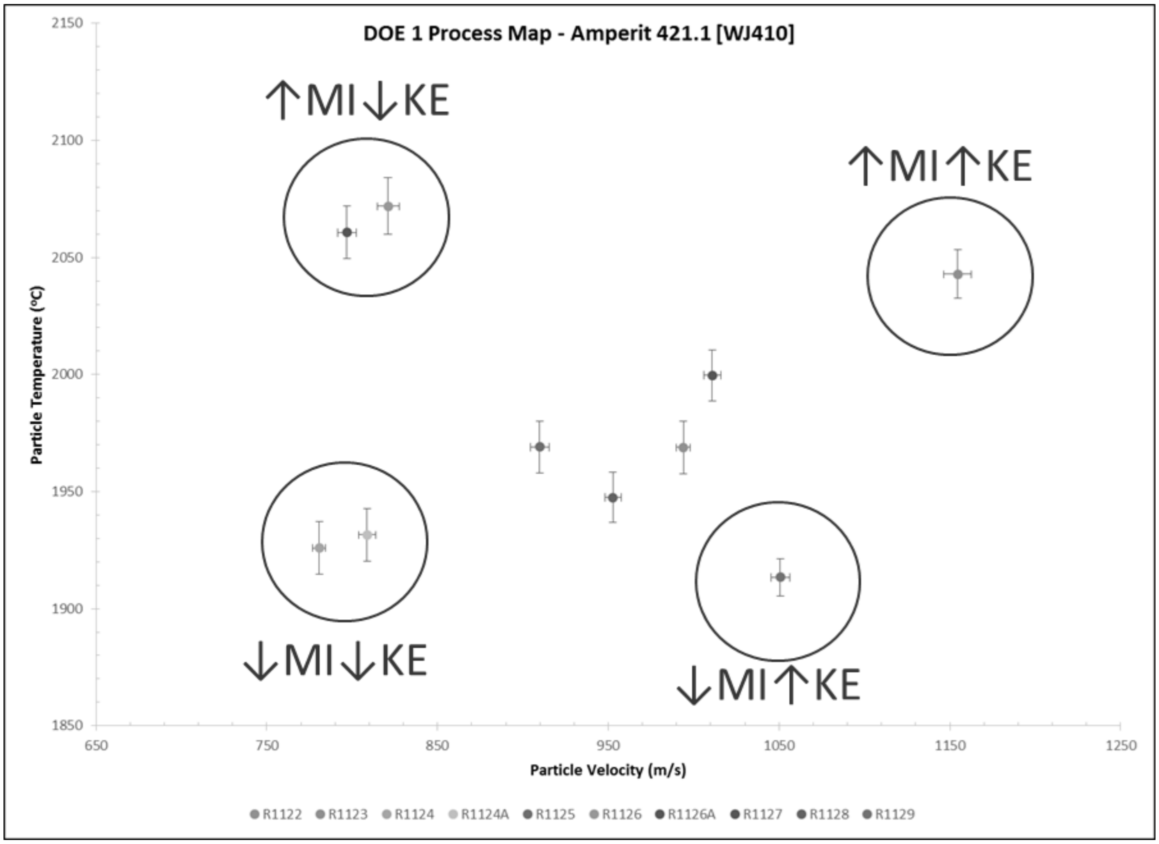

FIGURE 40: *D.O.E. 1 Process Map showing High/Low MI Group and High/Low KE Group*

The first order process map for D.O.E. 1 can be seen with a typical structure of an HVOF LF sprayed Ni alloy powder with four main groupings with high/low melting index and high/low kinetic energy on a linear trend. The error bars for velocity tend to be small whereas the error in the temperature measurement has a higher standard deviation due to the nature of the diagnostic sensor and the plume dynamics. The effect of increasing the combustion pressure as well as decreasing spray distance can be seen to increase the kinetic energy of the particles as well as increasing the melting index with higher A/F ratios. The higher MI groupings tend to have denser microstructure due to the increased melting and flattening of the particles that are incident onto the substrate. The higher kinetic energy grouping with produce a semi-dense coating but due to inefficient melting of the particles would tend to have inclusions or voids in the coating. Both the high MI and low KE, low MI and low KE groups have repeat runs which differ by very small amounts which exhibit the repeatability of the process as well as the diagnostic sensor measurements.

4.1.1.2. STRESS-STATE MEASUREMENTS

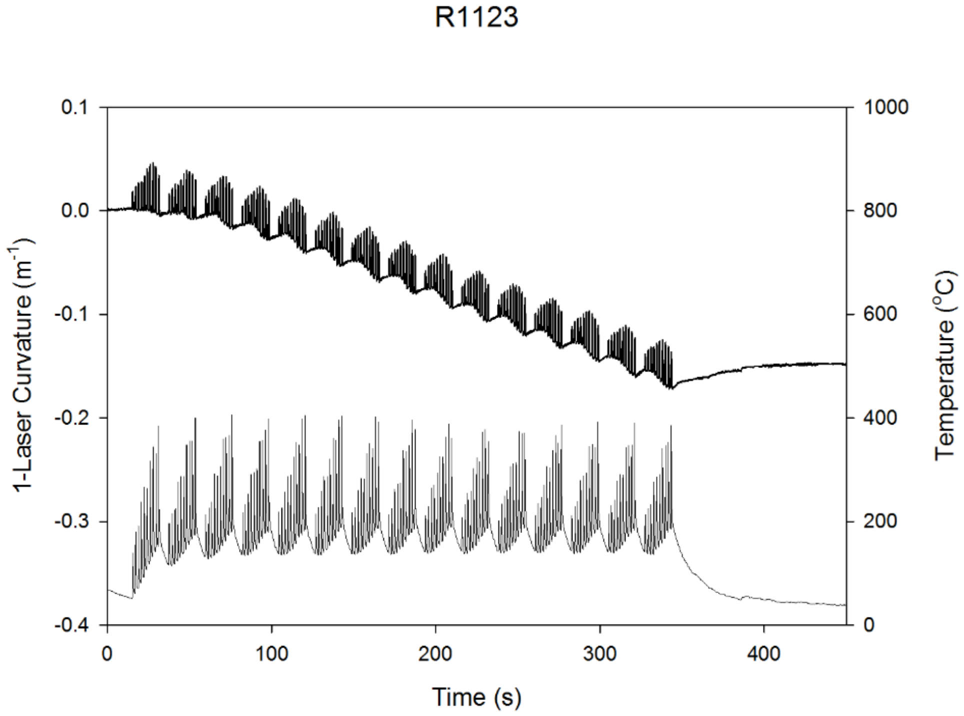

FIGURE 41: *ICP Output for R1123*

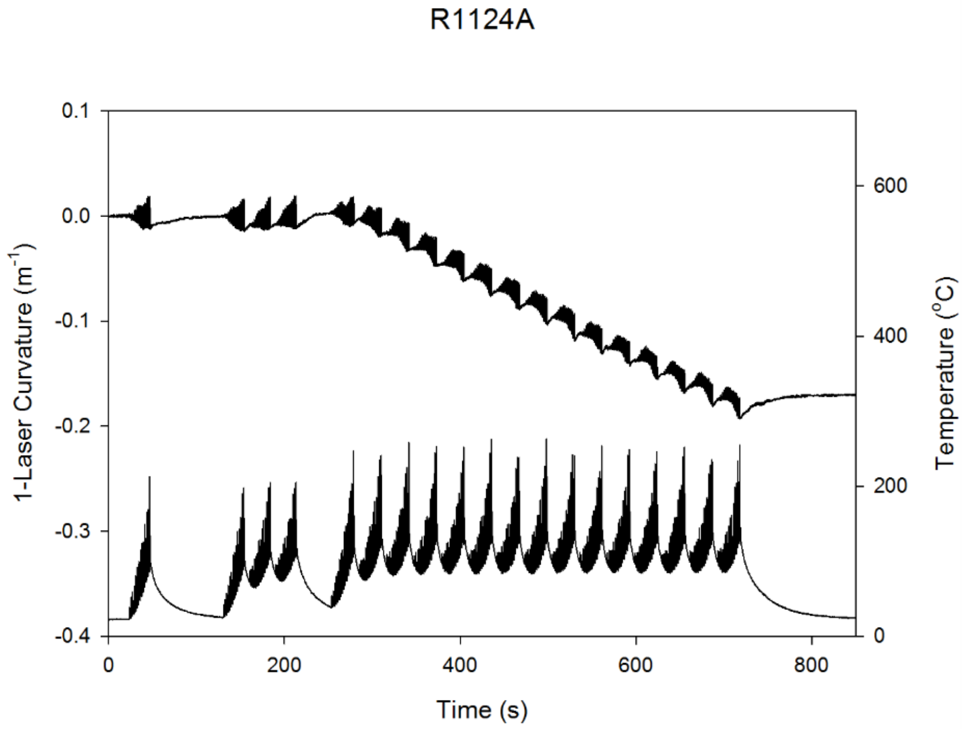

FIGURE 42: *ICP Output for R1124A*

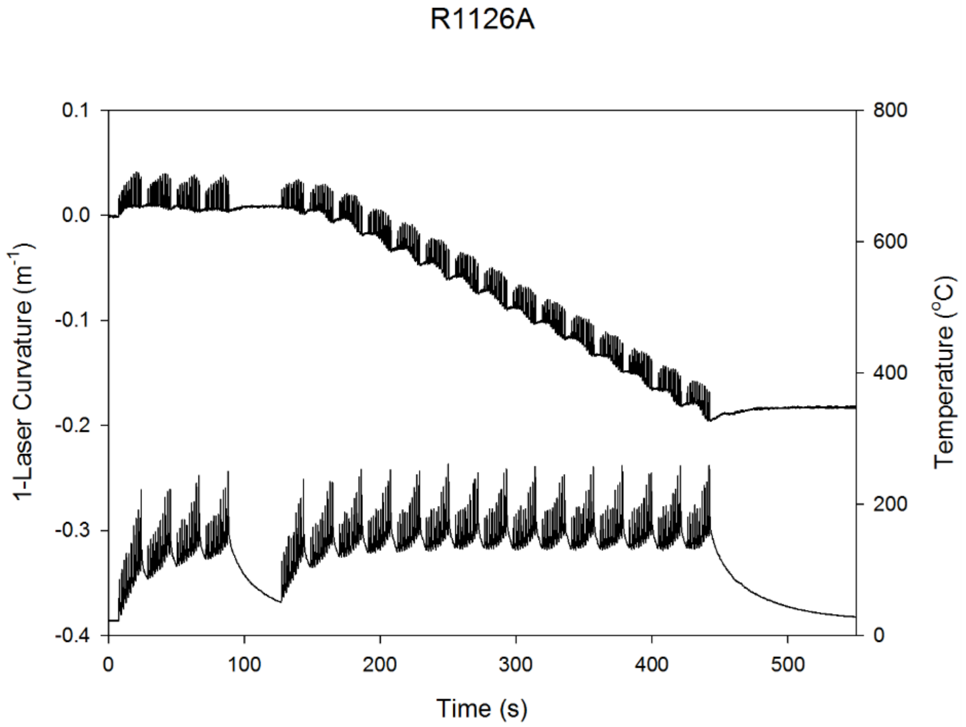

FIGURE 43: *ICP Output for R1126A*

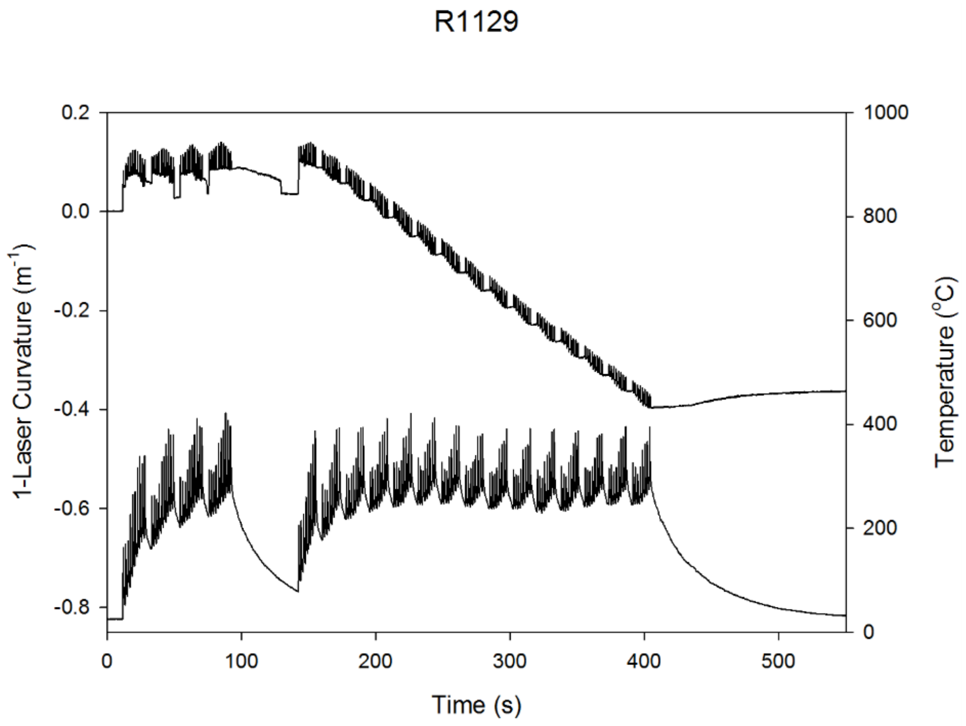

FIGURE 44: *ICP Output for R1129*

The stress-state measurements for D.O.E. 1 can be seen in the format obtained from the ICP sensor being time vs. beam curvature and substrate temperature. The curvature is typical of an HVOF LF sprayed Ni alloy powder having a high compressive evolving stress with some initial peening stress due to the high velocity. The bond coating tends to have a low thermal stress due to the coefficient of thermal expansion difference between Ni alloy and steel being low. The measurements were taken with no cooling air to create a more realistic stress-state in the coating. The conditions with higher KE will tend to increase the evolving stress due to the high energy particles impacting the coating, as well as the beam curvature amplitude starts to dampen as the thickness increases which is typical. The residual stress in the coating can be seen to be relatively the same in the four groupings with the high KE group having almost double due to the high velocity and low melting of the particles.

4.1.1.3. MICROSTRUCTURE

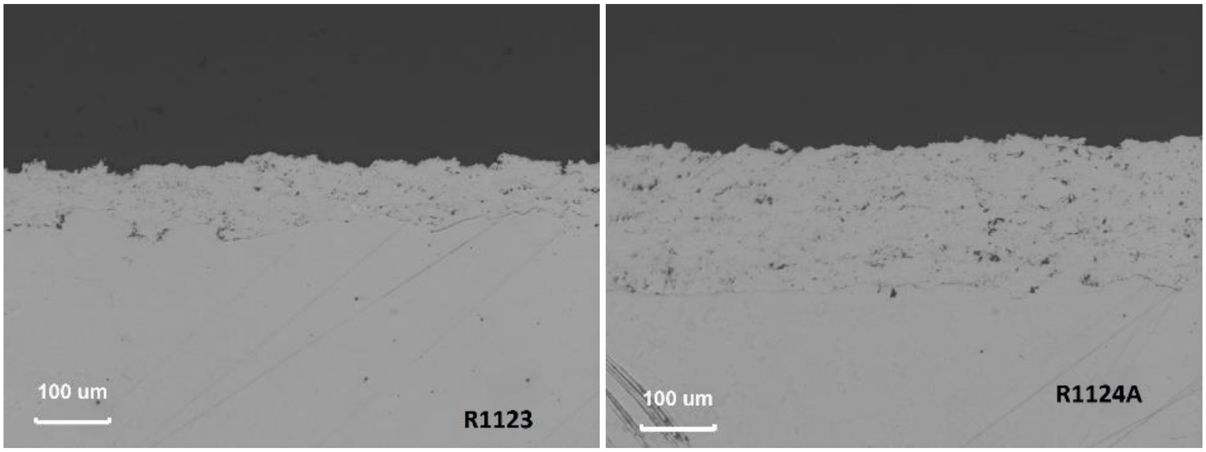

FIGURE 45: *Microstructure for R1123 and R1124A*

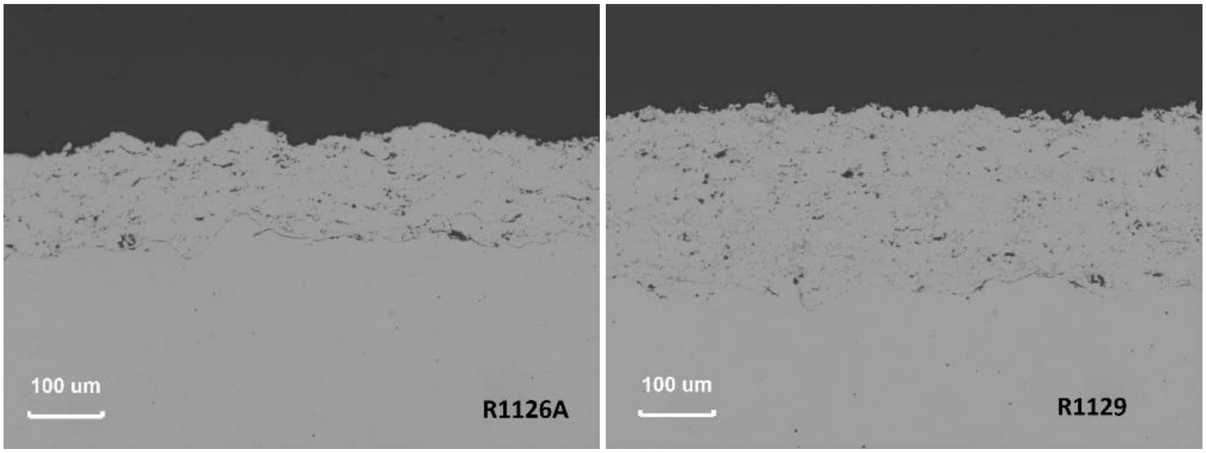

FIGURE 46: *Microstructure for R1126A and R1129*

The microstructual analysis of the four main groupings can be seen with a nominal change in the different groupings. The coatings tend to be dense with some inclusions and voids due to incomplete particle melting, as well as the high melting index group showing signs of oxide growth in the interlamellar splat boundaries due to the superoxidation of the particles in flight.

4.1.2. D.O.E. 2

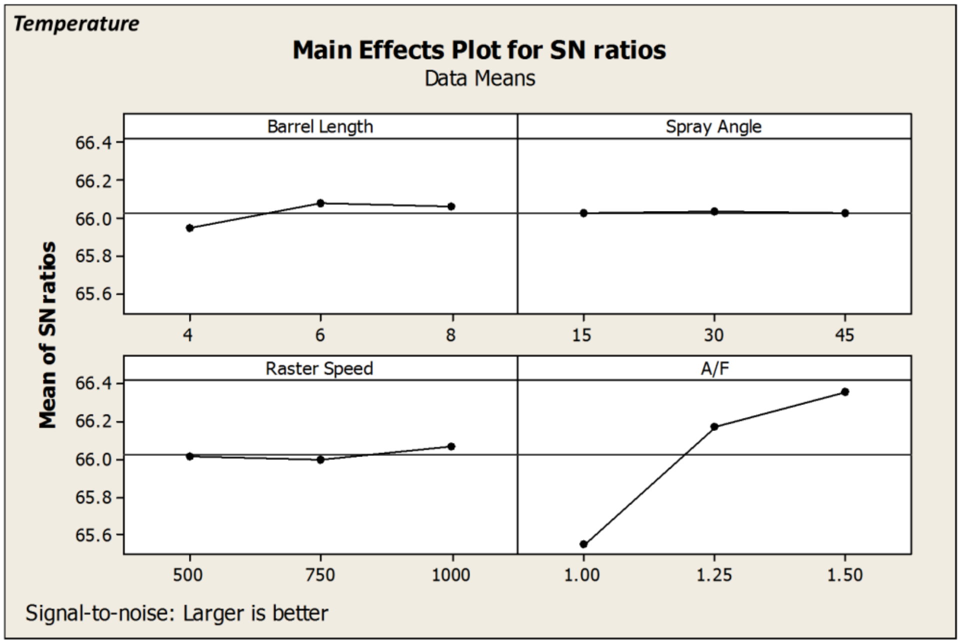

FIGURE 47: *D.O.E. 2 Main Effects plot for Temperature SN Ratios*

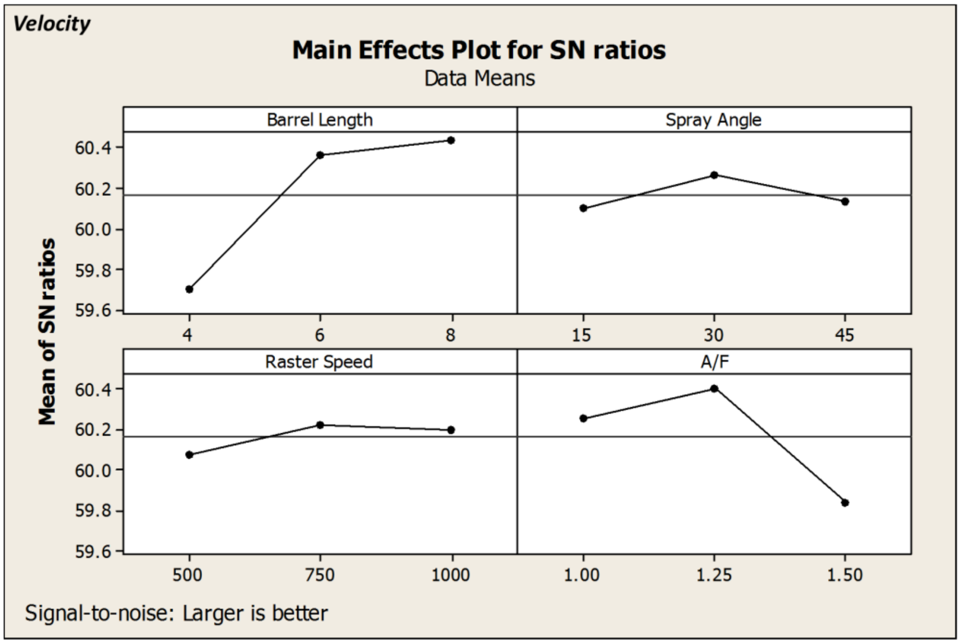

FIGURE 48: *D.O.E. 2 Main Effects plot for Velocity SN Ratios*

The main effects plots for SN #'s for D.O.E. 2 can be seen with only four input variables and increasing to three levels to see a clearer trend in the output. The output parameter values that can be seen to have a great effect on temperature and velocity are barrel length and A/F ratio where spray angle and raster speed can be omitted. There can be seen a larger deviation from linear trend in the increased number of levels as increasing the barrel length has a great effect from 4-6 inch yet a much smaller increase from 6-8 inch. The A/F ratio can also be seen to have a greater amount of non-linearity as increasing from 1.0-1.25 increases the velocity and temperature yet from 1.25-1.50 decreases the velocity while the temperature increases only a small amount.

4.1.2.1. PROCESS MAPS

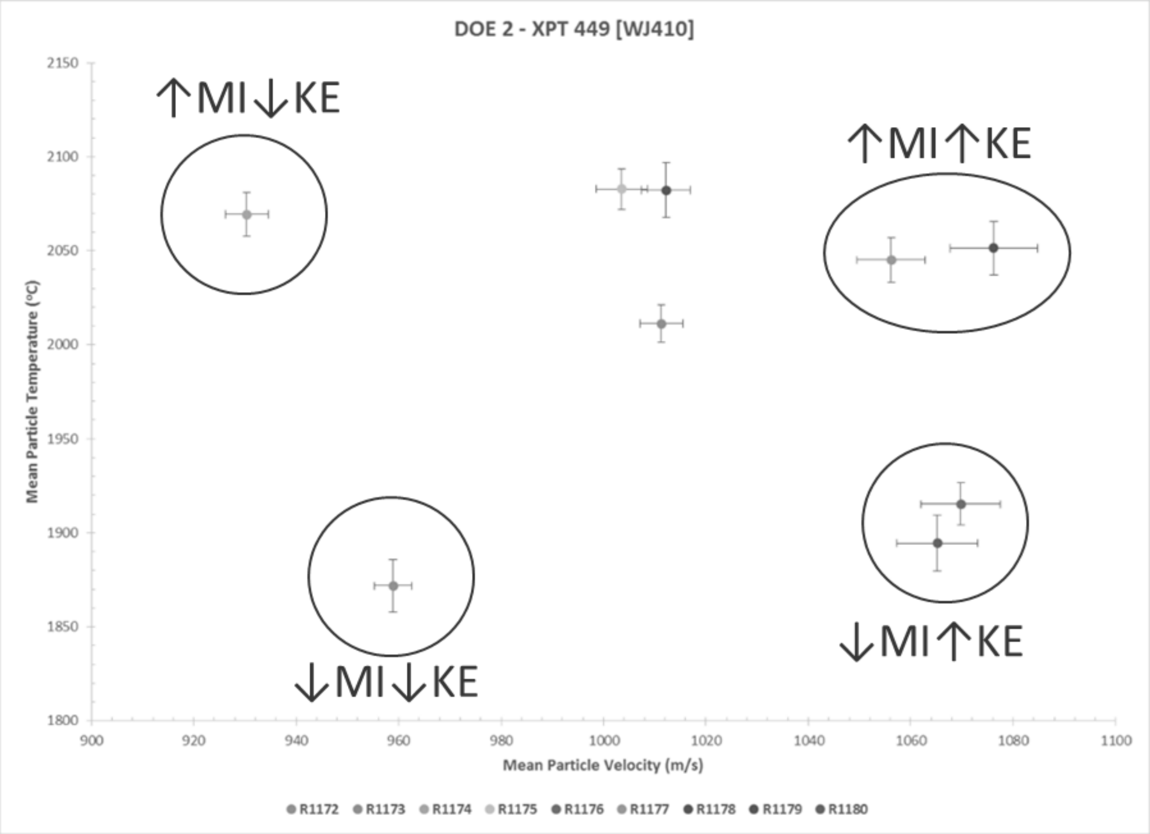

FIGURE 49: *D.O.E. 2 Process Map showing High/Low MI Group and High/Low KE Group*

The first order process map for D.O.E. 2 can be seen with the same four groupings as was seen in D.O.E. 1 with some slight differences. The high MI and KE group as well as low MI and high KE group have repeat runs showing the consistency of the measurement as well as the repeatability of the process. The velocity can be seen to be affected in the high condition group due to some variation in the combustion pressure caused by fluctuations in the controller kerosene back pressure supply. This group also has a larger error than the other groups due to the same inconsistency seen by the torch with kerosene supply which skew the results.

4.1.2.2. STRESS-STATE MEASUREMENTS

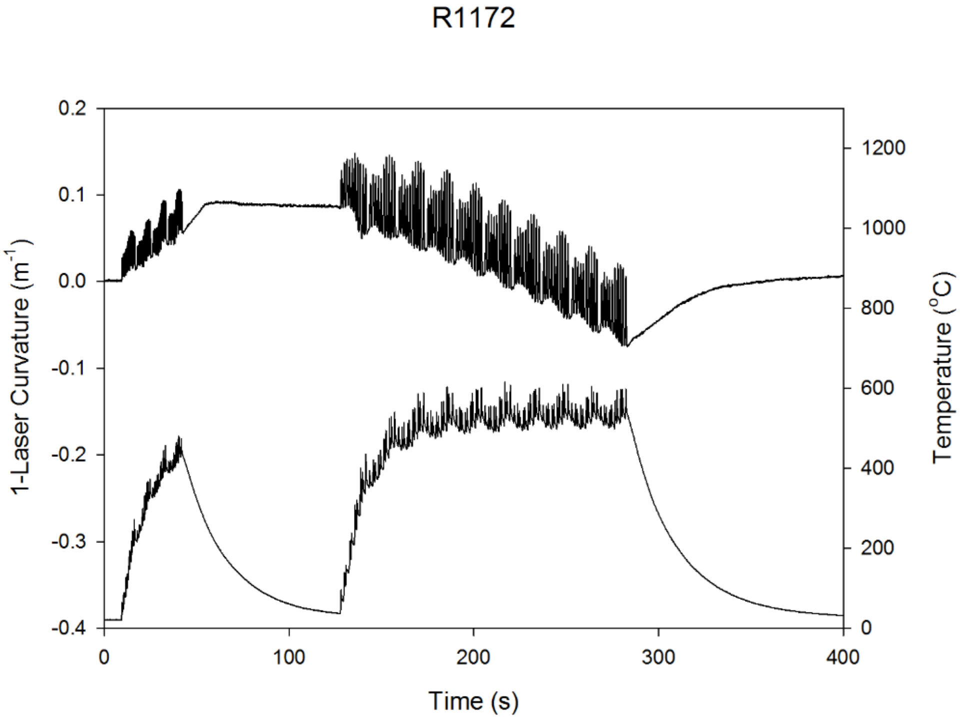

FIGURE 50: *ICP Output for R1172*

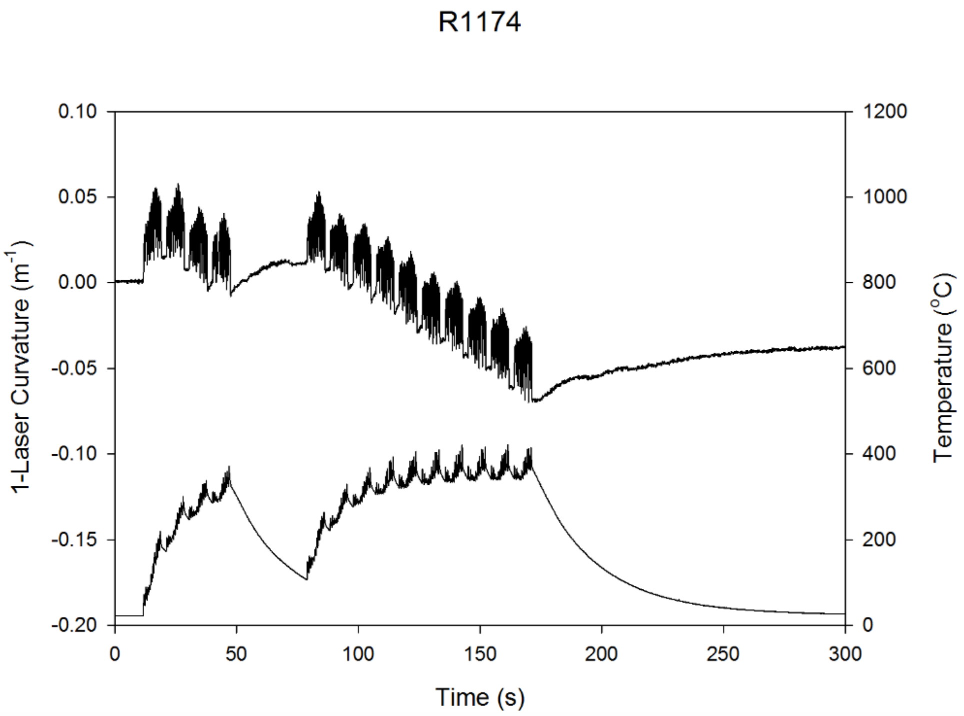

FIGURE 51: *ICP Output for R1174*

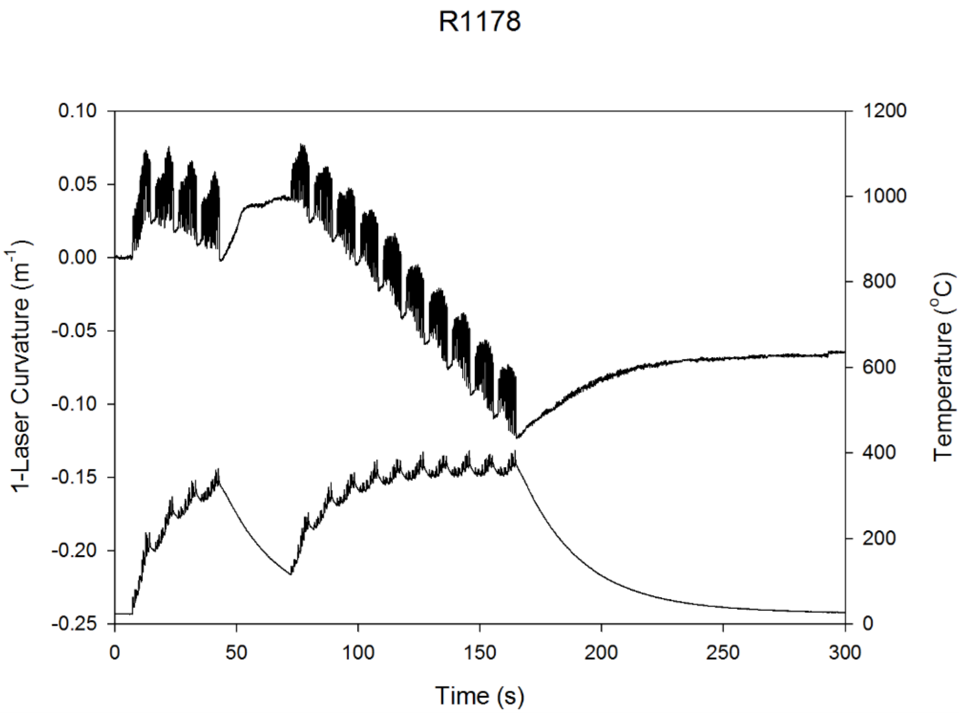

FIGURE 52: *ICP Output for R1178*

The following figures display the typical ICP output for an HVOF LF sprayed Ni alloy, which are very similar to the stress-state measurements from D.O.E. 1 where only the powder composition changed. The same large compressive evolving stress with low thermal stress and nominal residual stress. The high KE group exhibits a large peening stress during the first pass due to the high velocity of the powder incident onto the substrate and reaches a steady state as the coating thickness increases. The effects seen by the substrate can only be measured during the first or second pass as after this the interaction changes from adhesive forces to cohesive forces due to the particles being incident onto already deposited particles.

4.1.2.3. MICROSTRUCTURE

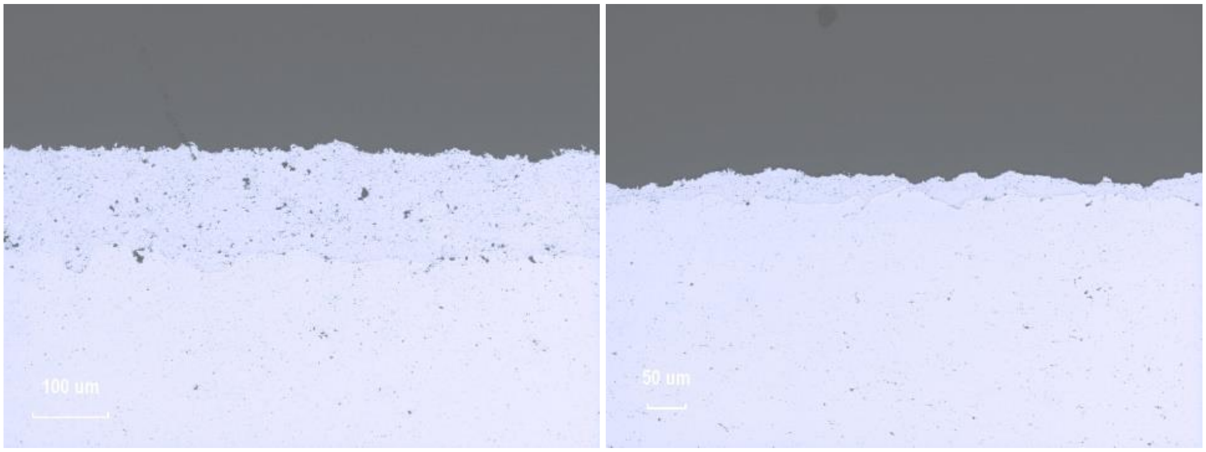

FIGURE 53: *Microstructure for R1172 and R1174*

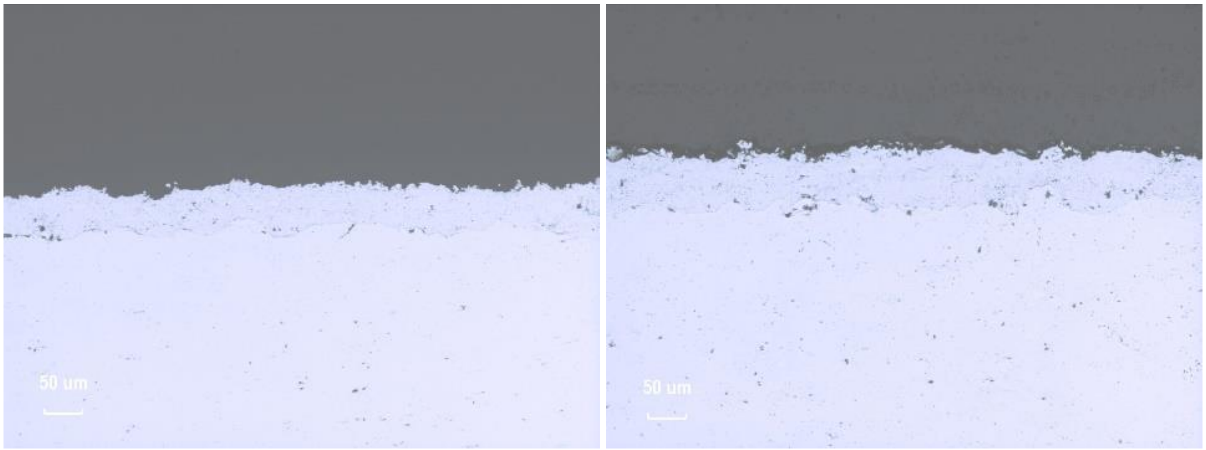

FIGURE 54: *Microstructure for R1178 and R1180*

The microstructural analysis for D.O.E. 2 can be seen with a nominal structure with a dense coating including some voids and inclusions. The largest difference that can be seen in all four images is the high MI group where the effect of a high A/F ratio is very apparent with dark oxide stringers seen in the interlamallar splat boundaries due to the superoxidiation of the particles, causing the coating to have a weaker adhesive bond to the substrate as well as lower cohesive bonding between splats.

4.1.3. D.O.E. 3

4.1.3.1. PROCESS MAPS

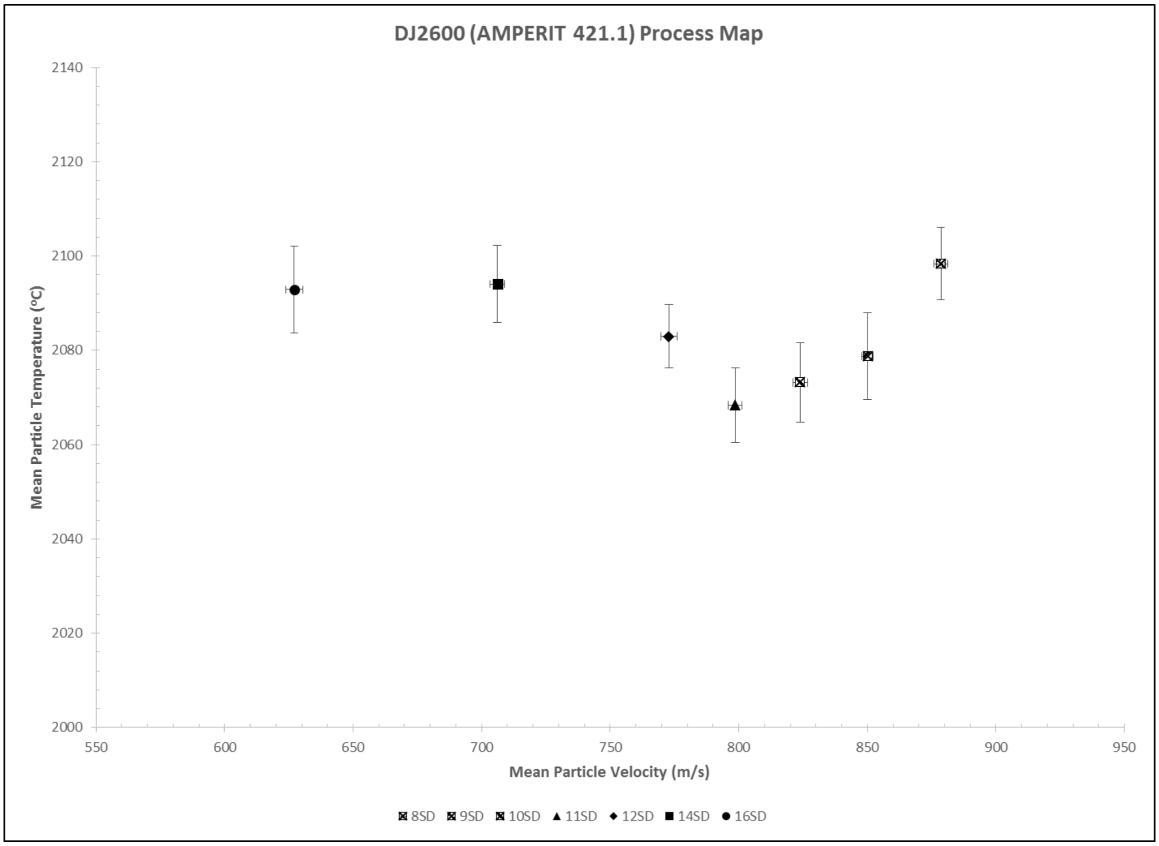

FIGURE 55: *D.O.E. 3 Process Map using DJ2600 and AMPERIT 421.1*

The first order process map for D.O.E. 3 varies greatly from the previous maps due to the change from LF to GF process which uses gas fuel as well as a different torch design. This map shows the change in spray distance with a GF torch and how this will affect particle temperature and velocity as well as changes in linearity which are apparent. As the spray distance is increased from 8-11 inches the velocity decreases as well as as decreasing the temperature which is to be expected. There is a critical point where from 11-16 inch distance the temperature starts to increase and the velocity steadily decreases. This is a clear example of particle superoxidation in air as there is a critical amount of particle flight time where the particles start to oxidize and raise their temperature again which is seen here by the diagnostic sensor. The working spray distance of the GF torch is typically 8-10 inches which is evident here as after this distance the particle dynamics change drastically in terms of oxidation, which for a bond coating is not desired.

4.1.3.2. STRESS-STATE MEASUREMENTS

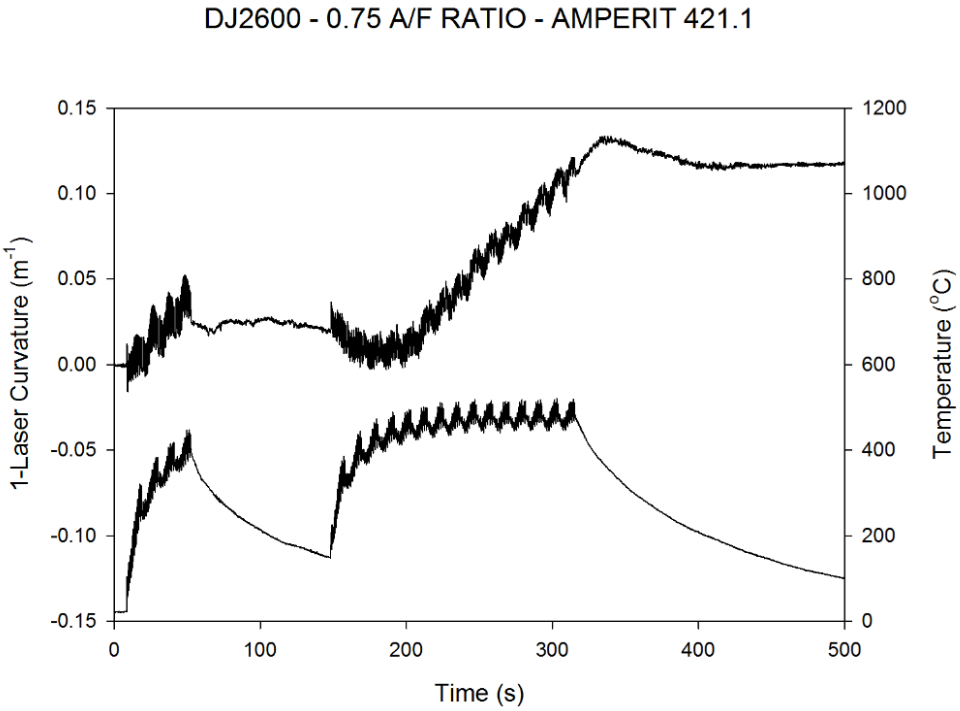

FIGURE 56: *ICP output for DJ2600 with an A/F = 0.75*

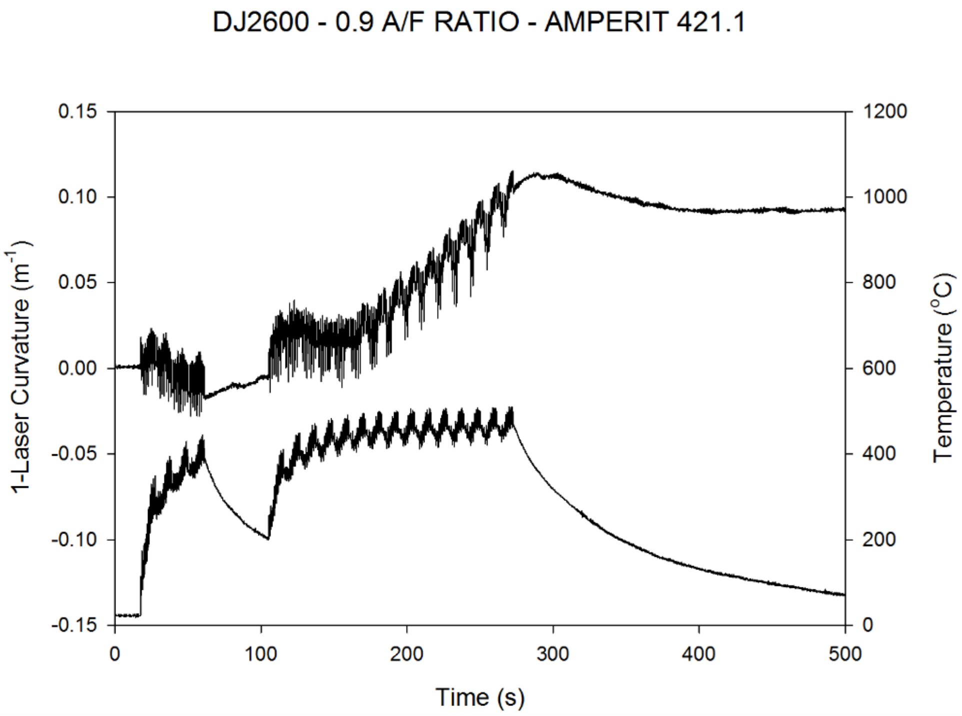

FIGURE 57: *ICP output for DJ2600 with an A/F = 0.9*

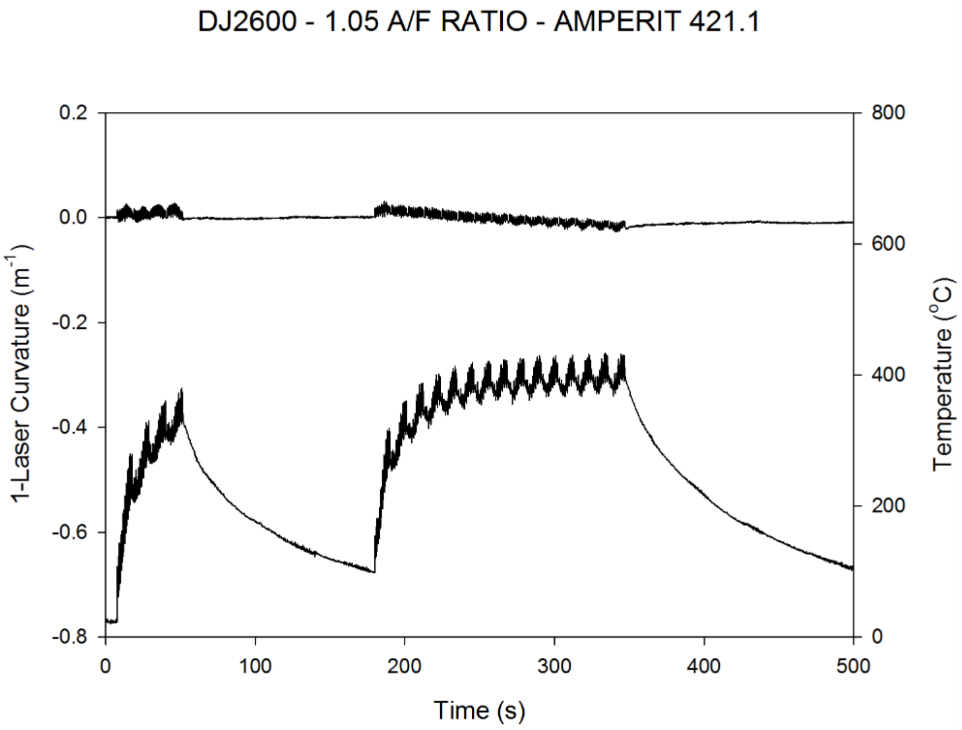

FIGURE 58: *ICP output for DJ2600 with an A/F = 1.05*

The stress-state measurements taken from the ICP sensor can be seen to also be very different when switching from LF to GF processing and is evident here. The large evolving stress is seen to reverse from compressive in LF to tensile in GF which is typical when spraying Ni alloys with GF torches. This is caused by the difference in the torch design where instead of a peening stress there is a more compressive evolving stress during passes 1-4 which as the coating builds up it starts to change to tensile and increases linearly from this point. The stress amplitude as well as evolving stress can be seen to change with increasing A/F ratio where an oxidizing condition will produce a more neutral residual stress in the coating. The spray distance of the GF torch tends to be much closer than with a LF torch and this can tend to cause a change in the evolving stress as well as how the coating builds upon itself at higher velocities.

4.1.3.3. MICROSTRUCTURE

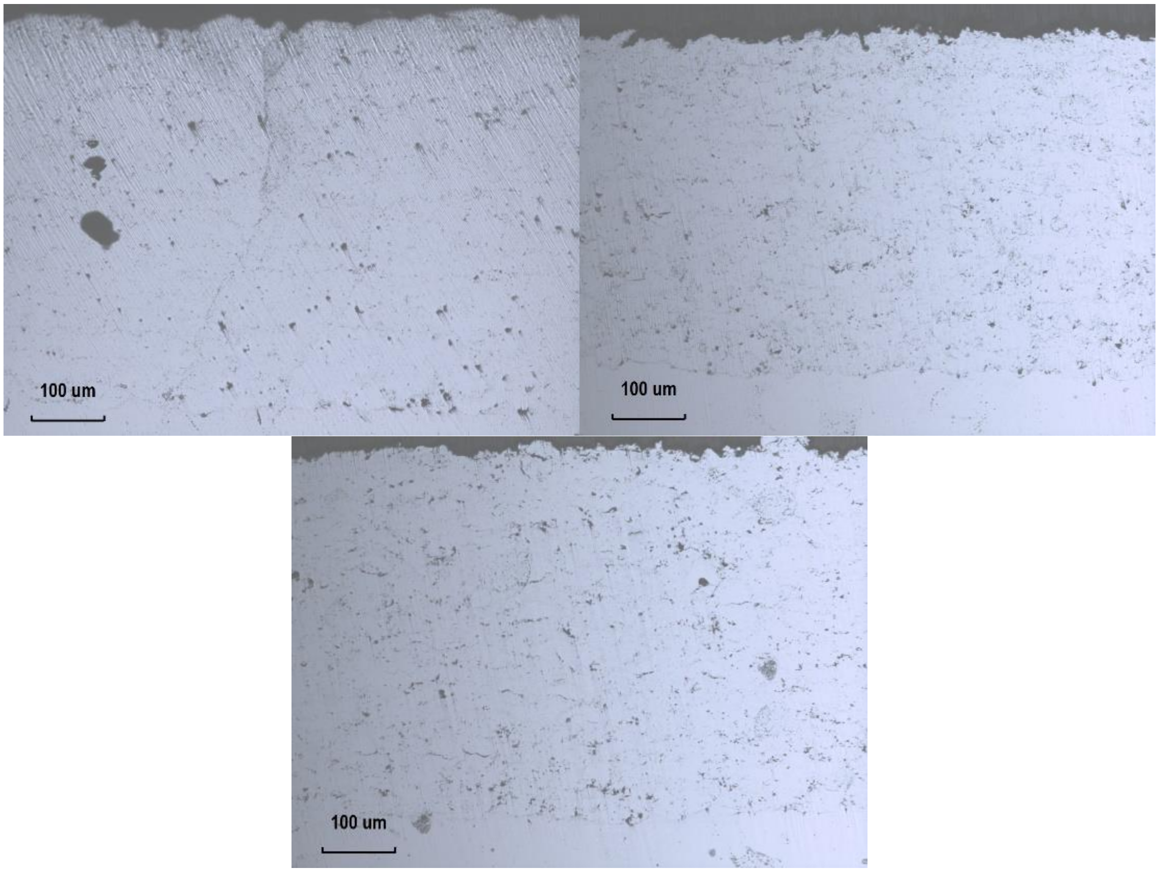

FIGURE 59: *DJ2600 Microstructure with A/F ratios LTR of 0.75, 0.9, and 1.0*

The microstructure of an HVOF GF sprayed Ni alloy is seen here with typical coating density as well as fewer voids and inclusions compared to a LF process. The A/F ratio is seen here increasing from left to right and slightly more oxides are present in the higher A/F ratio conditions which is to be expected, and is much less than with the LF process. This can be due to the GF torch having a shroud gas which is typically air which tends to protect the powder during flight, where using a pure nitrogen shroud is preferred due to the inert nature of the gas. There can also be seen a large void in one of the coatings which could be caused by a foreign object impacting the coating during spraying, but could also be from specimen grinding and polishing.

4.2. APS

4.2.1. PROCESS MAPS

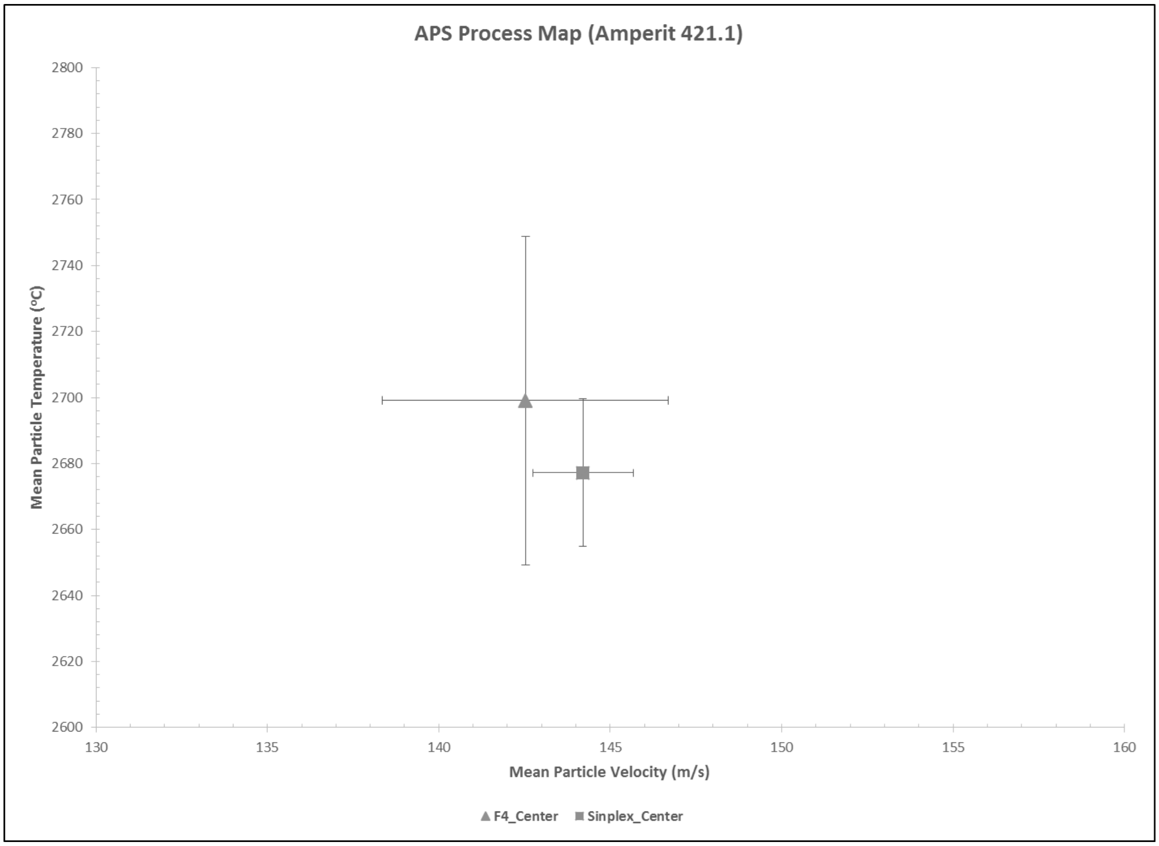

FIGURE 60: *APS Process Map using AMPERIT 421.1*

A comparative process map is seen here with mean particle temperature and velocity for two different single cathode APS torches. The main objective for spraying bond coating powder with an APS torch was purely for a comparison to the HVOF process and not intended to produce significant results. A major observation to be made is that the APS process produces particle temperatures 800-1000 °C higher than with the HVOF process, which is attributed to the extreme heat contained in the thermal plasma. The particles are superheated in the plasma and are projected through air to the substrate, which the particles superoxidize due to the extreme temperature and the oxygen contained in air. The velocity is very low compared to HVOF which is to be expected due to the nature of the plasma torch design.

4.2.2. STRESS-STATE MEASUREMENTS

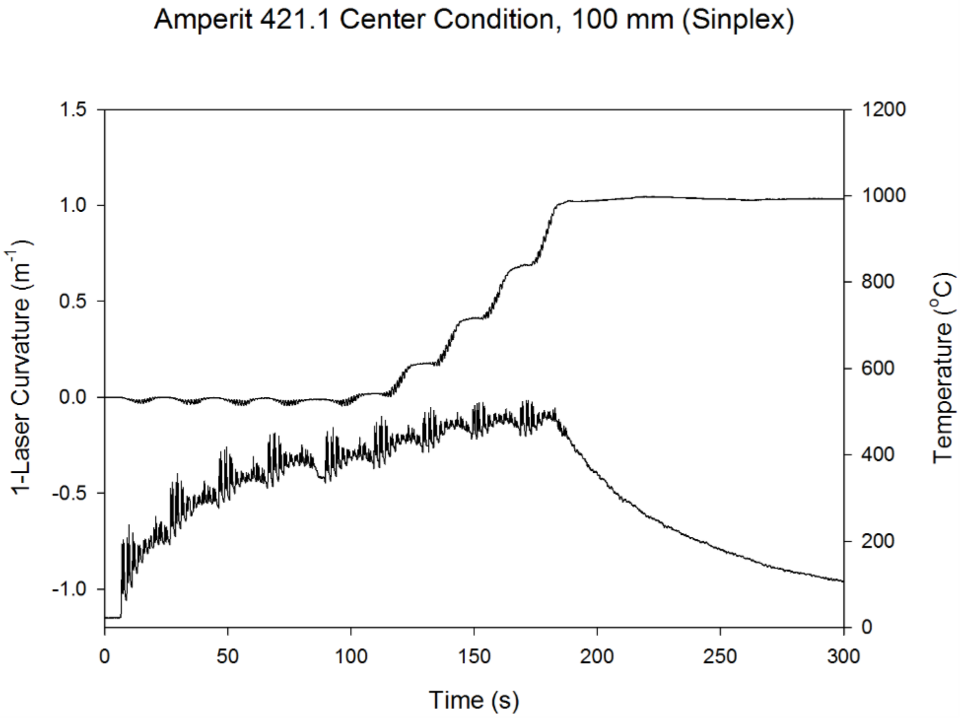

FIGURE 61: ICP Output for APS Sinplex

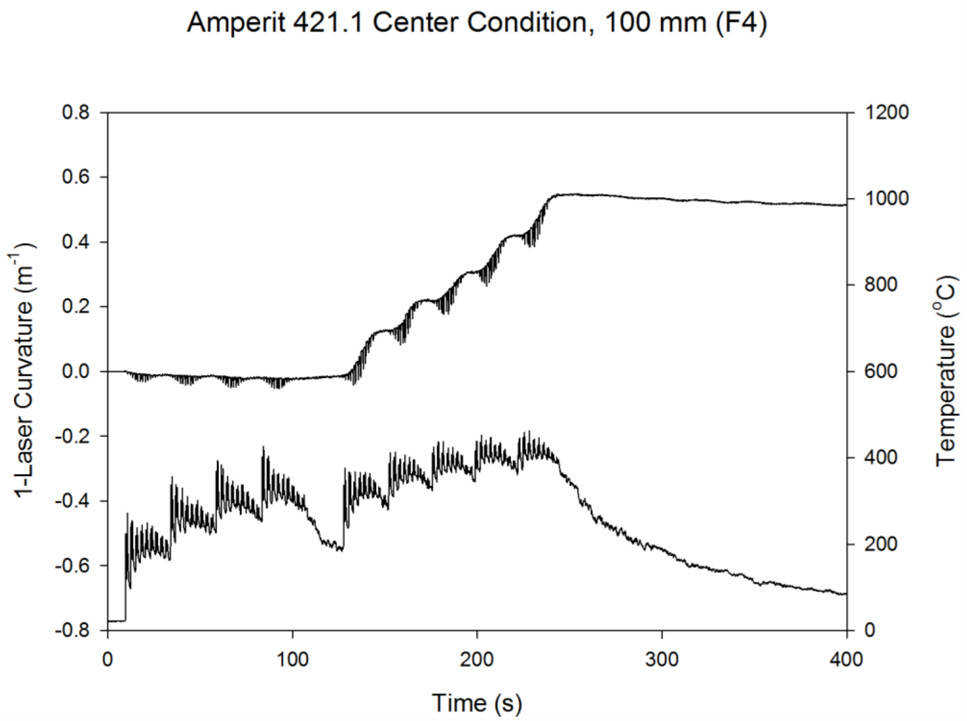

FIGURE 62: ICP Output for APS F4

The stress-state measurements taken by the ICP sensor displayed here are typical of an APS sprayed metallic powder with a tensile evolving stress and little thermal stress. The main difference between the two different torches is that the Sinplex has twice the residual stress in the coating as compared to the F4 style torch. This difference can be attributed to the fact that the simplex torch is a newer design and has a much higher application rate than the F4 building up more stress in the coating both during deposition as well as after cooling.

4.2.3. MICROSTRUCTURE

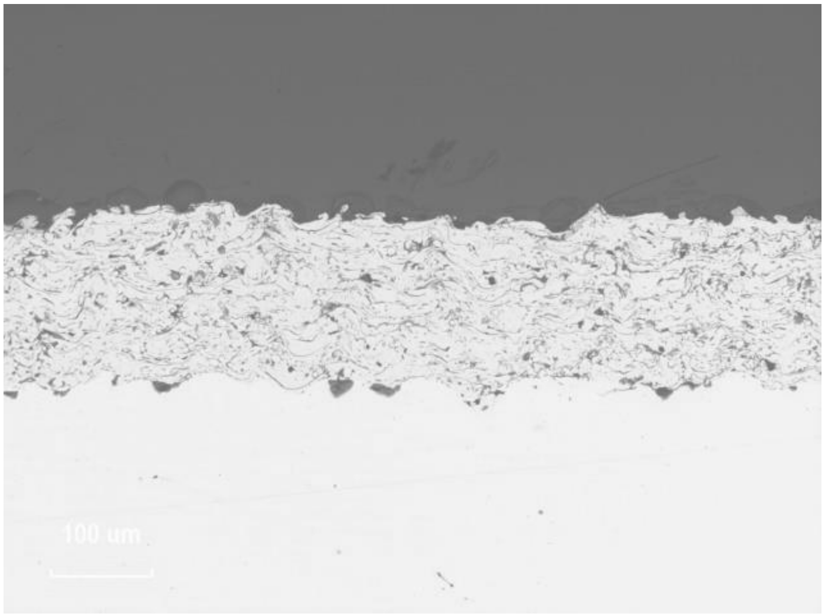

FIGURE 63: *APS sprayed AMPERIT 421.1 with F4*

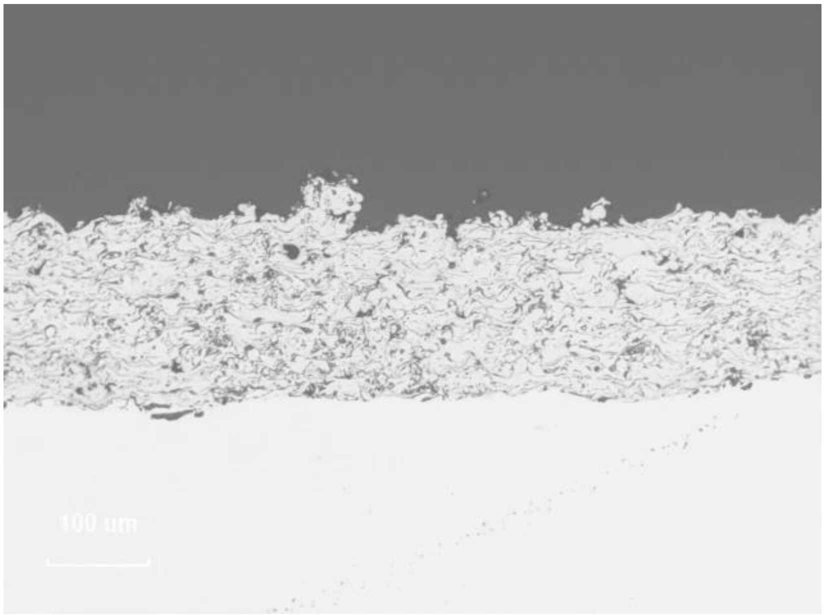

FIGURE 64: *APS Sprayed AMPERIT 421.1 with Sinplex*

The nominal microstructure of an APS sprayed metallic powder is represented in these cross-sectional images where the coating tends to be less dense and semi-porous. The presence of dark lines, called oxide stringers, are the superoxidized particles that have grown a TGO scale prematurely during coating deposition. This is the main cause of APS bond coating adhesive failure as well as poor thermal cycling performance. The simplex style torch has a slightly higher amount of oxide stringers in the coating due to some hot spots in the plasma.

4.3. ADHESION TESTING

Sample #	***Process***	***Torch***	***A/F***	***Thickness (µm)***
1	EPOXY	N/A	N/A	N/A
2	EPOXY	N/A	N/A	N/A
3	HVOF	WJ410	1.00	450
4	HVOF	WJ410	1.00	800
5	HVOF	WJ410	1.00	1200
6	HVOF	WJ410	0.85	500
7	HVOF	WJ410	1.00	500
8	HVOF	WJ410	1.50	500
9	HVOF	DJ2600	0.85	500
10	HVOF	DJ2600	1.00	500
11	HVOF	DJ2600	1.15	500
12	HVOF	WJ410	1.00	500
13	HVOF	JP5000	1.00	500
14	HVOF	JP5000	1.50	500
15	APS	F4	N/A	650
16	APS	F4	N/A	650
17	APS	SIN	N/A	1000
18	APS	SIN	N/A	1000

All JP500/WJ410 Samples sprayed at 12 inch Spray Distance

All DJ2600 Samples sprayed at 10 inch Spray Distance

All APS Samples sprayed at 100 mm Spray Distance

HVOF Feed Rate = 70 g/min

APS Feed Rate = 60 g/min

F4 Conditions: I = 350 A, PG = 35.5, SG = 2.0, CG = 1.5
Sinplex Conditions: I = 300 A, PG = 35.5, SG = 2.0, CG 1.5
3 Samples/Experiment
54 Samples Total

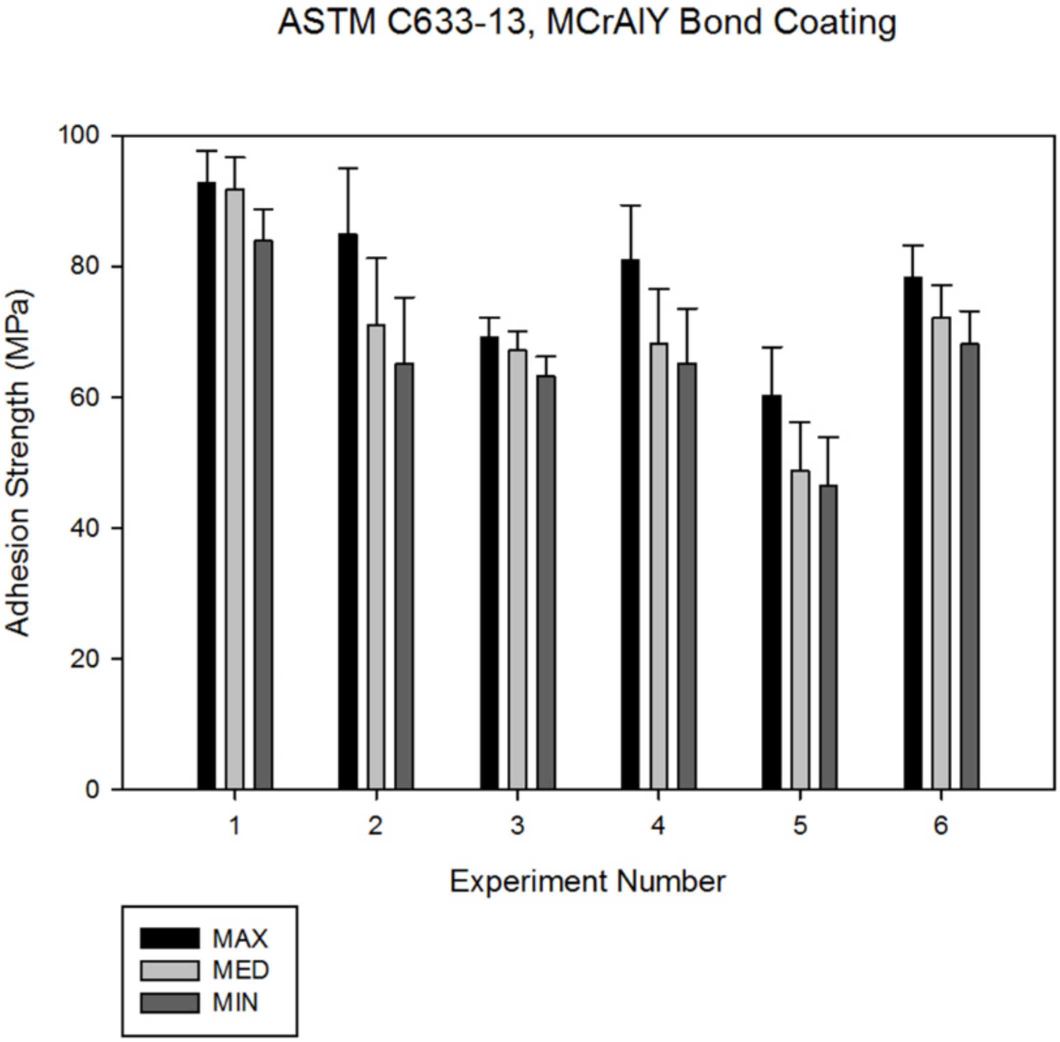

FIGURE 65: *Bond Strength Values, Experiments 1 – 6*

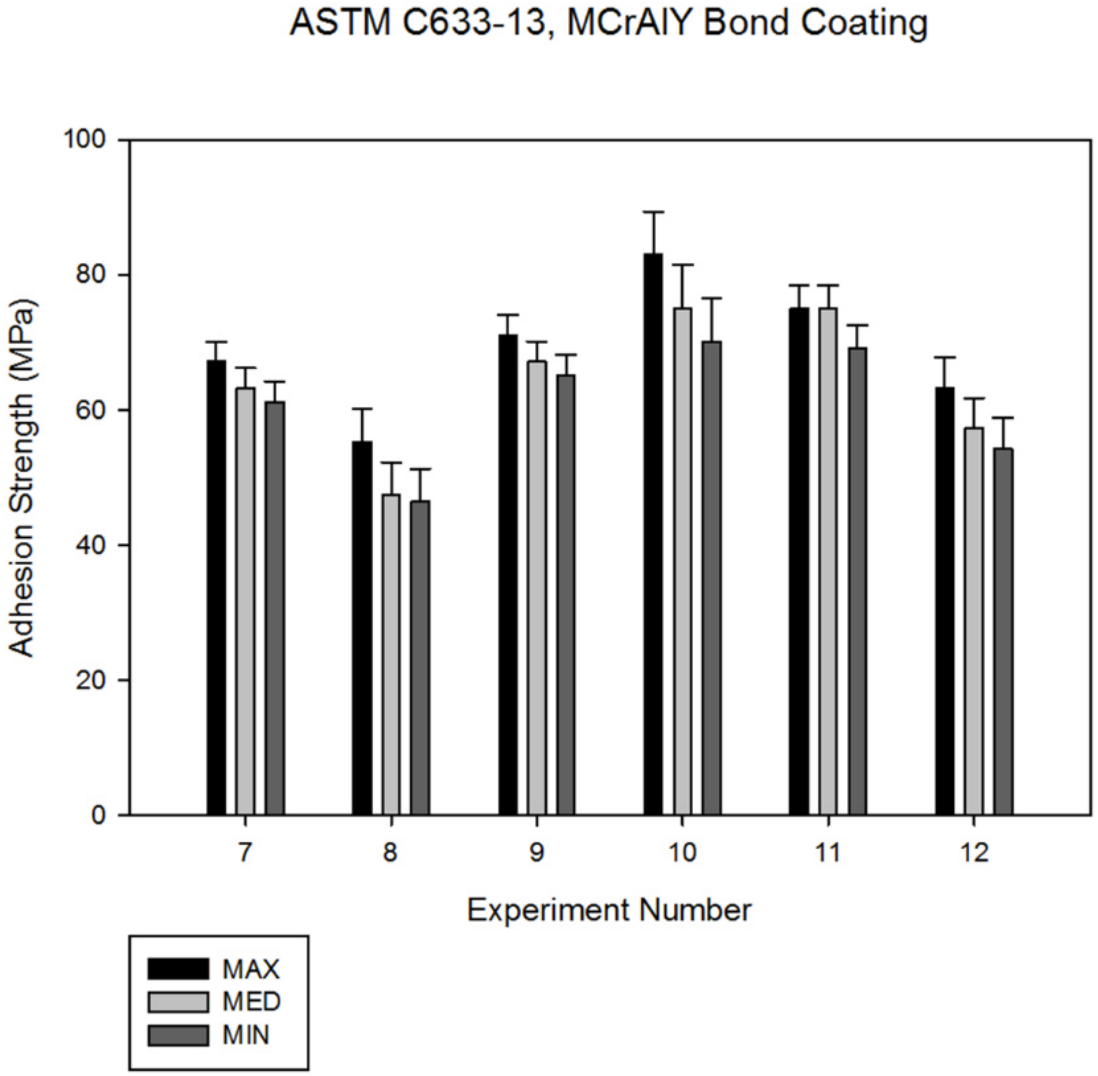

FIGURE 66: *Bond Strength Values, Experiments 7 – 12*

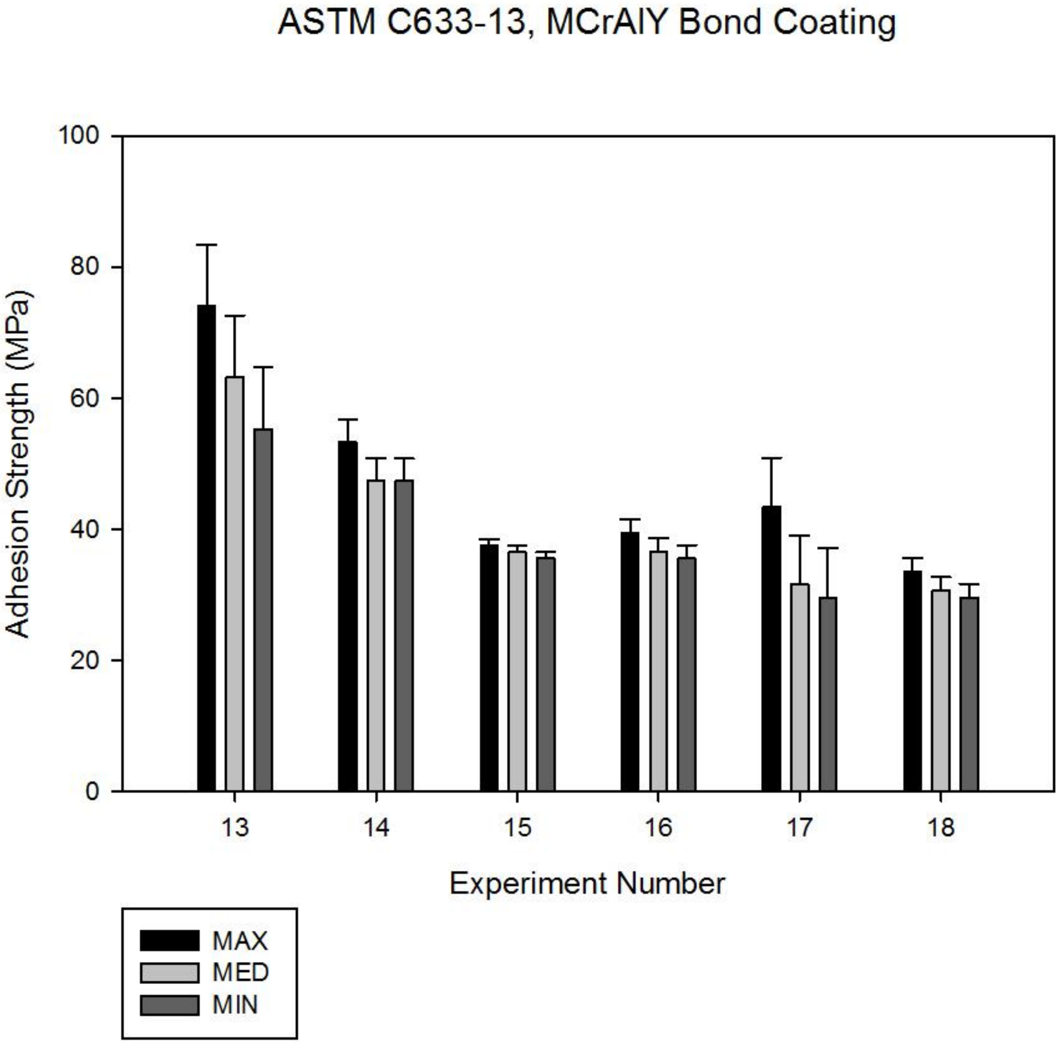

FIGURE 67: *Bond Strength Values, Experiments 13 – 18*

The results of the adhesion testing confirmed the process-property trends laid out in the introduction with 3 samples per experiment and a total of 18 experiments. Numbers 1-2 are an epoxy baseline test with a mean bond strength in excess of 90 MPa which is sufficient enough for HVOF sprayed coatings. Experiments 3-5 were sprayed with an HVOF LF WJ410 torch with varying coating thickness to see the effects of coating thickness on adhesion strength where between 800-1200 microns seems to be a critical value before decreasing the adhesion strength of the coating. Experiments 6-8 were sprayed with an HVOF LF WJ410 torch with increasing A/F ratio with the effect of the higher oxidizing flame reducing the bond strength due to pre-oxidation of the powder during deposition. Experiments 9-11 were sprayed with an HVOF GF DJ2600 torch which achieved the highest bond strength of all the samples as well as showing an increase in bond strength with increasing A/F ratio then a slight decrease after the stoichiometric condition is surpassed. Experiments 12-14 were sprayed with an HVOF LF WJ410/JP5000 torch which were a repeat run and an increasing A/F ratio which showed approximately the same bond strength as runs 6-8. Experiments 15-18 were sprayed with an APS F4/Sinplex torch and have the lowest mean bond strength of all the runs due to the superoxidation of the powder in the extreme heat of the plasma.

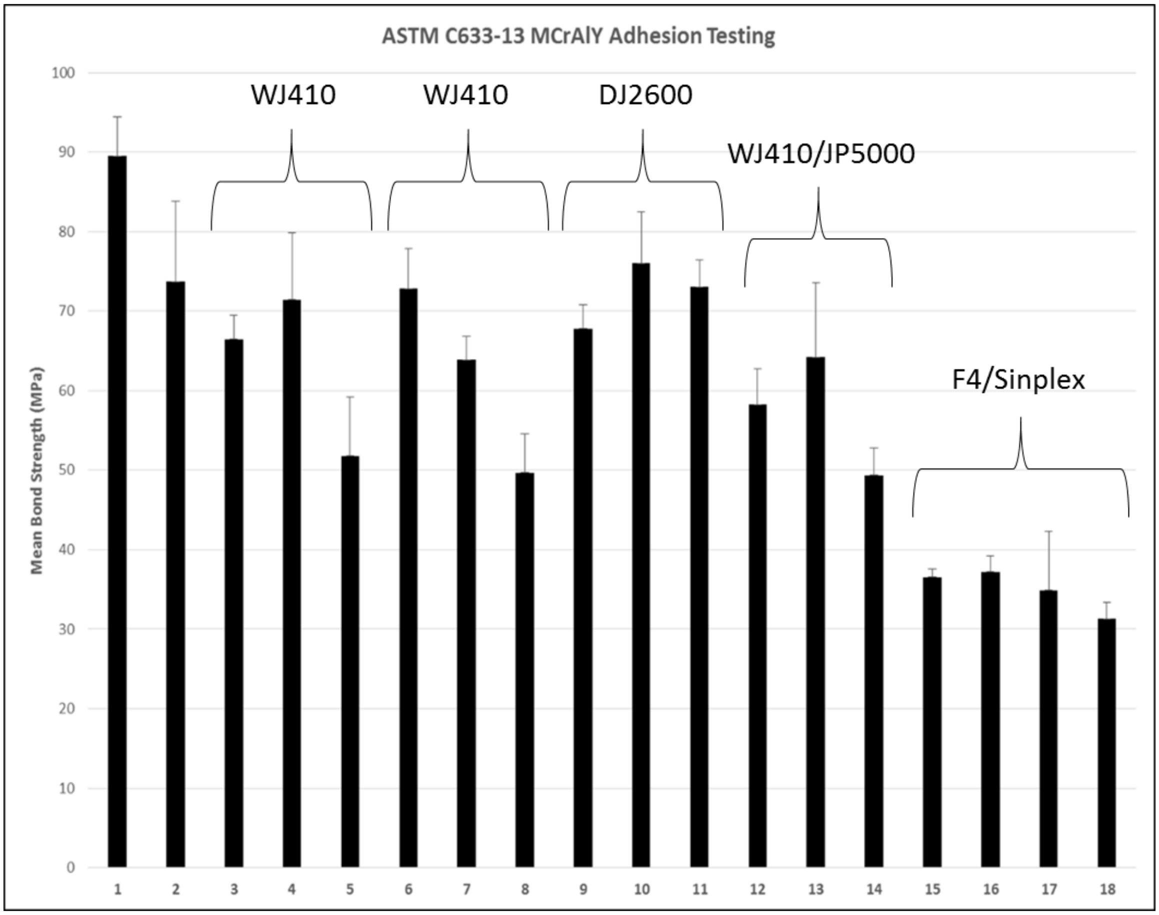

FIGURE 68: *Mean Bond Strength, All Experiments*

4.4. THERMAL CYCLING

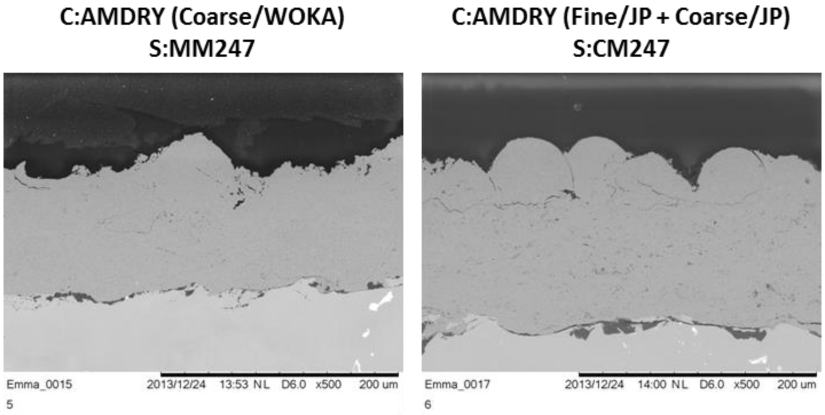
C:AMDRY (Coarse/WOKA)
S:MM247

C:AMDRY (Fine/JP + Coarse/JP)
S:CM247

Element	Measured Composition (wt. %)
Ni	48.1
Co	21.2
Cr	17.0
Al	12.8

Element	Measured Composition (wt. %)
Ni	46.1
Co	21.6
Cr	17.4
Al	13.8

FIGURE 69: *LF HVOF sprayed AMDRY 386-4 after 24 HR Thermal Cycle*

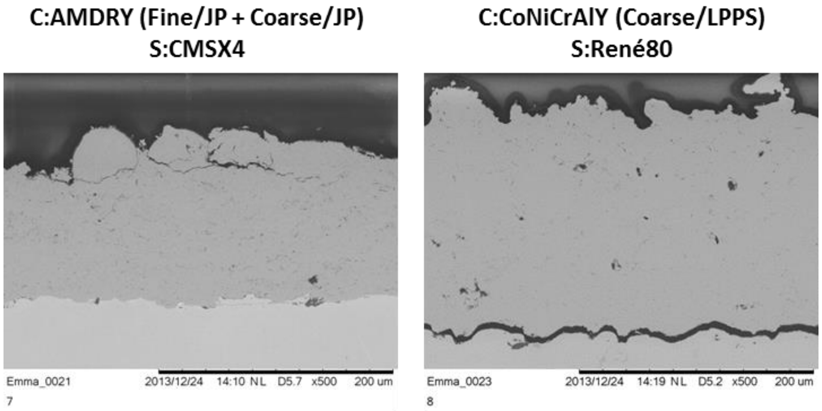
C:AMDRY (Fine/JP + Coarse/JP)
S:CMSX4

C:CoNiCrAlY (Coarse/LPPS)
S:René80

Element	Measured Composition (wt. %)
Ni	47.4
Co	21.8
Cr	17.4
Al	12.3

Element	Measured Composition (wt. %)
Ni	33.2
Co	36.6
Cr	21.3
Al	8.1

FIGURE 70: *LF HVOF and LPPS sprayed AMDRY 386-4 after 24 HR Thermal Cycle*

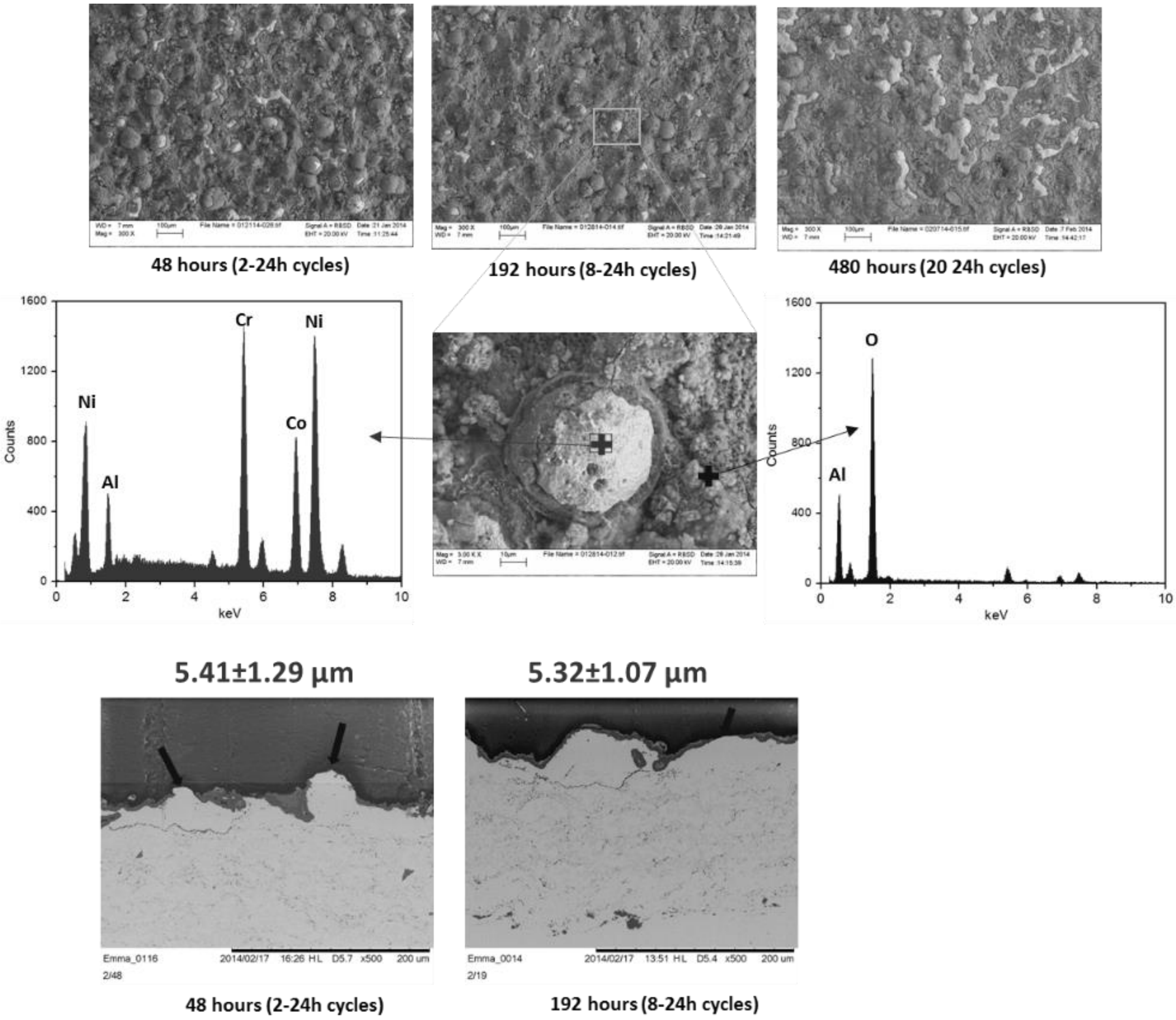

FIGURE 71: *HVOF sprayed AMDRY 386-2, 386-4 on Rene 80 substrate*

The thermal cycling of HVOF LF sprayed bond coating show mixed results in terms of TGO growth where above can be seen the TGO interface after 48 hrs, 192 hrs, and 480 hrs of furnace cycling. It is very apparent that after 480 hrs there is a significant amount of TGO growth on the outside of the particles and is confirmed with EDX spectroscopy showing the chemical element mapping of both the MCrAlY alloy and the TGO scale that is grown on top. The TGO growth assumes a parabolic exponential asymptotic relationship after a critical amount of thermal cycles which is seen to be between 192-480 hrs which is equivalent to 8-20 (24 hr) cycles. The TGO thickness was measured to be 5.41 microns after 2 cycles and approximately the same after 8 cycles which this coating achieved the critical amount of thermal cycles before the TGO stopped growing. There was no significant composition change seen fine and coarse powder yet a large difference when considering the LPPS sprayed coatings where there is a much larger decrease of Ni and Al in the coating which is leeched out to grow the TGO layer.

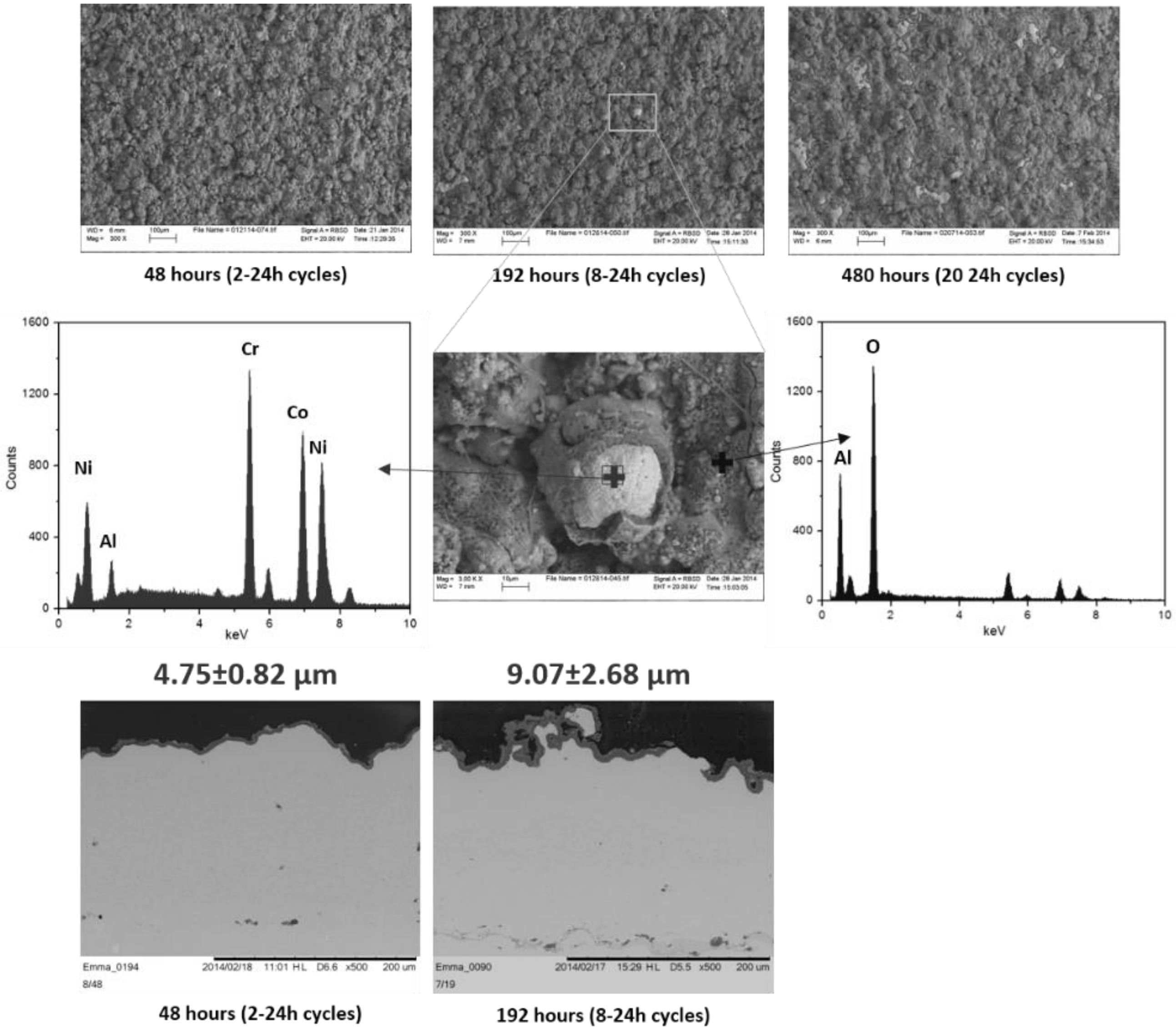
48 hours (2-24h cycles)

192 hours (8-24h cycles)

480 hours (20 24h cycles)

4.75±0.82 µm

9.07±2.68 µm

48 hours (2-24h cycles)

192 hours (8-24h cycles)

FIGURE 72: *LPPS sprayed CoNiCrAlY on Rene 80 substrate*

The thermal cycling results of the LPPS sprayed MCrAlY powder show much different results than that of the HVOF sprayed coatings. After 8 cycles the powder is seen to grow little to no TGO layer on the powder and not until 20 cycles can there be seen a significant amount of TGO growth. The TGO scale was measured to be 4.75 microns after 2 cycles and increased to 9.07 microns after 8 cycles which does not reach a critical thickness until more cycling is done to the coating. This is a major difference seen in HVOF and LPPS sprayed coatings where the latter can be explained by the oxygen deficient environment in which the coating is sprayed. This vacuum creates a semi-inert atmosphere inside the chamber which drastically reduces the amount of pre-oxidation of the bond coating when being deposited. Another observation to be made is that by pre-oxidizing the powder to some degree in HVOF sprayed coatings may create this critical asymptotic thickness where the TGO stops growing, as in the LPPS coating the TGO layer continues to grow after 8 cycles.

4.5. DISCUSSION

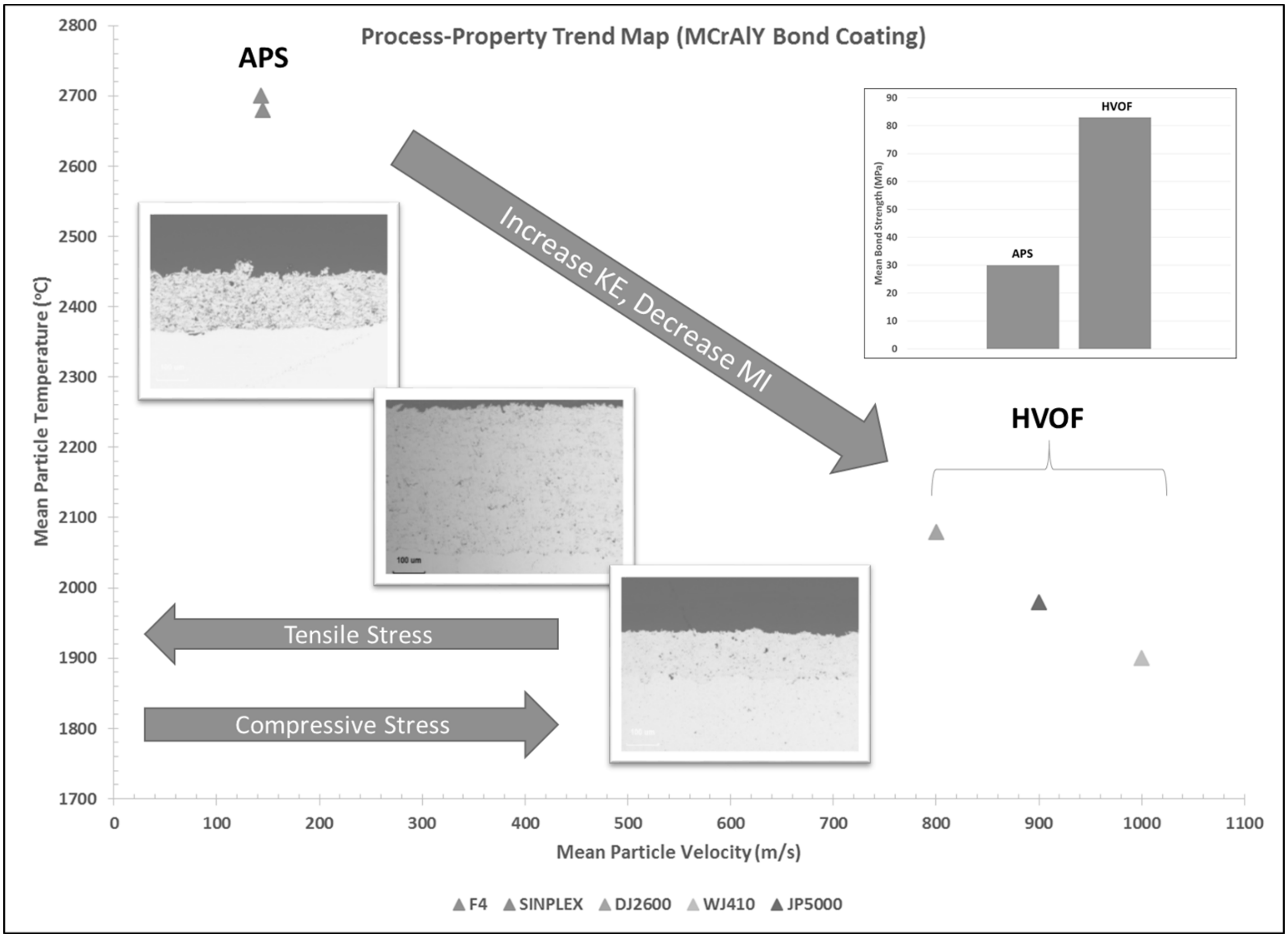

FIGURE 73: *Complete 1st Order Process-Property Trend Map*

The results of the proceeding experiments show clear trends in the process-property relations described in the introduction of the document, which are now discussed in detail corresponding to the design of experiments, adhesion testing, and thermal cycling. The trends can be seen to have both a linear response as well as an asymptotic exponential saturation with respect to the growth of the TGO layer. The type of thermal spray processing used to deposit the coatings can be seen to have a drastic effect on both the adhesion strength of the coating as well as the TGO layer growth under thermal cycling, which are linked to the process-property trends.

D.O.E. 1 was performed to understand the effects of varying the barrel length, feed rate, spray distance, combustion pressure, A/F ratio, spray angle, and to a lesser extent the substrate roughness. The resulting data analysis shows the mean values and SN ratios obtained with respect to mean particle temperature and velocity using the Accuraspray sensor showing the effect the feed rate and A/F ratio have on the temperature of the particles, being that higher feed rates tend to quench the flame and higher A/F ratios tend to pre-oxidize the powder increasing the temperature. The variables having the greatest effect on velocity can be seen to be the spray distance and combustion pressure, being that a larger spray distance will allow the particles to lose energy and therefor slow down, and the higher combustion pressure lends more energy to the particles and therefor speeds them up.

The ICP stress-state measurements show the typical compressive evolving stress and residual stress after cooling, involved with HVOF sprayed MCrAlY powder using a liquid-fuel torch. The largest evolving stress can be seen in R1129, this is due to the low MI and high KE of the particles, which are not fully molten but have a high velocity and tend to peen the surface of the substrate and also the coating to some extent as it builds up. The microstructural analysis for these four runs are displayed of which the densification of the coating with the high MI and high KE group of R1123, low MI and low KE of R1124A having semi-molten particles that do not flatten out, high MI and low KE of R1126A being flattened splats but not as dense as the high KE, and the low MI and high KE of R1129 which is a dense coating but some of the semi-molten particles can be seen in the cohesive regions in the coating, which also had the highest compressive residual stress.

D.O.E. 2 was performed to understand the effects of barrel length, spray angle, raster speed, and A/F ratio, and a different powder chemistry. The processing combination used was with a JP5000/WJ410 liquid-fuel torch and Sulzer-Metco XPT449 pure NiCoCrAlY powder without any other reactive rare earth elements. It can be seen from the SN ratio plots that the greatest effect on the mean particle temperature is again the A/F ratio while the high ratios pre-oxidize the powder and raise the temperature, being an exothermic process. The greatest effect on mean particle velocity was barrel length and A/F ratio, the longer barrels apply a longer dwell time to the particles and can impart extra energy from the plume as well as A/F, the higher above stoichiometric ratio that is applied, the extra oxygen raises the temperature of the particles and in doing so slightly increases the MI and flattens out the particles, creating more air drag and slowing them down. The stress-states of these coatings are very similar to that of D.O.E. 1 having the characteristic compressive evolving/residual stress as well as high stress amplitude due to the high velocity of the particles. The data for R1180 shows some downfalls to using the ICP sensor in that it is only accurate if set up and used properly, where here the beam was not secured onto the sensor well enough and the lasers read a curvature that was not accurate.

The microstructural analysis for D.O.E. 2 is very similar to that of D.O.E. 1 having similar parameters yet R1172 is noticeably different, being a low MI and low KE particle, it is not fully molten and has low energy therefor the splats do not flatted out and can leave voids in the coating, which can yield poor adhesion strength. The relative coating thicknesses are different due to spray angle change, where a larger angle away from normal to the surface lowers the deposition efficiency and therefor yields a thinner coating. Given the results from D.O.E. 1 and 2 further experiments were performed using the DJ2600 gas-fuel torch, which also consequently had the highest bond strength out of all the different processes. The spray distance for the DJ2600 is closer than the liquid fuel torches being in the range of 8 – 10 inches as opposed to 10 – 14 for a JP5000/WJ410 type. The step size of the gas-fuel torch is also smaller being only 3 mm whereas for the liquid-fuel torch it is 5 mm, this is due to the small volume of the plume. The effect of increasing the spray distance can be seen to lower the velocity of the particles as well as a decrease in temperature up to 11 inches where after this it starts to increase again, a sign of pre-oxidation of the powder.

D.O.E. 3 was performed in order to compare the process-property differences between gas-fuel and liquid-fuel HVOF torches. The DJ2600 GF torch shows a comparative process map when compared to the LF torches, having a slightly higher mean particle temperature, whereas it can be seen that the spray distance has a large effect on the mean particle velocity, where a range of 8 – 10 inches is recommended to have sufficient coating density. It is interesting to note that the MCrAlY powder, AMPERIT 421.1 sprayed with the DJ2600 gas-fuel torch has a tensile evolving/residual stress with A/F ratios in the range of 0.75 – 0.9, whereas with liquid-fuel torches it displays a heavy compressive evolving/residual stress. The MCrAlY powder sprayed with an A/F = 1.05 had a slight compressive evolving/residual stress which after cooling was close to be neutral stress. This is very hard to achieve in HVOF sprayed MCrAlY powders, or in metallic powders in general, as they almost always have a compressing evolving/residual stress. This may lead to the higher bond strength of the coatings as they do not have a high amount of interfacial surface energy built into the coating. The DJ2600 also has a unique feature where it uses a gas shroud to envelope the plume and adds an oxygen deficient region which helps to minimize pre-oxidation of the powder. This shroud gas can either be air, which is itself 80% N_2, or pure N_2 which would be ideal in protecting the high temperature particles during flight.

The APS process is a high temperature, low velocity deposition system as can be seen with velocities rarely reaching 180 m/s, as opposed to HVOF which can reach as high as 1000 m/s. This tends to make a porous metallic coating which is heavily oxidized as can be seen from the dark oxide stringers in the microstructure. The ICP data shows a tensile evolving/residual stress which is indicative of APS sprayed metallic powders. This can lower the bond strength of the coating, along with the superoxidation of the particles produces a very poor MCrAlY coating. The visible differences in the coatings are not extremely obvious yet with the Sinplex sprayed coating there can be seen dark lines on the interlamellar splat regions which is a sign of superoxidation. The design of the Sinplex torch uses what is called a neutral stack which allows the plasma to flow a longer distance without reaching the anode and can produce a hotter plasma, which is very bad for metallic coatings, especially MCrAlY bond coatings.

The method of measuring the TGO growth on the surface of the MCrAlY bond coatings has been explained in section 1.14., the data and analysis was performed by a post-doctoral staff member at the CTSR at SBU. These samples include different types of NSA substrates as well as HVOF and LPPS sprayed samples. The relative chemistry of the coatings were analyzed using energy dispersive x-ray spectroscopy (EDX) inside an SEM which can show a depletion in both Al and Cr in the coatings as a function of TGO growth. The relative thickness of the TGO was calculated with an SEM after various cycles inside the furnace, which can be subjective as this is a visual inspection method, a more accurate method would be to use thermogravimetric analysis, where the weight change of the coating is measured as a function of thermal cycling.

It is interesting to note that in the HVOF sprayed MCrAlY the TGO growth reaches an asymptotic relationship after 8 cycles and reaches a maximum thickness of 5.40 μm ± 1.0 μm whereas in the LPPS sprayed CoNiCrAlY, the TGO continues to grow after 8 cycles where it reached a value of 9.07 μm ± 0.82 μm. This could be due to the different chemistry of the powder where AMDRY 386-2 has many reactive elements which prevent further growth of the TGO, whereas the CoNiCrAlY has a greater percentage of Co and has no reactive elements which could hinder the TGO growth. The TGO scale layer can be seen to build up around the particles in the coating and propogate outward in a spherical manner, this is due to the morphology of the particles. The TGO tends to crack and break off due to the build-up of stresses which are analogous to the microcracking mechanisms seen in a TBC, this exposes the MCrAlY coating underneath and can allow a pathway for oxidation of the bond coating.

The procedure to test the bond strength of thermal spray coatings was explained in detail in section 1.13., where the proceeding data and analysis was performed at the CTSR at SBU. All samples were tested on an Instron tensile testing machine with a strain rate of 0.013 mm/s and the maxiumum load was recorded, and the mean bond strength of the coating was calculated from the applied loads. It will be shown that processing the MCrAlY coatings with high A/F ratios will lower the bond strength of the coating due to the pre-oxidation of the powder during deposition. The matrix of samples as well as the mean bond strength data are displayed below. All samples were fairly repeatable with a mean standard deviation of approximately, $\sigma = 4.68$ with the exception of experiment 2 which had a $\sigma = 10.13$ due to the fact that the epoxy had an additive, or thickening agent mixed in, which lowered the adhesion strength and consequently was not used. The DJ2600 (Samples 9 – 11) had the highest bond strength with a mean value of 72.0 MPa, and a maximum value of 76.04 MPa.This can be attributable to the very low residual stress in the coating, as well as the design of the torch which incorporates a gas shroud and protects the powder from pre-oxidizing during deposition. The process with the lowest bond strength was APS where F4 had a mean value of 34.89 MPa and a maximum of 42.0 MPa, whereas Sinplex had a mean value of 31.27 and a maximum of 37.0 MPa. This is due to the high temperature of the plasma which superheats the MCrAlY powder and superoxidizes the particles leeching out AlO and CrO, which shows up as a green tint on the coating, as well as black oxide stringers in the microstructure of the coating.

The effect of coating thickness on overall bond strength can be seen in samples 3 – 5 where the thicknesses were 450, 800, and 1200 μm. The mean bond strength increases with a coating thickness from 450 – 800 μm and decrease as the coating reaches 1200 μm due to the large amount of residual stress in the coating. The overall effect of increasing A/F ratio on mean bond strength can be seen in samples 6 – 8 where the bond strength decreases by a factor of 10 as the A/F ratio increases from 0.85 – 1.5 where the high oxygen content will pre-oxidize the coating and therefor weaken the interface. The JP5000 and WJ410 have almost identical mean bond strengths due to the fact that they are the same design of torch and also have interchangeable parts. The optimal processing technique, based on the results of these experiments would be to use a DJ2600 gas-fuel torch with a stoichiometric A/F ratio, with a N_2 shroud and AMPERIT 421.1 NiCoCrAlTaReHfSiY powder.

5. CONCLUSION

It is crucial to gain a deeper understanding of the variables affecting the performance of modern gas-turbine engines, which comes down to improving the thermal efficiency of the engine. It is understood that increasing the hot-section inlet temperature is proportional to increasing the fuel efficiency of the engine, driving the need for higher temperatures. Out of this comes the drive for innovation, where refractory materials are needed that can withstand the harsh environment inside the turbine. The melting point of nickel-cobalt based superalloy materials is fixed, yet the inlet temperatures far exceed this value, this is achieved by using highly engineered thermal barrier coatings (TBC). These TBC's need to withstand temperatures in excess of 1700 ^{o}C as well as having excellent corrosion properties. The combination of using a nickel-cobalt based bond coating as well as a ceramic top coating can effectively protect the turbine blades and mitigate the heat flux seen by the substrate. The standard operating procedure (SOP) for applying the TBC is using thermal spray processing, which can produce unique microstructures in the coating, improving the thermal properties of the coating, as well as being fiscally justified in being used by original equipment manufacturers (OEM) in their gas-turbine engines.

The subtleties of thermal spray processing, specifically in terms of bond coatings, has been shown in the proceeding experiments, where using both high-velocity oxygen fuel (HVOF), atmospheric plasma spray (APS), and low-pressure plasma spray (LPPS), can drastically affect the properties of the as-sprayed bond coating. These effects are displayed in the process-property trends that can be seen as a product of first understanding the variables involved in each process, using design of experiment (D.O.E.) techniques, standard data acquisition and testing techniques, as well as in-situ diagnostics to monitor the process variations. The crucial properties of the bond coating is known to be a high adhesion strength to the substrate, as well as an optimized thermal cycling response in terms of the thermally grown oxide (TGO) layer that is grown on the as-sprayed coating surface. These properties directly affect the thermal cycle life of the TBC where the root cause of coating failure has been seen to be the stress build-up in the TGO-Top Coating interfacial region, caused by rapid growth of the TGO layer itself. Understanding the process-property trends relating to the TGO growth is extremely important when processing the bond coating. The adhesion strength of the coating can be seen to be affected by pre-oxidation of powder during deposition wherein using highly oxidizing HVOF parameters, as well as high-temperature APS, can drastically lower the adhesion strength of the coating. It has been shown that decreasing the particle flight time, increasing the particle dwell time, using stoichiometric/reducing HVOF conditions, using a non-carbon rich fuel such as hydrogen, and depositing the bond coating in a vacuum environment all increase both the adhesion strength of the coating as well as somewhat decreasing the TGO growth acceleration. These process-property trends are crucial to TBC processing and are constantly studied by OEM's to create gas-turbine engines with increasing fuel efficiency.

6. REFERENCES

1. “Massachusetts Institute of Technology Gas Turbine Lab". Web.mit.edu. 1939-08-27.
2. Eckardt, D. and Rufli, P. "Advanced Gas Turbine Technology - ABB/ BBC Historical Firsts", ASME J. Eng. Gas Turb. Power, 2002, p. 124, 542-549
3. Waumans, T.; Vleugels, P.; Peirs, J.; Al-Bender, F.; Reynaerts, D. (2006)."Rotordynamic behaviour of a micro-turbine rotor on air bearings: modelling techniques and experimental verification, p. 182" (PDF). ISMA. International Conference on Noise and Vibration Engineering.
4. "Mechanical Engineering "Power & Energy," June 2004 - "A Year of Turbulence," Feature Article". Memagazine.org.
5. Sudhangshu Bose, *“High-temperature coatings”,* Butterworth-Heineman 2007
6. Callister W.J., *“Materials Science and Engineering: An Introduction”*, 8th Ed, 2010
7. Porter D.A., *“Phase Transformations in Metals and Alloys”*, 3rd Ed, 2011
8. Kalpakjian S., *“Manufacturing: Engineering and Technology”*, 7th Ed, 2014
9. Singh, Antariksh Rao Pratap, “*Mechanisms of Ordered Gamma Prime Precipitation in Nickel Base Superalloys*.” Denton, Texas. UNT Digital Library.
10. Reed, Roger C., *“The Superalloys: Fundamentals and Applications.”* Cambridge, UK: Cambridge UP, 2006.
11. Klein, L., Y. Shen, M. S. Killian, and S. Virtanen. *"Effect of B and Cr on the High Temperature Oxidation Behavior of Novel γ/γ'Strengthened Co-base Superalloys."* Corrosion Science 53 (2011): 2713-720.
12. Shinagawa, K., Toshihiro Omori, Katsunari Oikawa, Ryosuke Kainuma, and Kiyohito Ishida. *"Ductility Enhancement by Boron Addition in Co–Al–W High-temperature Alloys."* Scripta Materialia 61.6 (2009): 612-15.
13. Matweb.com/DataSheet/Special Metals INCONEL 718
14. Anthony, John W.; Bideaux, Richard A.; Bladh, Kenneth W. and Nichols, Monte C., ed. (1997). "Corundum" (PDF). *Handbook of Mineralogy*. III(Halides, Hydroxides, Oxides). Chantilly, VA, US: Mineralogical Society of America.
15. Pauling, L. (1932). "The Nature of the Chemical Bond. IV. The Energy of Single Bonds and the Relative Electronegativity of Atoms". *Journal of the American Chemical Society* **54** (9): 3570–3582.
16. Robert S. Mulliken, *Journal of Chemical Physics*, **1934**, *2*, 782.
17. John O'M. Bockris and Amulya K. N. Reddy (1970). *Modern Electrochemistry*. Plenum Press. pp. 352–3.
18. K. Kendall (1994). "Adhesion: Molecules and Mechanics".*Science* **263** (5154): 1720–5.
19. F. London, "The General Theory of Molecular Forces" (1936).
20. Sharfrin, E.; Zisman, William A. (1960). "Constitutive relations in the wetting of low energy surfaces and the theory of the retraction method of preparing monolayers".*The Journal of Physical Chemistry***64** (5): 519–524.

21. Eustathopoulos, N.; Nicholas, M.G. and Drevet B. (1999). *Wettability at high temperatures*. Oxford, UK: Pergamon.
22. Sulzer-Metco, *"Thermal Spray Materials Guide"*, PDF, 2014
23. Sulzer-Metco, *"Nickel Cobalt Chromium Aluminum Yttrium (NiCoCrAlY) Thermal Spray Powders"*, Material Product Data Sheet, PDF, 2014
24. H.C. Starck, *"AMPERIT Thermal Spray Powders"*, PDF, 2014
25. Young, David John (2008). *High Temperature Oxidation and Corrosion of Metals*.
26. Branan, Carl (2005-08-16). *Rules of thumb for chemical engineers: A manual of quick, accurate solutions to everyday process engineering*
27. Liang, Yan-Jie; Chai, Li-Yuan; Liu, Hui; Min, Xiao-Bo; Mahmood, Qaisar; Zhang, Hai-Jing; Ke, Yong (2012). "Hydrothermal sulfidation of zinc-containing neutralization sludge for zinc recovery and stabilization". *Minerals Engineering***25**: 14.
28. Rott, N. (1990). "Note on the history of the Reynolds number". *Annual Review of Fluid Mechanics* **22** (1): 1–11.
29. Padture N.P., *"Thermal Barrier Coatings for Gas-Turbine Engine Applications"*, **Science 296, 280** (2002)
30. Sturrock, Peter A. (1994). *Plasma Physics: An Introduction to the Theory of Astrophysical, Geophysical & Laboratory Plasmas*. Cambridge University Press.
31. Kuroda, Seiji; Kawakita, Jin; Watanabe, Makoto; Katanoda, Hiroshi (2008). "Warm spraying—a novel coating process based on high-velocity impact of solid particles". *Sci. Technol. Adv. Mater.* **9** (3)
32. Paulussen, S; Rego, R; Goossens, O; Vangeneugden, D; Rose, K (2005). "Plasma polymerization of hybrid organic–inorganic monomers in an atmospheric pressure dielectric barrier discharge". *Surface and Coatings Technology* **200**: 672.
33. R. Suryanarayanan (1993). *Plasma Spraying: Theory and Applications*. World Scientific Pub Co Inc. p. 211.
34. Wang et al., *"Melting index characterization and thermal conductivity model of plasma sprayed YSZ coatings"*, **Journal of the European Ceramic Society 32**, 2012
35. Karlsson A.M., *"The displacement of the thermally grown oxide in thermal barrier systems upon temperature cycling"*, **Materials Science and Engineering A351**, 2002
36. Chen et al., *"Oxidation and crack nucleation/growth in an air-plasma-sprayed thermal barrier coating with NiCrAlY bond coat"*, **Surface and Coatings Technology 197**, 2004
37. Lee et al., *"Phase transformation and bond coat oxidation behavior of plasma-sprayed zirconia thermal barrier coating"*, **Surface and Coatings Technology 124**, 2000
38. Sampath et al., *"Role of thermal spray processing method on the microstructure, residual stress and properties of coatings: an integrates study for Ni-5 wt.% Al bond coats"*, **Materials Science and Engineering A364**, 2003
39. Sulzer-Metco, *"Thermal Spray Equipment Guide V10"*, PDF, 2014
40. Miller R. A., *"Thermal Barrier Coatings for Aircraft Engines: History and Directions"*, **ASM International 42**, 2000

41. Vaßen et al., *"Process diagnostics in suspension plasma spraying"*, **Surface and Coatings Technology 205**, 2010
42. Vaßen et al., *"Stress distributions in plasma-sprayed thermal barrier coatings as a function of interface roughness and oxide scale thickness"*, **Surface and Coatings Technology 161**, 2001
43. Vaßen et al., *"Thermophysical properties and thermal cycling behavior of plasma sprayed thick thermal barrier coatings"*, **Surface and Coatings Technology 192**, 2004
44. Sampath et al., *"In-situ measurement of residual stresses and elastic moduli in thermal sprayed coatings"*, **Acta Materialia 51**, 2002
45. Vaßen et al., *"Advanced thermal spray technologies for applications in energy systems"*, **Surface and Coatings Technology 202**, 2008
46. Vaßen et al., *"Overview on advanced thermal barrier coatings"*, **Surface and Coatings Technology 205**, 2010
47. Vaßen et al., *"Development of a micromechanical life prediction model for plasma sprayed thermal barrier coatings"*, **Materials Science and Engineering A303**, 2000
48. Vaßen et al., *"Order-disorder transformation in a NiCoCrAlY Bond Coat Alloy at High Temperature"*, **Scripta Materialia 43**, 2000
49. Fraley et al., *"Design of Experiments via Taguchi Methods: Orthogonal Arrays"*, **The Michigan Chemical Process Dynamics and Controls Open Text Book**, 2007
50. Sohn et al., *"Thermal cycling of EB-PVD/MCrAlY thermal barrier coatings: Microstructural development and spallation mechanisms"*, **Surface and Coatings Technology 146 – 147**, 2001
51. ASTM Standard C633-13, *"Standard Test Method for Adhesion or Cohesion Strength of Thermal Spray Coatings"*, **ASTM International**, 2014